Addis Ababa University
Addis Ababa Institute of Technology
School of Electrical and Computer Engineering

ROTOR POSITION EXTRACTION BY CARRIER FREQUENCY COMPONENT METHOD (CFCM) IN SPACE VECTOR MODULATION (SVM) FOR IPM DRIVES

A thesis submitted to Addis Ababa Institute of Technology, School of Graduate Studies, Addis Ababa University

in partial fulfillment of the requirement for the Degree of Master of Science in Electrical Engineering (*Electrical Control Engineering*)

By

Nebiyu Tenaye Woldegebriel

Advisor: Dr. Mengesha Mamo

ADDIS ABABA, ETHIOPIA
SEPTEMBER 2015

Addis Ababa University
Addis Ababa Institute of Technology
School of Electrical and Computer Engineering

ROTOR POSITION EXTRACTION BY CARRIER FREQUENCY COMPONENT METHOD (CFCM) IN SPACE VECTOR MODULATION (SVM) FOR IPM DRIVES

By Nebiyu Tenaye Woldegebriel

APPROVED BY BOARD OF EXAMINERS

Dean, School of Graduate Committee	Signature
Dr. Mengesha Mamo Advisor	Signature
Internal Examiner	Signature
External Examiner	Signature

ACKNOWLEDGMENT

During my graduate study, several persons, including the academic and supporting staffs of School of Electrical and Computer Engineering (SECE), dearest friends and, of course, my family, have collaborated directly and indirectly to my thesis work. Therefore, I would like to recognize their contribution and express my gratitude in this section.

I would like to start by expressing a sincere acknowledgment to my advisor, *Dr. Mengesha Mamo*, for his guidance, support and encouragement. He has been an excellent advisor and mentor demonstrating high level of patience and continuous help. His deep knowledge to the subject matter contributed a lot in this paper. His guidance was undoubtedly great.

At last, but not least, I would like to express my gratitude to my family and colleges in SECE for their encouragement, unconditional support, confidence in me and love.

TABLE OF CONTENTS

LIST OF FIGURES

LIST OF TABLES

LIST OF ABREVIATIONS

PMSM	……	Permanent Magnet Synchronous Motor
AC	……	Alternating Current
DC	……	Direct Current
ACIM	……	Alternating Current Induction Motor
BLDC	……	Brushless Direct Current
FOC	……	Field Oriented Control
IPM	……	Interior Permanent Magnet
HVDC	……	High Voltage Direct Current
EMF	……	Electromotive Force
CFCM	……	Carrier Frequency Component Method
PM	……	Permanent Magnet
SVM	……	Space Vector Modulation
PI	……	Proportional Integral
IPMSM	……	Interior Permanent Magnet Synchronous Motor
SM	……	Synchronous Machine
VFD	……	Variable-Frequency Drive
MTPA	……	Maximum Torque per Ampere
SPWM	……	Sinusoidal Pulse Width Modulation
PWM	……	Pulse Width Modulation
VSI	……	Voltage Source Inverter
IPMM	……	Interior Permanent Magnet Motor
TF	……	Transfer Function
THD	……	Total Harmonic Distortion
FFT	……	Fast Fourier Transform
2D	……	Two Dimension
3D	……	Three Dimension
FACTS	……	Flexible AC Transmission Systems
MAM	……	Magnetic Anisotropy Method

LIST OF NOTATIONS

e	……	Error
τ	……	Time Constant
$\approx$	……	Approximately Equal To
Ω	……	Ohm
ω	……	Speed
$[\,]^{\text{™}}$	……	Trade Mark
$(\,)^{-1}$	……	Inverse
θ	……	Rotor Position
λ_f	……	Permanent Magnet Flux Linkage
J	……	Inertia, Performance Index
B	……	Viscous Friction Dumping Constant, Performance Index
ω_0	……	Minimal Natural Frequency
T_s	……	Sampling Time
K	……	Gain
L	……	Inductance
V	……	Voltage
I	……	Current
ρ	……	Time Domain Derivative Operator d/dt
T	……	Torque
P	……	Power
p	……	Number of Poles
e_f	……	Back Electromotive Force

ABSTRACT

Sensorless drive of interior permanent magnet (IPM) synchronous motors is possible because the motors' rotor position information is attached to stator inductance (due to magnetic saliency) and back electromotive force (EMF). The vector controlled sensorless drive, which uses the inductance variation of this motor, comprises a cascaded feedback and single loop SISO control systems.

A cascade PI controller is introduced. The inner feedback loop performs the control of *q*-axis voltage according to the required *q*-axis current obtained from speed controlling outer loop. The position of the motor is obtained by using high frequency injected signal component of the stator's currents. High frequency signals increase the bandwidth and reliability of the band pass filter. But further increase in injection frequency results higher THD. In order to find the exact position of the rotor from this saliency, two stationary reference frames are used. PI controller is also introduced for the single loop *d*-axis feedback system. This loop operates the regulation of the *d*-axis current for MTPA operation.

An SVPWM is used to generate an efficient VSI switching sequence from the reference voltages obtained from the vector controller. The performance of this PWM technique is compared with the sinusoidal PWM in terms of total harmonic distortion (THD) and DC bus voltage conversion ratio.

The *d-q* frame mathematical model of IPMSM, transformed using Park's and Clarke's transformation, is investigated on SIMULINK® SimPowerSystems™. The models are based on a per-unit (*pu*) analysis.

Simulation results show that, SVPWM has a 22% low THD value than SPWM, and it improves the DC bus voltage conversion by 7%. The rotor's position is successfully extracted from the high frequency component of rotor current for different motor operations, and the speed response of the control of the drive system is smooth.

Key Words: Interior Permanent Magnet (IPM) Motor, Vector Controlled Motor Drives, Space Vector Pulse width Modulated (SVPWM) voltage source inverter, SIMULINK® SimPowerSystems™/ MATLAB®

CHAPTER 1
INTRODUCTION

1.1 BACKGROUND

The permanent magnet synchronous motor (PMSM) can be thought of as a cross between an AC induction motor (ACIM) and a brushless DC motor (BLDC). They have rotor structures similar to BLDC motors which contain permanent magnets. However, their stator structure resembles that of ACIM, where the windings are constructed in such a way as to produce a sinusoidal flux density in the air-gap of the machine. As a result, they perform best when driven by sinusoidal waveforms. Unlike their ACIM, PMSM motors perform poorly with open-loop scalar V/Hz control, since there is no rotor coil to provide mechanical damping in transient conditions. Field Oriented Control (FOC) is the most popular control technique used with PMSMs. As a result, torque ripple can be extremely low, on par with that of ACIMs. PMSM motors provide higher power density for their size compared to ACIMs. This is because with an induction machine, part of the stator current is required to "induce" rotor current in order to produce rotor flux. These additional currents generate heat within the motor. However, the rotor flux is already established in a PMSM by the permanent magnets on the rotor.

Most PMSMs utilize permanent magnets, which are mounted on the surface of the rotor. This makes the motor appear magnetically "round", and the motor torque is the result of the reactive force between the magnets on the rotor and the electromagnets of the stator. This results in the optimum torque angle being 90 degrees, which is obtained by regulating the d-axis current to zero in a typical FOC application. However, some PMSMs have magnets that are buried inside of the rotor structure. These motors are called Interior Permanent Magnet, or IPM motors. As a result, the radial flux is more concentrated at certain spatial angles than it is at others. This gives rise to an additional torque component called reluctance torque, which is caused by the change of motor inductance along the concentrated and non-concentrated flux paths. This causes the optimum FOC torque angle to be greater than 90 degrees, which requires regulating the d-axis current to be a fixed negative ratio of the q-axis current. This negative d-axis current also results in field weakening, which reduces the flux density along the d-axis, which in turn partially lowers the core losses. As a result, IPM motors boast even higher power output for a given frame size. These

motors are becoming increasingly popular as traction motors in hybrid vehicles, as well as variable speed applications for appliances and HVAC.

The saliency exhibited by IPM motors can also provide an additional benefit in sensorless control applications. In many cases, the saliency signature is strong enough that it can be used to determine rotor position at standstill and low speed operating conditions. Some sensorless FOC designs use saliency mapping at low speeds, and then transition to a back-EMF observer model as the motor speeds up.

Nowadays, IPM synchronous motors [1] are very important in a wide variety of industrial applications. The operational accuracy (both in position and speed) and power consumption of other motors have always been the main issue. The usage of permanent magnet ac motors or PM synchronous was found to eliminate the usage of excitation/field currents. Therefore, the power consumption of these motors is very less than that of the non PM motors. The position or speed control of these PM motors has been being modified through time. Because of the non-suitable environment for sensors, sensorless drives have been more practical. Wide varieties of sensorless drives for PM motors are available.

By designing a rotor magnetic circuit such that the inductance varies as a function of rotor angle, the reluctance torque can be produced in addition to the mutual reaction torque of synchronous motors. This class of IPM synchronous motors can be considered as the reluctance synchronous motor and the PM synchronous motor combined in one unit. It is now very popular in industrial and military applications by providing high power density and high efficiency compared to other types of motors.

1.2 PROBLEM DESCRIPTION

The interior PM synchronous motor [1] is well known for its wide range torque reluctance and mutual reaction torque. IPM is a preferable motor for linear translational and rotational motions. Due to the above reasons sensorless low speed control of IPM will facilitate production and ensures high efficiency operations. As of this time, rotor position extraction based on carrier

frequency component method (CFCM) using two reference frames is available. The above deducted method uses triangular PWM for high frequency injection.

The position information of IPM synchronous motors [2] is attached to the stator's inductance (due to magnetic saliency) and back electromotive force (EMF). Consequently, control of such motors without a sensor (mechanical rotor position detector) is generally based on rotor position estimation from measured or estimated values of either or both of these two electrical quantities. At extremely low speed and standstill (from 0 – 10% base speed) the back EMF is very small resulting in unstable control, therefore, rotor position estimation from stator inductance variation with rotor position is effective in the lower speed lower range including zero speed. For 10% base speed and above the back EMF is suitable and can be estimated from measured fundamental stator terminal quantities using motor models and has been effectively used to estimate rotor speed and position; the sensorless drive of trapezoidal brushless DC motor drive and high speed PM-Synchronous motors [3] use this method.

Among the various methods of inductance estimation and rotor position extraction, high frequency signal injection [2], [4] is the most common used method to estimate or calculate the inductance and, hence, the rotor position. This method is not applicable for higher speed drives and the injection signal frequency should be chosen between the inverter switching (carrier) frequency and motor fundamental frequency. The decrease and the closeness of the injection frequency will result torque ripple and acoustic noise, and filtering difficulty, respectively.

Since, from [5] and [6], space vector modulation (SVM) technique is more advantageous over triangular PWM in many ways, high frequency injection using SVM technique should provide better operational and control efficiency. Improving the efficiency of the IPM synchronous motor operation in any way will help to improve industry productivity and energy consumption, because energy losses due to converter switching and harmonics are very smaller in SVM technique than in other PWM techniques.

1.3 OBJECTIVES OF THE THESIS

1.3.1 General Objectives

The general objective of the thesis is to show the improvements of sensorless control of IPM drives using carrier frequency component method for small speed drives by using SVM technique.

1.3.2 Specific Objectives

The specific objectives of the thesis are;

i. To study the mathematical model of IPMSM for saliency drive system.
ii. To study, implement and simulate IPM drive systems by using SVM.
iii. To extract rotor position from the carrier frequency of the input current signal.
iv. To design vector controlled IPM drive system using PI controller for the SVM implemented system.
v. To design and develop the virtual equivalent of each components and evaluate the responses and performances using SIMULINK® and MATLAB®.
vi. To evaluate the performance of the virtual equivalent of the overall drive system using SIMULINK® and MATLAB®.

1.4 CONTRIBUTION OF THE THESIS

The main contributions of this thesis are:

i. The two-reference frame model of PMSM has been used in some drive systems. In this thesis, this model, which is the d-q model, is employed and concludes the important role it plays in rotating magnetic field modeling.
ii. This thesis uses the saliency of IPMSM, which requires analyzing the high frequency component of the stator current. Introduces the analysis of high frequency components of stator currents only for rotor position extraction.
iii. The thesis proposes SVM-modulated signal to be mixed and injected with a very high frequency sinusoidal signal, which is intern filtered and used for analysis

purpose as in (ii). This idea is relatively new and shows the application of SVM for low speed IPM drive system.

iv. Since SVM is a digital modulation technique, its result can improve the performance of the drive system. SVM results in an optimized algorithm for real time control system.

1.5 OUTLINE OF THE THESIS

The thesis comprises six chapters and each chapter focuses on different specifics of the sensorless IPM drive. The first chapter (Chapter-1) presents the background and problem description of IPMM drive system, and the objectives and contribution of the thesis. The mathematical modeling of IPMSM in *d-q* axis and its equivalent circuit with the core literatures review are presented in Chapter-2. Chapter-3 presents the concepts of sensorless drive system, vector (field oriented) control, SVPWM technique and, of course, the powerful software tool used SIMULINK®'s Simpowersystems™. The design of important controllers and feedback loop is presented in Chapter-4. In this chapter, the definition of two reference frames is used as a core concept to extract the position of the rotor from the high frequency injected signal component of the stator current. The design of *d*-axis and *q*-axis currents PI controllers and speed PI controller is also presented in this chapter. In the 5th Chapter, the performance of the proposed PWM-technique, which is SVMPWM, is studied. The speed and torque performance in both directions of the drive system with respect to the corresponding performance variables, currents and voltages, are also presented and analyzed in this chapter. From these studies, conclusions, recommendations and future works are presented in the 6th Chapter.

CHAPTER 2
PERMANENT MAGNET SYNCHRONOUS MOTORS

2.1 INTRODUCTION

The permanent magnet synchronous motor is cross between an induction motor and brushless DC motor. Like a brushless DC motor, it has a permanent magnet rotor and windings on the stator. However, the stator structure with windings constructed to produce a sinusoidal flux density in the air-gap of the machine resembles that of an induction motor. Permanent magnet synchronous motors' power density is higher than induction motors with the same ratings since there is no stator power dedicated to magnetic field production. Today, these motors are designed to be more powerful while also having a lower mass and lower moment of inertia. Hence, they are commonly used in industrial automation for traction, robotics or aerospace, where greater power and heightened intelligence are require.

Some of the key characteristics of PMSM are:

- Close relative of the brushless DC motor
- Permanent magnet rotor and windings on the stator
- Sinusoidal back electromagnetic field (EMF) waveforms of the windings
- Controlled with sinusoid waveforms: matches the back EMF waveform of each winding.

Permanent magnet synchronous motors [9-10], [12], are broadly classified depending on the direction of field flux. The classifications are:

1. Radial field: the flux direction is along the radius of the machine.
2. Axial field: the flux direction is parallel to the rotor shaft.

The radial field PM machines are common whereas the axial field machines are coming into prominence in a small number of applications due to their higher power density and acceleration capacity than its counterpart. The axial field machines also have planar and easily adjustable air-gaps, and reduced noise and vibration levels. Note that, these are very desirable features in high-performance applications.

PMSMs can have different rotor types, depending on the placement of the magnets. The radial field version are shown below. The high power density synchronous machines have surface PMs with radial orientation whereas the interior magnet version is intended for high-speed applications. Regardless of the manner of mounting the PMs on the rotor, the basic principle of operation of the machine is same.

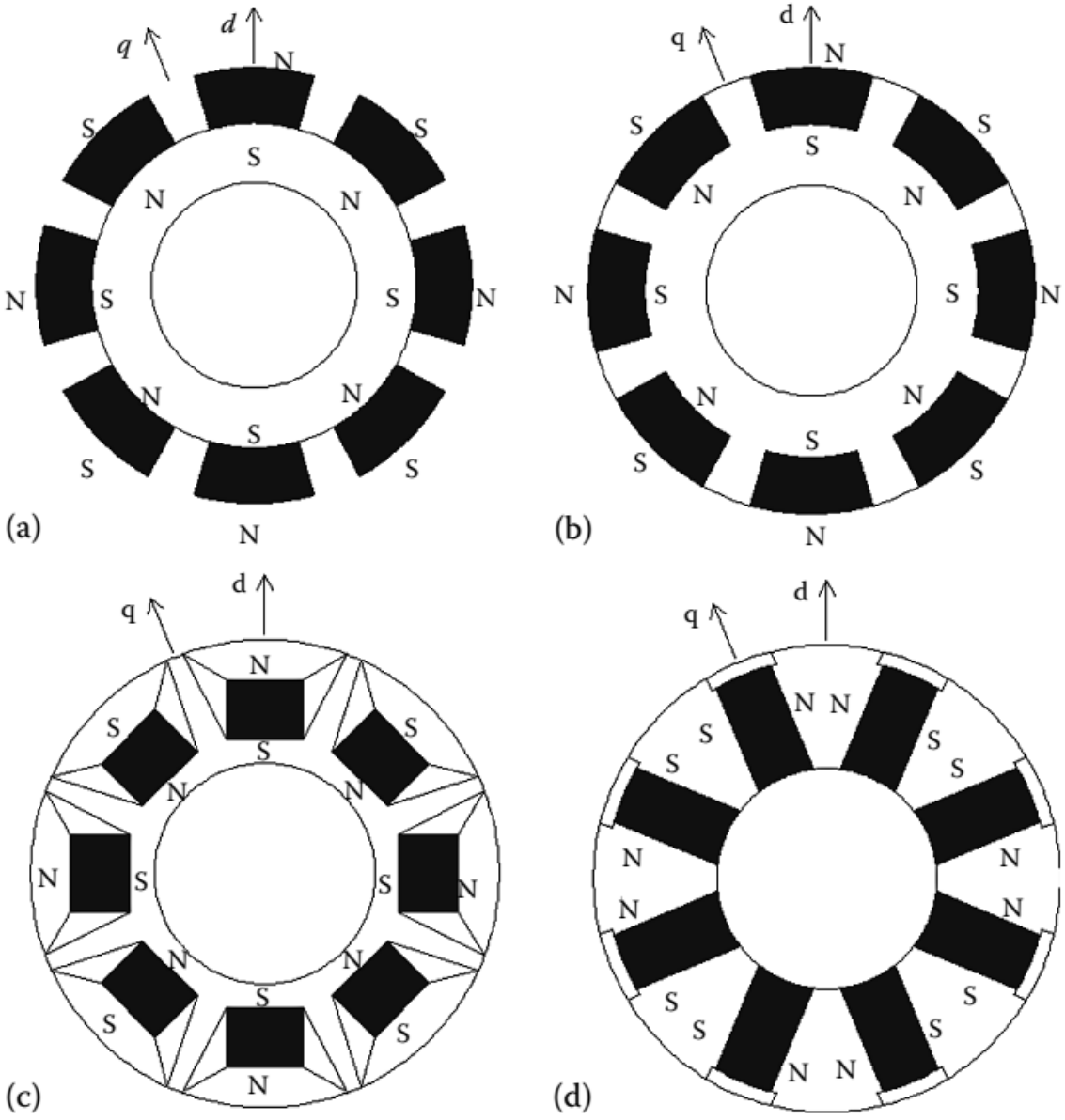

Figure 2. 1: *(a) Surface PM (SPM) synchronous machine. (b) Surface inset PM (SIPM) synchronous machine. (c) Interior PM (IPM) synchronous machine. (d) Interior PM synchronous machine with circumferential orientation.*

An important consequence of the method of mounting the rotor magnets is the difference between direct and quadrature axes inductance values (This will be explained later in this chapter).

Like any other AC machines, the PMSMs also have the same stator configurations depending on the number of phases. A distributed, Y-connected three-phase (or poly-phase) winding is used on the stator.

2.2 MATHEMATICAL MODEL OF IPMSM

2.2.1 Detailed Modeling of PMSM

A three-phase synchronous machine [9-14] can be generally modeled as shown in Figure-2 (a), where three stator (armature) windings on the stator, one field winding, and two damper windings on the rotor are depicted.

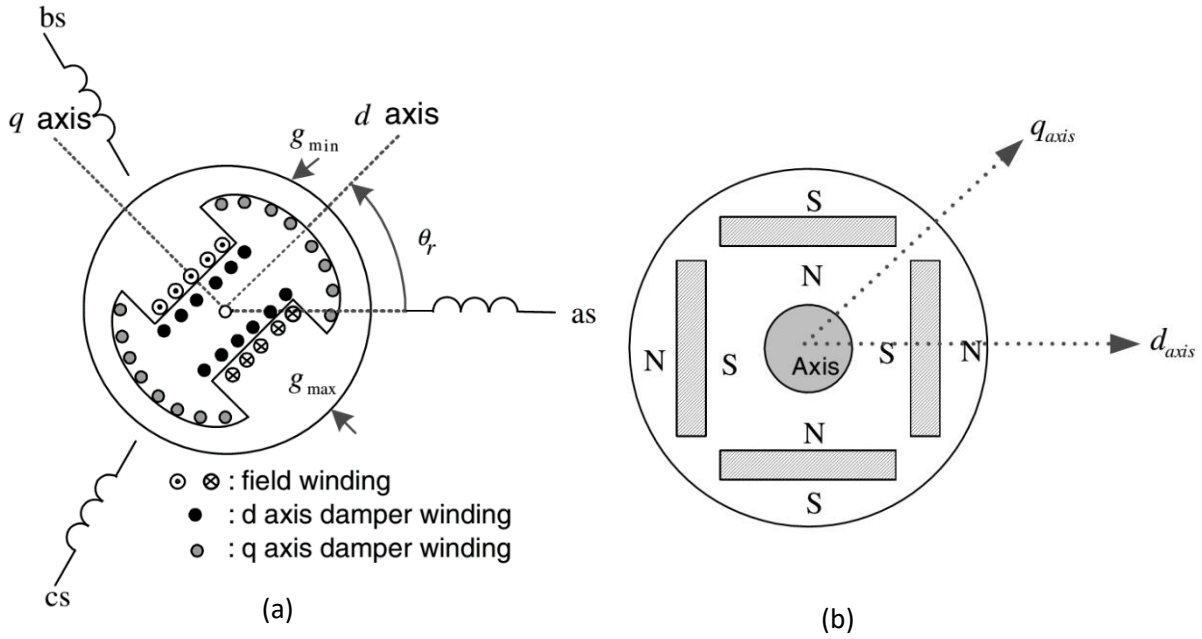

Figure 2. 2: *(a) Modeling of a three phase synchronous machine. (b) Cross-sectional view of the rotor of a four-pole IPMSM.*

The IPMSM has the magnet in the rotor, whose cross-sectional view is in Figure-2 (b). The IPMSM is designed to generate a sinusoidal back EMF, and there are no field windings and no damper windings. At any time t, the rotating rotor d-axis makes and angle θ_r with the fixed stator phase.

In PMSM the inductances vary as a function of the rotor angle. The two-phase (d-q) equivalent circuit model is used for analysis. The space vector form of the stator voltage equation in the stationary reference frame is given as:

$$V_s = R_s i_s + \frac{d\lambda_s}{dt} \tag{2.1}$$

Where R_s, V_s, i_s and λ_s are the resistance of the stator winding, complex space vectors of the three phase voltages, currents and flux linkages, all expressed in the stationary reference frame fixed to the stator, respectively, and are defined as:

$$\begin{aligned} V_s &= \left[V_{sa}(t) + e^{j2\pi/3} V_{sb}(t) + e^{j4\pi/3} V_{sc}(t) \right] \\ i_s &= \left[i_{sa}(t) + e^{j2\pi/3} i_{sb}(t) + e^{j4\pi/3} i_{sc}(t) \right] \\ \lambda_s &= \left[\lambda_{sa}(t) + e^{j2\pi/3} \lambda_{sb}(t) + e^{j4\pi/3} \lambda_{sc}(t) \right] \end{aligned} \tag{2.2}$$

Where, v_{sa}, v_{sb}, v_{sc} are the values of stator instantaneous phase voltages; i_{sa}, i_{sb}, i_{sc} are the values of stator instantaneous phase currents; λ_{sa}, λ_{sb}, λ_{sc} are the stator flux linkages and are given by:

$$\begin{aligned} \lambda_{sa} &= L_{aa} i_a + L_{ab} i_b + L_{ac} i_c + \lambda_{ra} \\ \lambda_{sb} &= L_{ba} i_a + L_{bb} i_b + L_{bc} i_c + \lambda_{rb} \\ \lambda_{sc} &= L_{ca} i_a + L_{cb} i_b + L_{cc} i_c + \lambda_{rc} \end{aligned} \tag{2.3}$$

Where L_{aa}, L_{bb}, and L_{cc} are the self-inductances of the stator *a*, *b* and *c* phase, respectively. L_{ab}, L_{bc} and L_{ca}, are the mutual inductances between the *ab*, *bc* and *ac* phases, respectively. λ_{ra}, λ_{rb} and λ_{rc} are the flux linkages that change depending on the rotor angle established in the stator *a*, *b*, and *c* phase windings, respectively, due to the presence of the permanent magnets on the rotor. They are expressed as:

$$\begin{aligned} \lambda_{ra} &= \lambda_r \cos\theta_r \\ \lambda_{rb} &= \lambda_r \cos(\theta_r - 120°) \\ \lambda_{rc} &= \lambda_r \cos(\theta_r + 120°) \end{aligned} \tag{2.4}$$

In equation (2.4), λ_r represents the peak flux linkage due to the permanent magnet. It is often referred to as the back-emf constant. Note that in the flux linkage equations, inductances are the functions of the rotor angle. Self-inductance of the stator a-phase winding, L_{aa} including leakage inductance and *a* and *b*-phase mutual inductance,

$$\begin{aligned} L_{ab} &= L_{bc} && \text{have the form} \\ L_{aa} &= L_{ls} + L_0 - L_{ms}\cos(2\theta_r) \\ L_{ab} &= L_{ba} = 1/2\, L_0 - L_{ms}\cos(2\theta_r) \end{aligned} \qquad 2.5$$

Where, L_{ls} is the leakage inductance of the stator winding due to the armature leakage flux, L_0 is the average inductance due to the space fundamental air-gap flux; $L_0 = ½(L_q + L_d)$, L_{ms} is the inductance fluctuation (saliency); due to the rotor position dependent on flux $L_{ms} = ½(L_d - L_q)$, similar to that of L_{aa} but with θ_r replaced by $(\theta_r - 2\pi/3)$ and $(\theta_r - 4\pi/3)$ for *b*-phase and *c*-phase self-inductances, L_{bb} and L_{cc} can also be obtained similarly. All stator inductances are represented in matrix form below:

$$\begin{aligned} L_{ss} &= \begin{bmatrix} L_{aa} & L_{ab} & L_{ac} \\ L_{ba} & L_{bb} & L_{bc} \\ L_{ca} & L_{cb} & L_{cc} \end{bmatrix} \\ &= \begin{bmatrix} L_{ls} + L_0 - L_{ms}\cos 2\theta_r & -0.5L_0 - L_{ms}\cos 2(\theta_r - \pi/3) & 0.5L_0 - L_{ms}\cos 2(\theta_r + \pi/3) \\ -0.5L_0 - L_{ms}\cos 2(\theta_r - \pi/3) & L_{ls} + L_0 - L_{ms}\cos 2(\theta_r - 2\pi/3) & -0.5L_0 - L_{ms}\cos 2(\theta_r - \pi) \\ 0.5L_0 - L_{ms}\cos 2(\theta_r + \pi/3) & -0.5L_0 - L_{ms}\cos 2(\theta_r - \pi) & L_{ls} + L_0 - L_{ms}\cos 2(\theta_r + 2\pi/3) \end{bmatrix} \end{aligned} \qquad 2.6$$

It is evident from equation (2.6) that the elements of L_{ss} are a function of the rotor angle which varies with time at the rate of the speed of rotation of the rotor. Under a three-phase balanced system, with no rotor damping circuit and knowing the flux linkages, stator currents, and resistances of the motor, the electrical three-phase dynamic equation in terms of phase variables can be arranged in matrix form similar to that of equation (2.1) and written as:

$$[V_s] = [r_s][i_s] + \frac{d[\lambda_s]}{dt} \qquad 2.7$$

Where,

$$\begin{aligned} [V_s] &= [V_{sa},\ V_{sb},\ V_{sc}](t) \\ [I_s] &= [i_{sa},\ \ i_{sb},\ i_{sc}](t) \\ [r_s] &= [r_{sa},\ \ r_{sb},\ r_{sc}] \\ [\lambda_s] &= [\lambda_{sa},\ \lambda_{sb},\ \lambda_{sc}](t) \end{aligned} \qquad 2.8$$

In equation (2.7), v_s, i_s, and λ_s refer to the three-phase stator voltages, currents, and flux linkages in matrix forms as shown in equation (2.8), respectively. Further all the phase resistances are equal and constant, $r_s = r_a = r_b = r_c$.

2.2.2 Park's Transformation and Dynamic d-q Modeling

L_{ss} presents computational difficulty (in equation-2.1) when used to solve the phase quantities directly. To obtain the phase currents from the flux linkages, the inverse of the time varying inductance matrix will have to be computed at every time step. The computation of the inverse at every time step is time consuming and could produce numerical stability problems. To remove the time-varying quantities in voltages, currents, flux linkages and phase inductances, stator quantities are transformed to a d-*q* rotating reference frame using Park's transformation. This results in the above equations having time-invariant coefficients. The idealized machines have the rotor windings along the *d*- and *q*-axes. Stator winding quantities need transformation from three phases to two-phase *d*-*q* rotor rotating reference frame. Park's transformation is used to transform the stator quantities to *d*-*q* reference frame, the *d*-axis aligned with the magnetic axis of the rotor and *q*-axis is leading the *d* axis by π/2 as shown in Figure-2. The original *d*-*q* Park's transformation $[T_{dq0}\theta_r]$ is applied to the stator quantities in equation 2.7 is given by:

$$\begin{aligned} [V_{dq0}] &= [T_{dq0}(\theta_r)][V_s] \\ [i_{dq0}] &= [T_{dq0}(\theta_r)][i_s] \\ [\lambda_{dq0}] &= [T_{dq0}(\theta_r)][\lambda_s] \end{aligned} \qquad 2.9$$

Where, $[T_{dq0}\theta_r]$ is Park's transformation matrix.

The *dq* transformation is a transformation of coordinates from the three-phase stationary coordinate system to the *dq* rotating coordinate system. This transformation is made in two steps:

1. a transformation from the three-phase stationary coordinate system to the two-phase, so-called *αβ*, stationary coordinate system, and
2. a transformation from the *αβ* stationary coordinate system to the *dq* rotating coordinate system.

These steps are shown in Figure 3. A representation of a vector in any n-dimensional space is accomplished through the product of a transpose n-dimensional vector (base) of coordinate units

and a vector representation of the vector, whose elements are corresponding projections on each coordinate axis, normalized by their unit values. In three-phase (three dimensional) space, it looks like this:

$$X_{abc} = \begin{bmatrix} a_u & b_u & c_u \end{bmatrix} \begin{bmatrix} x_a \\ x_b \\ x_c \end{bmatrix} \qquad 2.10$$

Assuming a balanced three-phase system ($x_o = 0$), a three-phase vector representation transforms to *dq* vector representation (zero-axis component is 0) through the transformation matrix $[T_{dq0}\theta_r]$, defined as:

$$[T_{dq0}\omega t] = \frac{2}{3}\begin{bmatrix} \cos(\omega t) & \cos(\omega t - 2/3\,\pi) & \cos(\omega t + 2/3\,\pi) \\ \sin(\omega t) & \sin(\omega t - 2/3\,\pi) & \sin(\omega t + 2/3\,\pi) \end{bmatrix} \qquad 2.11$$

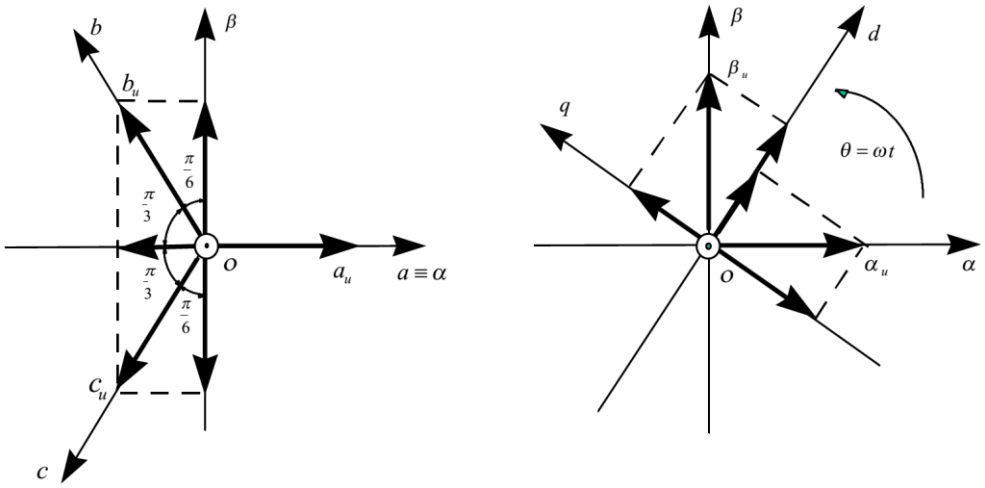

Figure 2. 3: *Park's transformation from three-phase to rotating dq0 coordinate system*

$$[\alpha_u \quad \beta_u \quad o_u] = [a_u \quad b_u \quad c_u]\frac{2}{3}\begin{bmatrix} 1 & 0 & \frac{1}{2} \\ -\frac{1}{2} & \frac{\sqrt{3}}{2} & \frac{1}{2} \\ -\frac{1}{2} & -\frac{\sqrt{3}}{2} & \frac{1}{2} \end{bmatrix}, \qquad [d_u \quad q_u \quad o_u] = [\alpha_v \quad \beta_v \quad o_v]\frac{2}{3}\begin{bmatrix} \cos(\theta_r) & -\sin(\theta_r) & 0 \\ \sin(\theta_r) & \cos(\theta_r) & 0 \\ 0 & 0 & 1 \end{bmatrix}$$

$$[d_u \quad q_u \quad o_u] = [a_u \quad b_u \quad c_u]\frac{2}{3}\begin{bmatrix} \cos(\theta_r) & -\sin(\theta_r) & \frac{1}{2} \\ \cos(\theta_r - \frac{2}{3}\pi) & -\sin(\theta_r - \frac{2}{3}\pi) & \frac{1}{2} \\ \cos(\theta_r + \frac{2}{3}\pi) & -\sin(\theta_r + \frac{2}{3}\pi) & \frac{1}{2} \end{bmatrix}$$

In other words, the transformation from X_{abc} (three phase coordinate) to X_{qd} (*dq* rotating coordinates is obtained through the multiplication of the vector X_{abc} by the matrix $[T_{dq0}\theta_r]$ (where $\theta_r = \omega t$) :

$$X_{dq} = [T_{dq0}\omega_r]\, X_{abc} \qquad 2.12$$

The inverse transformation matrix (from *dq* to *abc*) is defined as:

$$[T_{dq0}\theta_r]' = \begin{bmatrix} \cos(\theta_r) & -\sin(\theta_r) & \frac{1}{2} \\ \cos(\theta_r - \frac{2}{3}\pi) & -\sin(\theta_r - \frac{2}{3}\pi) & \frac{1}{2} \\ \cos(\theta_r + \frac{2}{3}\pi) & -\sin(\theta_r + \frac{2}{3}\pi) & \frac{1}{2} \end{bmatrix} \qquad 2.13$$

The inverse transformation is calculated as:

$$X_{abc} = [T_{dq0}\omega_r]'\, X_{dq} \qquad 2.14$$

Now, the transformation can be applied to the previous model of PMSM. The model of PMSM without damper winding can be developed on rotor reference frame (*dq-frame*) using the following assumptions:

1. Saturation is neglected
2. The induced EMF is sinusoidal
3. Eddy currents and hysteresis losses are negligible.
4. There are no field current dynamics.

Voltages equations are given by:

$$V_q = R_s i_q + \omega_r \lambda_d + \rho \lambda_q \quad 2.15$$

$$V_d = R_s i_d - \omega_r \lambda_q + \rho \lambda_d \quad 2.16$$

Flux Linkage are given by:

$$\lambda_q = L_q i_q \quad 2.17$$

$$\lambda_d = L_d i_d + \lambda_f \quad 2.18$$

Where, λ_f is Field flux linkage (in this case PM flux linkage), and

ρ is derivative operator (i.e. d/dt)

Substituting equations 2.17 and 2.18 into 2.15 and 2.16

$$V_q = R_s i_q + \omega_r (L_d i_d + \lambda_f) + \rho L_q i_q \quad 2.19$$

$$V_d = R_s i_d - \omega_r L_q i_q + \rho (L_d i_d + \lambda_f) \quad 2.20$$

Arranging equations 2.19 and 2.20 in matrix form

$$\begin{pmatrix} V_q \\ V_d \end{pmatrix} = \begin{pmatrix} R_s + \rho L_q & \omega_r L_d \\ -\omega_r L_q & R_s + \rho L_d \end{pmatrix} \begin{pmatrix} i_q \\ i_d \end{pmatrix} + \begin{pmatrix} \omega_r \lambda_f \\ \rho \lambda_f \end{pmatrix} \quad 2.21$$

Electromechanical power developed by the machine can be obtained from the component of the input power that is transferred across the air gap. The total input power to the machine is given by:

$$P_{in} = v_a i_a + v_b i_b + v_c i_c + v_f i_f + v_g i_g \quad W \quad 2.22$$

When the stator phase quantities are transformed to the rotor dq0 reference frame that rotates at a speed of $\omega_r = d\theta_r/dt$, equation (2.22) becomes:

$$\begin{aligned} P_{in} &= \frac{3}{2}(v_q i_q + v_d i_d) + 3 v_0 i_0 + v_f i_f + v_g i_g \quad W \\ &= \frac{3}{2}\left(r_s (i_q^2 + i_d^2) + i_q \frac{d\lambda_q}{dt} + i_d \frac{d\lambda_d}{dt} + \omega_r (\lambda_d i_d - \lambda_q i_q) \right) \\ &\quad + 3 i_0^2 r_o + 3 i_0 \frac{d\lambda_0}{dt} + i_f^2 r_f + i_f \frac{d\lambda_f}{dt} + i_g^2 r_g + i_g \frac{d\lambda_g}{dt} \end{aligned} \quad 2.23$$

Eliminating terms in equation (2.23) with *ohmic* losses and the rate of change in magnetic energy, the above expression of the electromechanical power developed reduces to:

$$P_e = \frac{3}{2} \omega_r (\lambda_d i_q - \lambda_q i_d) \quad W \quad 2.24$$

For a *P*-pole machine, $\omega_r = (P/2)\,\omega_m$, with ω_m being the rotor speed in mechanical radians per second. Thus, equation (2.24) for a *P*-pole machine can also be written as:

$$`P_e = \frac{3}{2}\frac{P}{2}\omega_m\left(\lambda_d i_q - \lambda_q i_d\right) \qquad W \tag{2.25}$$

Dividing the electromechanical power by mechanical speed of the rotor, we obtain the following expression for the electromechanical torque developed by a *P*-pole machine:

$$T_e = \frac{3}{2}\left(\frac{P}{2}\right)\left(\lambda_d i_q - \lambda_q i_d\right) \tag{2.26}$$

The mechanical torque equation is:

$$T_e = T_L + B\omega_m + J\frac{d\,\omega_m}{dt} \tag{2.27}$$

Solving for the rotor mechanical speed from equation 2.27, we obtain:

$$\omega_m = \int\left(\frac{T_e - T_L - B\omega_m}{J}\right)dt \tag{2.28}$$

and,

$$\omega_m = \omega_r\left(\frac{2}{P}\right) \tag{2.29}$$

In the above equations ω_r is the rotor's electrical speed, whereas, ω_m is the rotor's mechanical speed.

2.2.3 Equivalent Circuit of Interior PMSM

Equivalent circuits of the motors are used for study and simulation of motors. From the d-q modeling of the motor using the stator voltage equations the equivalent circuit of the motor can be derived. Assuming rotor d axis flux from the permanent magnets is represented by a constant current source as described in the following equation $\lambda_f = L_{md}\, i_f$, figure 4 is obtained.

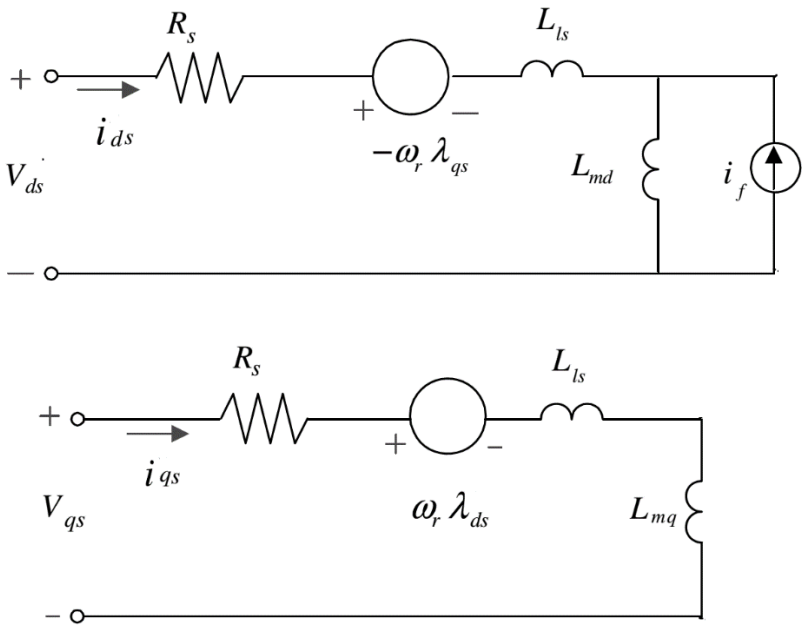

Figure 2. 4: *Equivalent circuit of an interior permanent magnet synchronous machine at rotor reference d–q axis*

2.3 LITERATURE REVIEW

Many papers regarding sensorless drive of PMSM and, of course IPMSM, in particular, have been published. A great and considerable care is taken to recognize and summarize publicly available and provided research papers.

1. **Mengesha Mamo, K. Izle, M. Sawamura and J. Oyama**, [2] proposed the extraction of rotor position from carrier signal component of the stator current. The carrier signal is injected to the stator through SPWM. The frequency of the signal is chosen in such a way that, it is in the range of the inverter's switching frequency and well above the fundamental operating frequency of the motor under study.

   The rotor's position is, then, extracted from the stator current i_a, i_b and i_c. These currents implicitly contain the inductance values L_q and L_d, from which the rotor position can be determined. For the position to be found, two stationary reference frames were defined. According to this paper, one of the stationary reference is α-β frame, which is a complex plane which can be determined from an *a-b-c* (three-phase frame/from only

two of the three phases) using Clark's transformation (it is discussed in *section-2.2.2*), and the other frame, *k-l*, is the same as *α-β* except that it is 45º behind the *α-β* frame. Before the three phase currents are transformed into the two stationary frame values, they are filtered in the carrier frequency range.

This thesis bases rotor position extraction method of this paper. In-spite of the SPWM technique used in here, this thesis proposes a more efficient PWM technique called space vector PWM.

2. **Jung-Ik Ha, Kozo Idle, Toshihiro Sawa, Seung-Ki Sul,** [3] proposed the IPM drive by identifying the rotor's initial position. A high frequency signal is injected to detect the position of the rotor from rotor's magnetic saliency. This paper uses the same approach as the paper in [2], except that this paper presents performance of the drive system. According to this paper, an IPM motor makes the magnetic and reluctance torque simultaneously and the high torque per current can be generated as:

$$T_e = \frac{3}{4} P\left\{\left(L_d - L_q\right) i_d + K_e\right\} i_q$$

To obtain the high reluctance torque and to hold high efficiency, the *d* axis current should be as in the figure below.

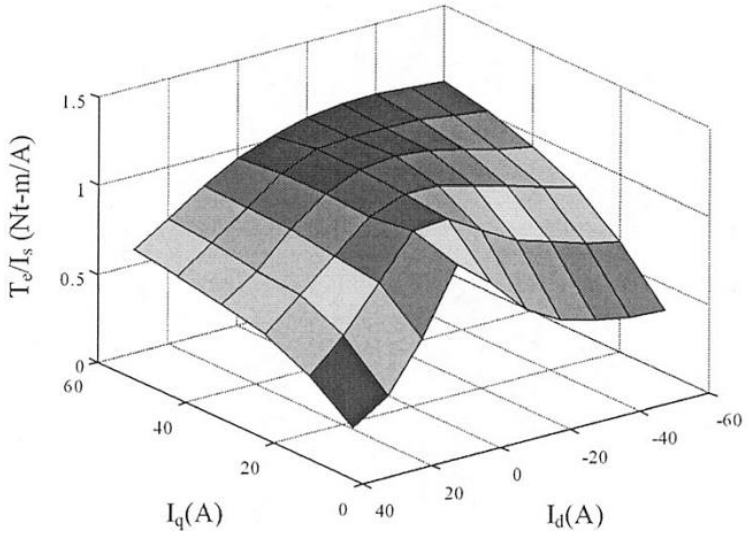

Figure 2. 5: *Characteristics of Output Torque. Torque per Current According to d-axis and q-axis Currents.*

From the figure, the characteristics of the torque produced are shown. For vector controlled IPMM drives, there is no negative current. For maximum torque per current drive, the current i_d should be zero. It is evident from the figure that the for $i_d = 0$, the torque is linearly dependent on the current i_q.

For this paper, the above torque performance is to be studied and the conclusions and arguments made from the study helped in generalizing and analysis purpose. Some of these are discussed as follows.

At zero or low speed, the high frequency impedance is dominated by the inductance.

There are voltages and current types in high frequency injection methods. The current injection method may have faster dynamic than the voltage one, but, in the case where the impedance difference decreases according to load condition, the controllability of the current type injection system can be easily lost under heavy load conditions.

3. **Dorin O. Neacsu,** [7] summarized the theory and performance of a three phase SVMPWM for VSIs, which is used in this paper. The paper started by analyzing the rotating space vector of a three phase balanced signal. This was because, it results a unique correspondence between a Space Vector in the complex plane and a three-phase system. The main advantages of this mathematical representation are:
    - Analysis of three-phase systems as a whole instead of looking at each phase,
    - It allows to use the properties of the vectorial rotation. Using rotation with ωt leads to an analysis in DC components by withdrawing the rotational effect.

    Then, the vertical analysis of a three phase VSI leads to the determination of the corresponding phase and line voltages and currents. The analytical approach used in this paper is somehow the same as in this thesis (as in Section-3.4). The detail of the analysis is left uncovered here.

    The six-step PWM technique is, mostly, covered in many papers before discussing the theory of operation of SVM techniques. This is also true for this paper, which used the six-step mode of operation with the vertical analysis of the three phases VSI. Which resulted in important relationships between the line and phase voltages and currents.

PWM is an algorithm that generates the switching function. Different PWMs produce different effects on converter loads. Performance indices are measured in respect with the modulation index:

$$m = \frac{V_S}{\frac{2}{3}V_{DC}}$$

Most used performance indices are:

- **Content in fundamental (z)**: represents the ratio between the RMS value of the fundamental of the output phase voltage (V_{L1}) and the RMS value of the output phase voltage (V_L).
- **Total Harmonic Distortion (THD)** coefficient:

$$THD_V = \frac{\sqrt{V_L^2 - V_{L1}^2}}{V_{L1}}$$

Other performance indices are also provided on the paper. Here, only those related to the voltage are shown.

The increased efficiency of SVM is due to the reduced inverter switchings compared to other types of PWM techniques like SPWM. In order to reduce the number of the inverter switchings, it is necessary to distribute the switching sequence in such a way that switching only one inverter leg at a time performs the transition from one state to the next. This results in starting the sampling period with one zero state and ending at the other state. This paper presented three main types of such switchings. This thesis uses symmetrically generated SVMs. The other two SVM algorithms are, namely, direct-inverse SVM and simple direct SVM.

4. **Stephen J. Dodds**, [28] proposed two settling time formulas that are to be derived numerically with the 5% and 2% criteria for the step responses of control systems having linear closed loop dynamics that may be designed by the method of pole assignment to have multiple closed loop poles. The proposed control system is to be implemented on digital processors like FPGA and ASIC DSPs, which are the latest drive control systems central part.

This paper is restricted to single input, single output plants but a similar approach may be taken for the control of multivariable plants. The design approach presented in this paper is a simple 'top-down' one in which the starting point is the desired performance in terms of the settling time with *zero overshoot* in the step response. It is important to note that if control energy is an important factor, then the settling time can be adjusted to minimize this within the constraint of maximum allowable settling time, attention also being paid to robustness (external disturbance rejection and insensitivity to plant modeling errors).

For a non-overshooting response the closed loop system must have convenient negative real poles, according to the TF:

$$\frac{y(s)}{y_r(s)} = \left(\frac{1}{1 + s\tau_c} \right)^n$$

Where, y is the measured and controlled output, y_r is the reference input, and τ_c is the closed loop time constant, i.e., the time constant of each of the n first order systems which when connected in a chain will yield the desired nth order closed loop dynamics. It can be shown that the general expression of the step response of the closed loop system defined by the above equation is:

$$y(t) = Y_r \left[1 - \sum_{i=0}^{n-1} \frac{1}{i!} \left(\frac{t}{\tau_c} \right)^i e^{-t/\tau_c} \right]$$

After a series of numerical computations, the 5% and 2% settling time formulas are derived. The accuracy assessment of the formulas are made and the paper proved that up to a 6^{th} order characteristic polynomial the formulas work very fine. The derivation of the formulas and performance evaluations are included in the paper.

CHAPTER 3
METHODOLOGY

3.1 INTRODUCTION

These days, the applications of sensorless drives have been preferable due to performance characteristics of sensors under extreme temperature and other environmental conditions. In addition to this, some drive systems' position and speed determination (extraction) technique does not require motor parameters at all. This makes the control of any drive system to be the same for the same motor type irrespective of the motor ratings and parameters. These sensorless drives can be controlled using either scalar or vector control techniques. Scalar controls are simple to implement and offer good steady state response; however, the dynamics are slow because the transients are not controlled. To obtain high precision and good dynamics, vector control schemes have been invented for use with closed-loop feedback controls. The controller controls the switching pattern of an inverter that is directly connected to the motor under study. The discussion in this thesis is limited to the vector control of sensorless drive of IPMSM and circles around the new switching pattern generation technique called space vector PWM.

3.2 DESCRIPTION OF SENSORLESS DRIVE SYSTEM OF IPMSM

The motor drive consists of five main components, the PM motor, SVPWM, inverter, control unit and the rotor position determination block. The components are connected as shown in Figure 3.1.

3.2.1 Sensorless Rotor Position Detection Methods

There are mainly two different methods to obtain the rotor position without the use of mechanical sensors, the back electromotive force or back EMF method and the signal injection method [15]. A new, third method that uses the characteristics of the magnetic material is also available.

3.2.1.1 *Back EMF*

For medium and high speed, the dominating methods to detect the rotor position without using a mechanical sensor is to make use of the back electromotive force, back EMF, from the motor

model. [15] The underlying theory behind these methods is the motor equation of the stator, in equation (3.1), expressed in the *dq* reference frame.

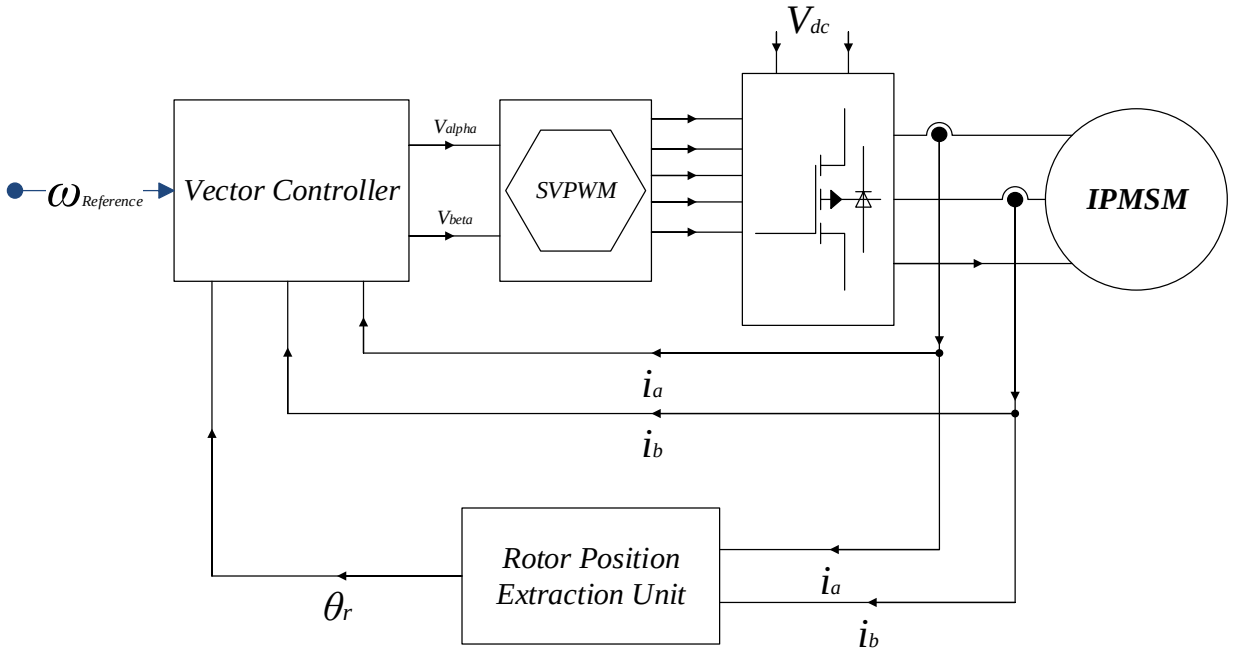

Figure 3. 1: *Block Diagram of Sensorless drive of IPMSM using SVPWM.*

In equation (3.2), the back EMF term, e_f is defined.

$$\vec{V}_{dq} = \frac{\vec{di}_{dq}}{dt} + R_{dq}\vec{i}_{dq} + \vec{e}_f \qquad 3.1$$

$$\vec{e}_f = j.\omega_r.\vec{\lambda}_{fdq} \qquad 3.2$$

In (3.1) and (3.2), the inductance, L_{dq}, the resistance, R_{dq}, and the magnetic flux generated from the permanent magnet in the rotor, λ_{fdq}, are all approximately known quantities. The current, i_{dq} and voltage, v_{dq}, can be measured; hence the motor equation can be solved for the electrical rotor speed, ω_r. Finally an integration of the speed dependent back EMF term, results in an achieved rotor position.

The limitations of the back EMF methods are the fact that the detection possibility is proportional to the speed; the ability diminishes at low rotor speed and stand still. The explanation to this is that the amplitude of the back EMF will be small since e_f, as can be seen in equation (3.2), is proportional to ω_r. Hence, the terms with the inductance and resistance in equation (3.1) will

become dominant compared to the back EMF, meaning, the motor equation element containing the information regarding the position gets too small to detect.

3.2.1.2 Magnetic Anisotropy Method

A new method to determine position during low-speed and in standstill is the Magnetic Anisotropy Method (MAM). Instead of using saliency in the rotor to determine the position, anisotropies effects in the permanent magnets are used. The physical properties are different in different directions depending on the direction of the measurement. The frequency of the applied carrier voltage is set to 100-500 kHz instead of 0.5-3 kHz that is more common in other signal injection methods; hence an additional signal generator has to be utilized. In industrial applications this has to be a chip, with the ability to generate such a high signal.

High frequency voltages are applied in one phase and the response is measured in all 3 phases. This type of measurement is performed for all three phases and from this information the rotor position can be extracted. Unfortunately this method is undeveloped, e.g. the temperature dependence of the anisotropic properties has not been examined and satisfactory results have not been obtained in practical experiments. This means that the research in the area is concentrated in trying to explain the phenomena physically. The great advantage with this method would be that it has the theoretical possibility to work for salient as well as non-salient motors, where the permanent magnets do not saturate the stator teeth [16].

3.2.1.3 Signal Injection

The basic idea behind the signal injection methods [15], [11] is to add a high frequency signal in order to obtain the rotor position. The high frequency, typically 0.5 to 3 kHz, means that the resistance in the motor can be neglected and the current will depend on the inductance only. The applied signal can either be added with superposition on top of the fundamental voltage, or by modifying the fundamental PWM pattern to contain a voltage pulse that can be used to track the rotor position.

By injecting signals to an AC machine, the magnetic saliency according to the rotor position and/or the rotor flux linkage can be detected. And the detected saliency can be used to identify the rotor position. To enhance the control bandwidth, the injected signal should be high enough, but low

enough to be manipulated through PWM inverter and its associated controller. The magnetic saliency according to the rotor position is inherently available in the case of a salient rotor AC machine such as IPMSM.

Consider the voltage equations given in section 2.2

$$V_q = R_s i_q + \omega_r (L_d i_d + \lambda_f) + \rho L_q i_q \quad 3.3$$

$$V_d = R_s i_d - \omega_r L_q i_q + \rho (L_d i_d + \lambda_f) \quad 3.4$$

If the high-frequency signal injection for sensorless control is done at a low-speed region, the voltages in above equations due to the rotation of the machine can be neglected. And if the high-frequency signal is sinusoidal and the equivalent circuit of an AC machine is in the steady state in the viewpoint of the injected signal, the impedances at the high frequency on the *d* and *q* axis of the rotor reference frame can be approximated as:

$$Z_{qh} \approx \frac{V_{qh}}{i_{qh}} = R_s + \omega_h L_{qh} \quad 3.5$$

$$Z_{dh} \approx \frac{V_{dh}}{i_{dh}} = R_s + \omega_h L_{dh} \quad 3.6$$

Where, $L_{dh} = L_d|_{\omega=\omega h}$ at the *d*-axis, $L_{qh} = L_q|_{\omega=\omega h}$ at the *q*-axis and ω_h is the angular frequency of the injected signal (where L_{dh} and L_{qh} represent *d* and *q*-axes inductances at the injected high frequency).

Since the air gap at the *d* axis is larger than that at *q* axis from rotor structure, as shown in Figure-2.1, the inductance at the *d* axis is smaller than that at any other axis. At zero or low speed, the high-frequency impedance is dominated by the inductance. Therefore, the high-frequency impedance measured in the stationary reference frame can be expressed as equation (3.7). It can be easily derived from equations (3.5) and (3.6)

$$Z_h(\theta) = Z_{ha} - \frac{1}{2} Z_{hp} \cos 2(\theta_r - \theta) \quad 3.7$$

Where, Z_{ha} stands for the average value of the *d–q* impedance; that is, $Z_{ha} = \frac{Z_{dh}+Z_{qh}}{2}$, Z_{hp} stands for the difference of the impedance, $Z_{hp} = Z_{qh} - Z_{dh}$, and θ is the angle where minimum high-frequency impedance occurs.

In Figure 3.2, the impedance at the injected high-frequency signal according to the rotor position of a six-pole, 11-kW IPMSM is shown. As the frequency increases, the impedance difference increases. The average impedance, Z_{ha}, decreases as the magnitude of the fundamental frequency component of the stator current of an IPMSM increases, while the difference, Z_{hp}, increases as the current at the d axis increases. This comes from the saturation of the magnetic circuit of the IPMSM. At the rotor reference frame, the magnitude of the high-frequency impedance is minimum at the *d* or *–d* axes.

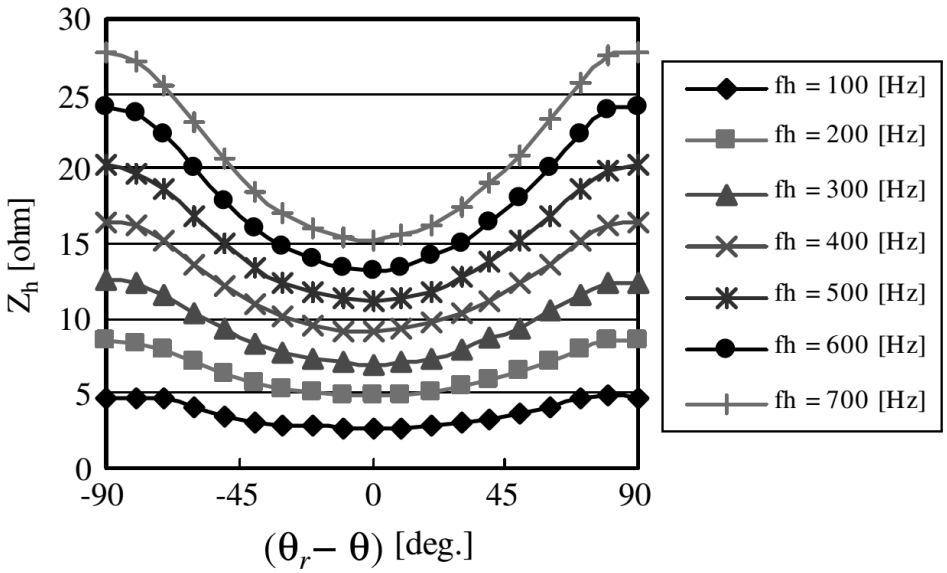

Figure 3. 2: *High-frequency impedance of a six-pole, 11-kW IPMSM at various injection frequencies (fh=ωh/2π) according to the injected angle oriented to the rotor angle with no load.*

Figure courtesy [11].

3.3 VECTOR CONTROL

Vector control [10], [17-18], also called field-oriented control (FOC), is a variable-frequency drive (VFD) control method where the stator currents of a three-phase AC electric motor are identified as two orthogonal components that can be visualized with a vector. One component defines the

magnetic flux of the motor, the other the torque. The control system of the drive calculates from the flux and torque references given by the drive's speed control the corresponding current component references. Typically proportional-integral (PI) controllers are used to keep the measured current components at their reference values. The SVM of the variable-frequency drive defines the transistor switching according to the stator voltage references that are the output of the PI current controllers.

Vector control accordingly provides a reference to generate a three-phase PWM motor voltage output derived from a complex voltage vector to control a complex current vector derived from motor's three-phase motor stator current input through projections or rotations back and forth between the three-phase speed and time dependent system and these vectors' rotating reference-frame two-coordinate time invariant system.

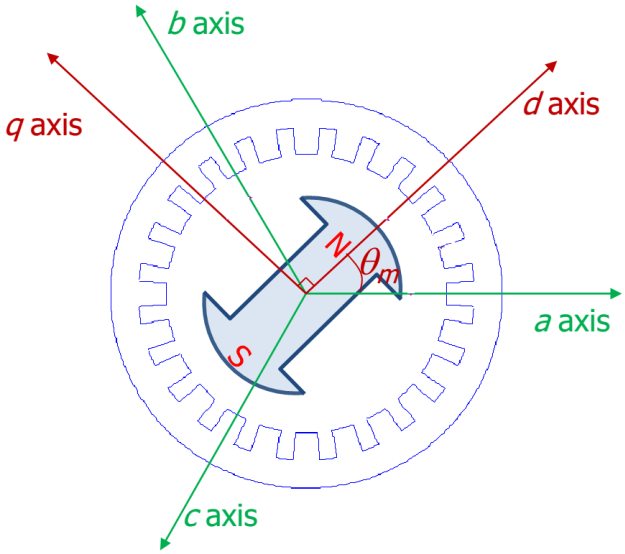

Figure 3. 3: *d-q Coordinate System Superimposed on Three-Phase Salient pole SM.*

Such complex stator motor current space vector can be defined in a *d-q* coordinate system with orthogonal components along *d* and *q* axes such that field flux linkage component of current is aligned along the *d* axis and torque component of current is aligned along the *q* axis. The SM's *d-q* coordinate system can be superimposed to the motor's instantaneous three-phase (*abc)* sinusoidal

system, as shown in Figure 3.3. Components of the *d-q* system current vector, allow conventional control such as PI control.

The torque of the IPMSM [11] can be represented as:

$$T_e = \frac{3}{2}\left(\frac{P}{2}\right)\left\{(L_d - L_q) i_d i_q - \lambda_f i_q\right\} \qquad 3.8$$

At rotor reference *d–q* frame derived at *Section-2.2.1*. It is the sum of the reluctance torque and the field torque. And, even if the field flux, λ_f, by the magnet is kept constant, the pair of i_d and i_q is enormous to generate the given torque reference, T_e^*. However, if the total losses are minimized at the given torque, the pair is uniquely decided. If the iron loss can be neglected, the minimization of the magnitude of the stator current vector, i_d, is the minimization of the copper loss, which is the only loss now considered. Such an operation is called a maximum torque per ampere (MTPA) operation, which gives the best efficiency while generating the given reference torque. Usually, the iron loss is relatively quite small compared to the copper loss at the rated operating conditions of IPMSM. In this context, the instantaneous speed control with MTPA operation involves:

a) Finding value of i_q^* (i_q reference) and setting i_d^* (i_d reference) zero, and
b) Regulating *d–q* voltages according to the current reference pair found.

All of these controls should be done instantaneously. If the parameters of IPMSM are constant regardless of the operating condition, the pair can be derived analytically at a particular speed.

A controller containing the components, as shown in Figure 3.4, carries out the above control mechanism. PI control loop for *d*-current is used to provide the control input voltage v_d. The rotor speed loop controller calculates the demand for *q*-current, which in turn provides the voltage component in *q*-axis v_q. The type of controller used for *q*-axis current is control system with cascaded PI controllers.

The voltage decoupling function takes the speed (ω_r) and the currents i_d and i_q, and computes the values for v_d and v_q by the relation given by equations (2.19) and (2.20) (in section-2.2.2).

vector (field oriented) controller for MTPA operation

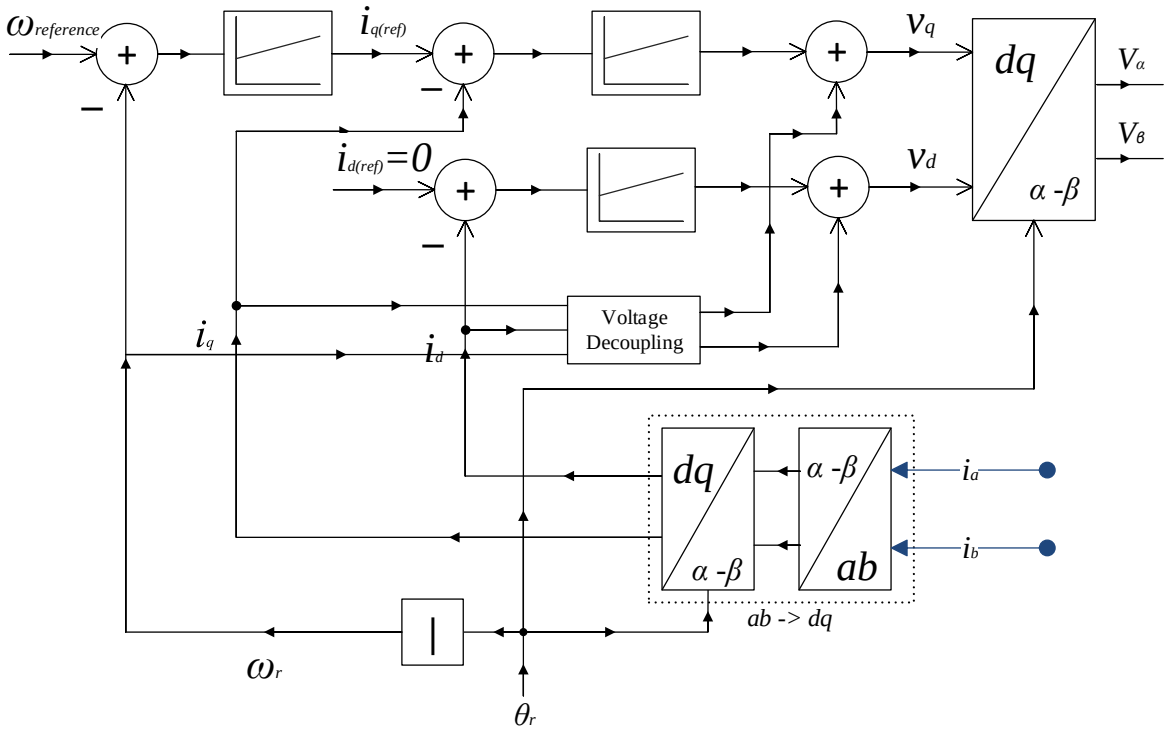

Figure 3. 4: *Field oriented control for IPMSM.*

3.4 SPACE VECTOR MODULATION TECHNIQUE

The Pulse Width Modulation (PWM) technique is applied in the inverter (DC/AC converter) to output an AC waveform with variable voltage and variable frequency for use in mostly variable speed motor drives. The input to the inverter is DC, obtained from either a controlled or uncontrolled rectifier. Hence, an inverter is a two-stage power converter that transforms first the grid AC to DC and then DC to AC. The PWM is the basic energy processing technique used in Power Electronic converters initially implemented with the analog technology using discrete electronic components. In the SVPWM technique, the duty cycles are computed rather than derived through comparison as in SPWM.

3.4.1 Principle of Space Vector PWM

The concept of the SVPWM [5-7] relies on the representation of the inverter output as space vectors or space phasors. Space vector representation of the output voltages of the inverter is realized for the implementation of SVPWM. Space vector simultaneously represents three-phase quantities as one rotating vector; hence each phase is not considered separately. The three phases are assumed as only one quantity. The space vector representation is valid for both transient and steady state conditions in contrast to phasor representation, which is valid only for steady state conditions. The concept of the space vector arises from the rotating air-gap MMF in a three-phase induction machine. By supplying balanced three-phase voltages to the three-phase balanced winding of a three-phase induction machine, rotating MMF is produced, which rotates at the same speed as that of individual voltages, with an amplitude of 1.5 times the individual voltage amplitude.

The space vector is defined as:

$$f_s = \frac{2}{3}\left[f_a + e^{j2\frac{\pi}{3}} f_b + e^{j4\frac{\pi}{3}} f_c \right] \qquad 3.9$$

Where f_a, f_b, and f_c are the three-phase quantities of voltages, currents, and fluxes. In the inverter PWM, the voltage space vectors are considered. The space vector at any given time maintains its magnitude. As time increases, the angle of the space vector increases, causing the vector to rotate with a frequency equal to that of the sinusoidal waveforms. When the output voltages of a three-phase six-step inverter are converted to a space vector and plotted on the complex plane, the corresponding space vector takes only on one of six discrete angles as time increases. The central idea of SVWPM is to generate appropriate PWM signals so that a vector with any desired angle can be generated.

Since the inverter can attain either +0.5V_{dc} or -0.5V_{dc} (if the DC bus has mid-point), or V_{dc} or 0, i.e. only two states, the total possible outputs are 2^3 = 8 (000, 001, 010, 011, 100, 101, 110,111). Here 0 indicates the upper switch is ‘OFF’ and 1 represents the upper switch is ‘ON.’ Thus, there are six active switching states (power flows from the input/DC link side of the inverter to the output/load side of the inverter) and two zero switching states (no power transfer from input/DC link to the load/load side). The operations of the lower switches are complimentary.

The power circuit topology of a three-phase voltage source inverter [19-20] is shown in Figure 3.5. Each power switch is a transistor or IGBT with anti-parallel diodes. The pole or leg voltages are denoted by a capital suffix letter like V_A, V_B, V_C and can attain the value +0.5 V_{dc} when the upper switch is operating and -0.5 V_{dc} when the lower switch is operating. The phase voltage applied to the load is denoted by the letters v_{an}, v_{bn}, v_{cn}. The operation of the upper and the lower switches are complimentary (a small dead band is provided in real time implementation).

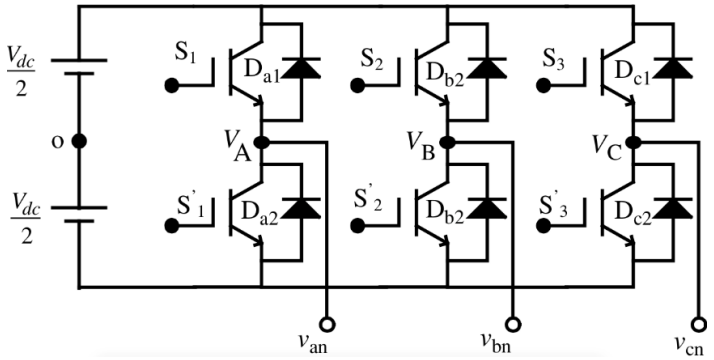

Figure 3. 5: *Power circuit topology of a three-phase voltage source inverter.*

The relationship between the leg voltage and switching signals are:

$$v_k = s_k v_{dc}; \quad k \in A,B,C \qquad 3.10$$

Where S_k = 1when the upper power switch is 'ON' and S_k = 0 when the lower switch is 'ON.' If the load is assumed to be a star connected three-phase, then the relation between the phase-to-neutral load voltage and the leg voltages can be written as:

$$\begin{aligned} V_A(t) &= v_a(t) + v_{nN}(t) \\ V_B(t) &= v_b(t) + v_{nN}(t) \\ V_C(t) &= v_c(t) + v_{nN}(t) \end{aligned} \qquad 3.11$$

Where v_{nN} is the voltage difference between the star point *n* of the load and the negative rail of the DC bus *N*, called the 'Common Mode Voltage'. This common mode voltage or neutral voltage is responsible for leakage bearing currents and their subsequent failure.

By adding each term of equation (3.11), and setting the sum of phase-to-neutral voltage to zero,

assuming a balanced three-phase voltage whose instantaneous sum is always zero, the following is obtained:

$$v_{nN}(t)=\frac{1}{3}\left[V_A(t)+V_B(t)+V_C(t)\right] \qquad 3.12$$

Substituting equation (3.12) back into equation (3.11), the following expressions for the phase-to-neutral voltage are obtained:

$$\begin{aligned} v_a(t)&=\frac{2}{3}V_A(t)-\frac{1}{3}\left[V_B(t)+V_C(t)\right] \\ v_b(t)&=\frac{2}{3}V_B(t)-\frac{1}{3}\left[V_A(t)+V_C(t)\right] \\ v_c(t)&=\frac{2}{3}V_C(t)-\frac{1}{3}\left[V_B(t)+V_A(t)\right] \end{aligned} \qquad 3.13$$

Equation (3.13) can also be written using the switching function definition of equation (3.10):

$$\begin{aligned} v_a(t)&=\left(\frac{v_{dc}}{3}\right)\left[2S_A-S_B-S_C\right] \\ v_b(t)&=\left(\frac{v_{dc}}{3}\right)\left[2S_B-S_A-S_C\right] \\ v_c(t)&=\left(\frac{v_{dc}}{3}\right)\left[2S_C-S_B-S_A\right] \end{aligned} \qquad 3.14$$

Orthogonal coordinates are used to represent the three-phase two-level inverter in the phase diagram. There are eight possible inverter states that can generate eight space vectors. These are given by the complex vector expressions:

$$\vec{V}_k(t)=\begin{cases}\frac{2}{3}V_{dc}e^{j(k-1)\frac{\pi}{3}} & if\ k=1,2,3,4,5,6 \\ 0 & if\ k=0,7.\end{cases} \qquad 3.15$$

The entire space is divided into six equal-size sectors of 60º. Two active vectors bound each sector. $\vec{V}_0$ and $\vec{V}_7$ (7 and 8) are two voltage vectors with zero amplitude located at the origin of the hexagon. The eight active and non-active state vectors are geometrically drawn in Figure 3.6 (a).

By using equations (3.9) and (3.15) the possible space vectors are computed and listed in Table 3.1. According to the Equations (3.11) to (3.15), the eight switching vectors, output line-to-neutral voltage (phase voltages), and output line-to-line voltages in terms of DC link V_{dc} are also given in Table 3.1.

Voltage Vectors	**Space Vector NO.**	**Switching States**	**Phase to Neutral Voltages**			**Line-to-Line Voltages**			**Phase-to-neutral Voltage Space Vectors**
		abc	V_{an}	V_{bn}	V_{cn}	V_{ab}	V_{bc}	V_{ca}	
V_0	7	000	0	0	0	0	0	0	0
V_5	5	001	$-\frac{V_{dc}}{3}$	$-\frac{V_{dc}}{3}$	$\frac{2V_{dc}}{3}$	0	-V_{dc}	V_{dc}	$\frac{2}{3}V_{dc}e^{j\frac{4\pi}{3}}$
V_3	3	010	$-\frac{V_{dc}}{3}$	$\frac{2V_{dc}}{3}$	$-\frac{V_{dc}}{3}$	- V_{dc}	V_{dc}	0	$\frac{2}{3}V_{dc}e^{j\frac{2\pi}{3}}$
V_4	4	011	$-\frac{2V_{dc}}{3}$	$\frac{V_{dc}}{3}$	$\frac{V_{dc}}{3}$	- V_{dc}	0	V_{dc}	$\frac{2}{3}V_{dc}e^{j\pi}$
V_1	1	100	$\frac{2V_{dc}}{3}$	$-\frac{V_{dc}}{3}$	$-\frac{V_{dc}}{3}$	V_{dc}	0	- V_{dc}	$\frac{2}{3}V_{dc}e^{j0}$
V_6	6	101	$\frac{V_{dc}}{3}$	$-\frac{2V_{dc}}{3}$	$\frac{V_{dc}}{3}$	V_{dc}	- V_{dc}	0	$\frac{2}{3}V_{dc}e^{j\frac{5\pi}{3}}$
V_2	2	110	$\frac{V_{dc}}{3}$	$\frac{V_{dc}}{3}$	$-\frac{2V_{dc}}{3}$	0	V_{dc}	- V_{dc}	$\frac{2}{3}V_{dc}e^{j\frac{\pi}{3}}$
V_7	8	111	0	0	0	0	0	0	0

Table 3. 1: *Vectors, Switching Vectors, Phase Voltages, and Line-to-Line Voltages as a Function of the DC Bus Voltage Vdc and Phase-to-neutral Space vector for a three-phase voltage source inverter.*

The reference voltage vector, V_s^*, rotates in space at an angular velocity $\omega = 2\pi f$, where f is the fundamental frequency of the inverter output voltage. When the reference voltage vector passes through each sector, different sets of switches as in Table 3.1 will be turned ON or OFF. As a result, when the reference voltage vector rotates through one revolution in space, the inverter output varies one electrical cycle over time. The inverter's output frequency coincides with the rotating speed of the reference voltage vector. The zero vectors $\vec{V}_0$ and $\vec{V}_7$ (7 and 8), and active vectors $\vec{V}_1$ to $\vec{V}_6$ do not move in space. They are referred to as stationary vectors. Figure 3.6(a) shows the reference vector V_s^* in the sixth sector.

The six active voltage space vectors are shown on the same graph with an equal magnitude of $2V_{dc}/3$ and a phase displacement of 60^o. The tips of the space vectors, when joined together, form a hexagon. The inverter cannot produce a desired reference voltage vector directly. It is possible to decompose the reference vector into vectors that lie on two adjacent active vectors and two zero vectors, which are located at the center of the hexagon.

Depending on the value of $|v_s^*|$, [21-22] SVPWM can has different characteristics. When the reference voltage vector is $|v_s^*| = (1/\sqrt{3})\ V_{dc}$ the maximum sinusoidal output is obtained and the trajectory is a circle inscribed inside the hexagon, called the linear modulation range. If the references increase more than this value, then the output cannot be realized by using the linear modulation technique and this is called the over-modulation region. Since the time of application of the zero space vector becomes negative, it does not make any physical sense. When the reference voltage vector is more than this limiting value of $|v_s^*| = 1/\sqrt{3}\ V_{dc}$, the inverter moves into the over-modulation region for $(1/\sqrt{3}\ )\ V_{dc} < |v_s^*| < (2/\pi)\ V_{dc}$. When the reference voltage vector is $|v_s^*| = (2/\pi)\ V_{dc}$, the inverter operates in the square wave mode or six-step mode, as shown in Figure 3.6(b).

The over-modulation region is further divided into two sub-modes, the over-modulation region-I ($0.5773 < |v_s^*| < 0.6061$) and the over-modulation region-II ($0.6061 < |v_s^*| < 0.6366$). In over-modulation region-I, the reference voltage space vector is modified in such a way that it becomes a 'distorted continuous reference voltage space vector.' The magnitude of the reference voltage vector is altered but the angle is not modified. However, in the over-modulation region-II, both the reference voltage space vector magnitude and the angles are modified in such a way that it becomes a 'distorted discontinuous reference voltage space vector.'

The reference voltage follows a circular trajectory in a linear modulation range and the output is sinusoidal. The reference trajectory will change in over-modulation and the trajectory will be a hexagon boundary when the inverter is operating in the six-step mode. In implementing the SVPWM, the reference voltage is synthesized by using the nearest two neighboring active vectors and zero vectors. The choice of the active vectors depends upon the sector number in which the reference is located. Hence, it is important to locate the position of the reference voltage. Once the reference vector is located, the vectors to be used for the SVPWM implementation to be identified.

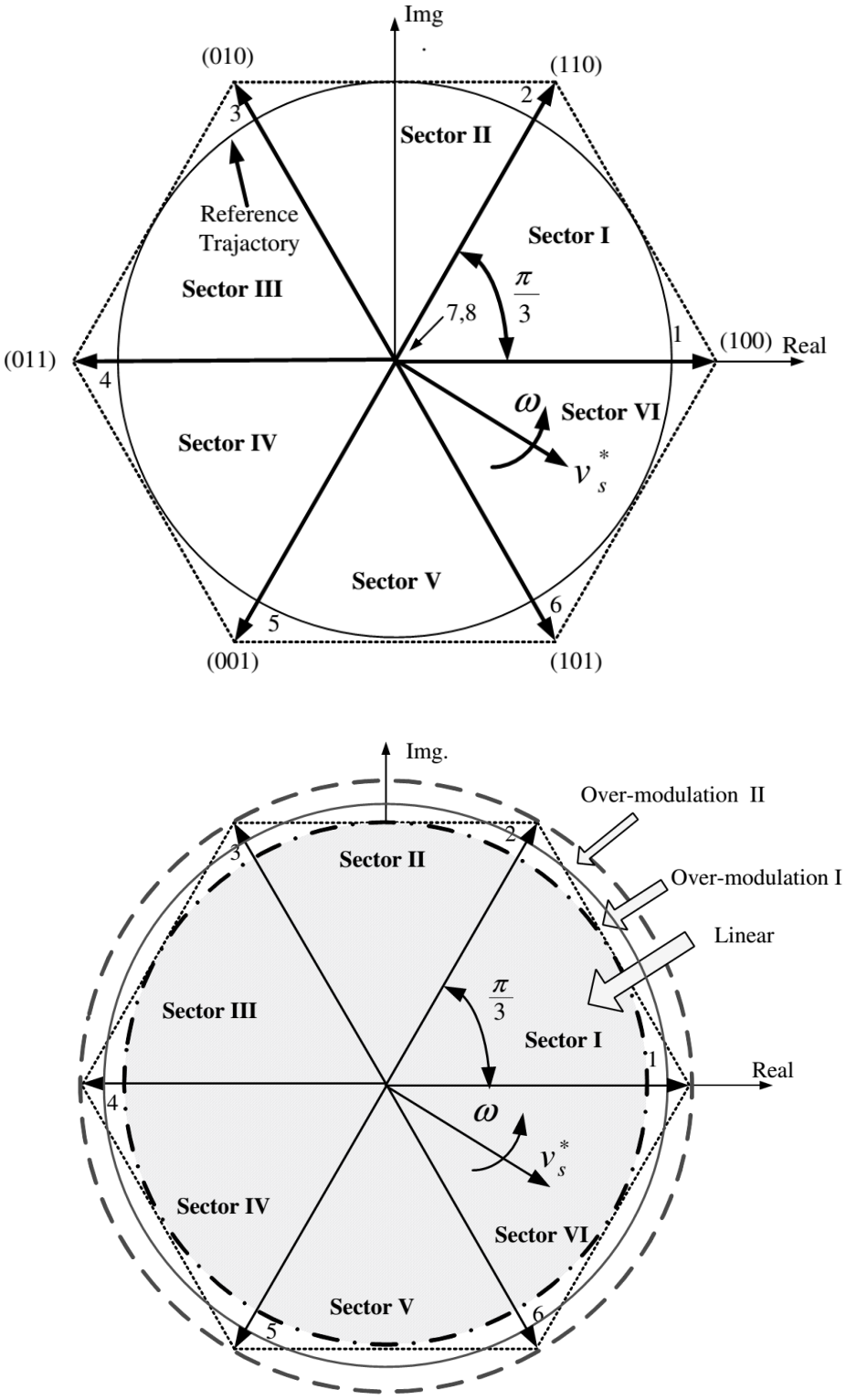

Figure 3. 6: *(A) Voltage space vector locations corresponding to different switching states, (b) Linear and over-modulation range.*

After identifying the vectors to be used, the next task is to find the time of application of each vector, called the 'dwell time'. The output voltage frequency of the inverter is the same as the speed of the reference voltage and the output voltage magnitude is the same as the magnitude of the reference voltage.

The maximum modulation index or the maximum output voltage that is achievable using the SVPWM technique is the radius of the largest circle that can be inscribed within the hexagon as in Figure 3.6(b). This circle is tangential to the midpoints of the lines joining the ends of the active space vector.

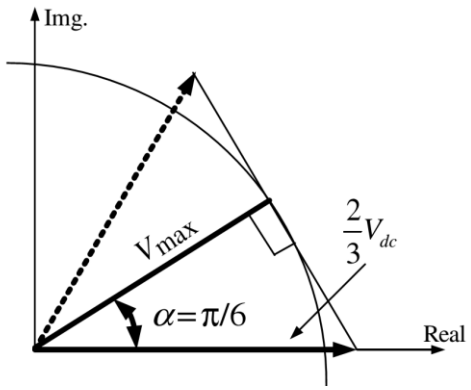

Figure 3. 7: *Determining the maximum possible output using SVPWM.*

Thus, the maximum obtainable fundamental output voltage is calculated from the right-angled triangle (Figure 3.7) as:

$$V_{max} = \left(\frac{2}{3}\right) V_{dc} \cos\left(\frac{\pi}{6}\right) = \frac{1}{\sqrt{3}} V_{dc} \qquad 3.16$$

The maximum possible output voltage using SPWM is 0.5 V_{dc} and hence the increase in the output, when using SVPWM, is $(2V_{dc}/3)/ (05V_{dc}) = 1.154$.

The time of application of the different space vectors are calculated using the '*equal volt-second principle*'. According to this principle, the product of the reference voltage and the sampling/switching time (T_s) must be equal to the product of the applied voltage vectors and their time of applications, assuming that the reference voltage remains fixed during the switching interval. When the reference voltage is in sector I, the reference voltage can be synthesized by

using the vectors V_1, V_2, and V_0 (zero vector), applied for time t_a, t_b, and t_o, respectively. Hence, using the equal volt-second principle, for sector I:

$$V_S^* T_S = V_1 t_a + V_2 t_b + V_0 t_0 \qquad 3.17(a)$$

Where; $$T_S = t_a + t_b + t_0 \qquad 3.17(b)$$

The space vectors are given as:

$$V_S^* = |V_S^*| e^{j\alpha} \qquad V_1 = \frac{2}{3} V_{dc} e^{j0} \qquad V_2 = \frac{2}{3} V_{dc} e^{j\frac{\pi}{3}} \qquad V_0 = 0 \qquad 3.18$$

Substituting equation (3.18) into equation (3.17a) and separating the real (α-axis) and imaginary (β-axis) components:

$$V_S^* \cos(\alpha) T_S = \frac{2}{3} V_{dc} t_a + \frac{2}{3} V_{dc} \cos(\frac{\pi}{3}) t_b \qquad 3.19(a)$$

$$V_S^* \sin(\alpha) T_S = \frac{2}{3} V_{dc} \sin(\frac{\pi}{3}) t_b \qquad 3.19(b)$$

Where; $\alpha = \pi/3$.

Solving equations (3.19a) and (3.19b) for the time of applications t_a and t_b:

$$\begin{aligned} t_a &= \frac{\sqrt{3}|V_S^*|}{V_{dc}} \sin(\frac{\pi}{3} - \alpha) T_S \\ t_b &= \frac{\sqrt{3}|V_S^*|}{V_{dc}} \sin(\alpha) T_S \\ t_0 &= T_S - t_a - t_b \end{aligned} \qquad 3.20$$

Generalizing the above equation for six sectors gives the following, where k = 1, 2 ...6 is the sector number:

$$\begin{aligned} t_a &= \frac{\sqrt{3}|V_S^*|}{V_{dc}} \sin(k\frac{\pi}{3} - \alpha) T_S \\ t_b &= \frac{\sqrt{3}|V_S^*|}{V_{dc}} \sin(\alpha - (k-1)\frac{\pi}{3}) T_S \\ t_0 &= T_S - t_a - t_b \end{aligned} \qquad 3.21$$

After locating the reference location and calculating the dwell time, the next step in SVPWM implementation is the determination of the switching sequence. The requirement is the minimum number of switchings to reduce switching loss; ideally one power switch should turn 'ON' and turn 'OFF' in one switching period.

In order to obtain a fixed switching frequency and optimum harmonic performance from SVPWM, each leg should change its state only once in each switching period. This is achieved by applying the zero state vectors followed by two adjacent active state vectors in a half switching period. The next half of the switching period is the mirror image of the first half. The total switching period is divided into seven parts, the zero vector (*000*) is applied for 1/4th of the total zero vector time, followed by the application of active vectors for half of their application time and then again zero vector (*111*) is applied for 1/4th of the zero vector time. This is then repeated in the next half of the switching period. This is how symmetrical SVPWM is obtained. The switching patterns showing the leg voltages in one switching period are depicted in Figure 3.8 for sectors I to VI.

Average leg voltages can be determined from the switching patterns of Figure 3.8, for example, for sector I:

$$\begin{aligned} V_{A,avg} &= \frac{(V_{dc}/2)}{T_S}[t_0 + t_a + t_b - t_0] \\ V_{B,avg} &= \frac{(V_{dc}/2)}{T_S}[t_0 - t_a + t_b - t_0] \\ V_{C,avg} &= \frac{(V_{dc}/2)}{T_S}[t_0 - t_a - t_b - t_0] \end{aligned} \qquad 3.22$$

Substituting the equation of time of applications from equation (3.20) into equation (3.22), the following is obtained for sector I and similarly can be derived for other sectors:

$$\begin{aligned} V_{A,avg} &= \frac{\sqrt{3}}{2}|V_s^*| \sin(\alpha + \frac{\pi}{3}) \\ V_{B,avg} &= \frac{3}{2}|V_s^*| \sin(\alpha - \frac{\pi}{6}) \\ V_{C,avg} &= -\frac{\sqrt{3}}{2}|V_s^*| \sin(\alpha + \frac{\pi}{3}) \end{aligned} \qquad 3.23$$

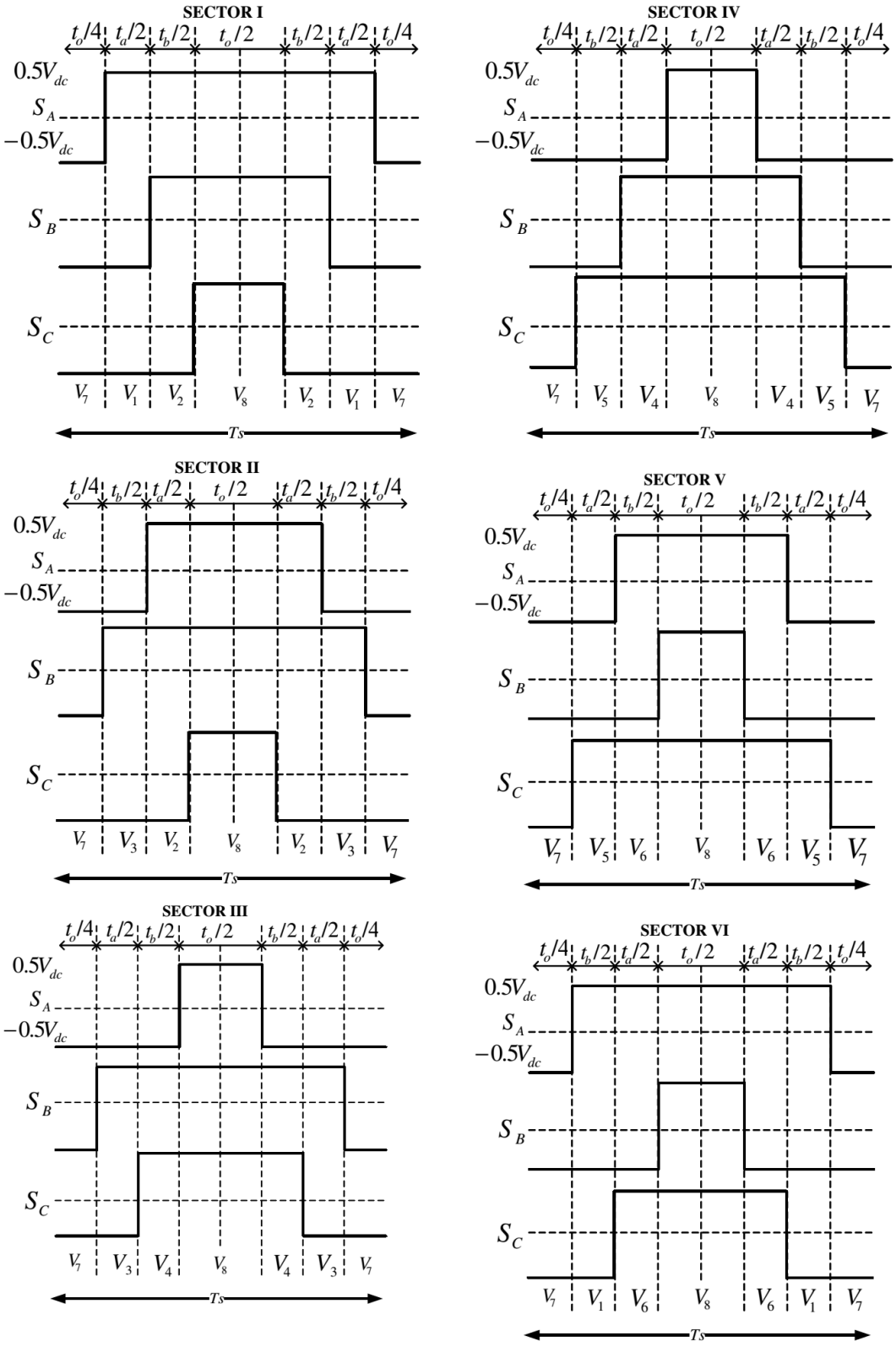

Figure 3. 8: *Switching pattern for SVPWM for sector I to VI.*

3.4.2 Modulation Characteristics and Harmonics of PWM

PWM signals are often compared by the percent of DC bus voltage conversion, number of switchings, algorithm efficiency and of course the harmonic distortion present. The maximum DC bus voltage that can be converted to AC in SPWM is half of the V_{DC}. According to *section-3.4.1*, the SVPWM technique converts 57.7% of the DC bus voltage. Since the rated current capabilities of the semiconductor devices remain the same, using SVM only increases the power conversion by 7.7%. The ease of implementation of SVM in DSPs and code efficiency, and changing the state of only one switch unlike SPWM makes the proposed PWM technique even more efficient both power wise and time wise.

If there is a signal with a fundamental frequency *f* (like a sinusoidal with frequency *f*), harmonics are every other sinusoidal components at frequencies multiples of the fundamental frequency (*2f*, *3f*, *4f* ...). These harmonics are important because they can be seen at the output of a system with some nonlinearity. The power in the harmonics represent how nonlinear the system is. If the system is linear, the output signal will be the linear combination of the input signals having the same frequency as the inputs. Then the signals are referred as linearly dependent.

Harmonics, most of the time, are not required and cause a distortion to the fundamental frequency component of the signal. The harmonic distortion, that is present in a signal, is measured as *Total Harmonic Distortion* (THD), and is sometimes referred as *Distortion Factor*. The *total harmonic distortion*, or THD, of a signal is a measurement of the harmonic distortion present and is defined as the ratio of the sum of the powers of all harmonic components to the power of the fundamental frequency. THD is used to characterize the linearity of audio systems and the power quality of electric power systems.

Total harmonic distortion, or THD, is the summation of all harmonic components of the voltage or current waveform compared against the fundamental component of the voltage or current wave:

$$THD = \frac{\sqrt{(V_2^2 + V_3^2 + V_4^2 + \ldots + V_n^2)}}{V_1} \qquad 3.24$$

The formula above shows the calculation for THD on a voltage signal. The end result is a percentage comparing the harmonic components to the fundamental component of a signal. *The higher the percentage, the more distortion that is present on the mains signal.*

In power systems, lower THD means reduction in peak currents, heating, emissions, and core loss in motors. Harmonics have existed on power systems from the time of the very first generators. However, the harmonic components were so small that their effects on systems were negligible. This was due to the lack of non-linear loads before the 1960s. Now days, the beginning of the era of non-linear loads which now include electronic ballasts, computer power supplies, fax machines, arc furnaces and variable frequency drives (VFDs). Harmonic distortion can have detrimental effects on electrical equipment. Unwanted distortion can increase the current in power systems which results in higher temperatures in neutral conductors and distribution transformers. Higher frequency harmonics cause additional core loss in motors which results in excessive heating of the motor core. These higher order harmonics can also interfere with communication transmission lines since they oscillate at the same frequencies as the transmit frequency. If left unchecked, increased temperatures and interference can greatly shorten the life of electronic equipment and cause damage to power systems and electric drive systems.

There is no national or international standard dictating THD limits on drive or any other systems. But [29] gives acceptable values of harmonic distortions.

CHAPTER 4
DRIVE SYSTEM AND CONTROLLER DESIGN

4.1 INTRODUCTION

The rotor position of IPMSM is to be extracted from the filtered carrier frequency components of stator currents. The filter, in this case, can be any analog filter like Butterworth or Chebyshev if it is to be implemented independently from the DSP microcontroller. If the whole system is to be implemented inside the DSP chip, the filter should be a digital filter. The specification of the filter, then, depends not only on the cut off frequencies, but also on the resolution (bit length of the processor). The rotor position will then be extracted from this component, which implicitly contains the value of the inductance values. In IPMSM, the ratio the *d* and *q* axis inductance values reach up to three on higher carrier frequencies.

The vector control consists of two sets of PI controllers separately for the *d* and *q* axis currents. In case of the *q* axis model, a cascade PI controller is used for the speed and current compensation. The reference value of *q* axis current is obtained from the speed PI controller and the current is, then, compensated by the other PI controller.

4.2 ROTOR POSITION EXTRACTION FROM CARRIER-FREQUENCY SIGNAL

As discussed in *section-3.2.1.3*, the high-frequency impedance measured in the stationary reference frame is expressed as shown in equation (4.1).

$$Z_h(\theta) = Z_{ha} - \frac{1}{2} Z_{hp} \cos 2(\theta_r - \theta) \qquad 4.1$$

Where, Z_{ha} stands for the average value of the *d*–*q* impedance; that is, $Z_{ha} = \frac{Z_{dh}+Z_{qh}}{2}$, Z_{hp} stands for the difference of the impedance, $Z_{hp} = Z_{qh} - Z_{dh}$. For low speed operation, the voltage drop associated with the stator resistance R_s is very small. Since the motor operates at lower voltage conditions. Hence, it is often neglected.

For a sinusoidal distributed stator winding and the rotor *d* axis aligned with phase *a* winding axis, as per *figure 2.2*, $\theta_r = 0$, from the above equation, (if the value of R_s is neglected and using trigonometric identity) we obtain a very attractive rotor position equation:

$$L_S(\theta) = L_{sum} - L_{diff}\cos 2(\theta) \qquad 4.2$$

Where, $L_{sum} = 0.5(L_q + L_d)$ and $L_{diff} = 0.5(L_q - L_d)$

In order to find the exact position of the rotor, we have to define two stationary reference frames against which the inductance variations are obtained, and, hence, the rotor position.

4.2.1 Defining Two Reference Frames for Inductance Measurement

IPMSMs are always modeled as salient-pole synchronous motors. Figure 4.1 [2] shows IPMSM as salient-pole synchronous motor with two stationary reference frames that are 45^o out of phase.

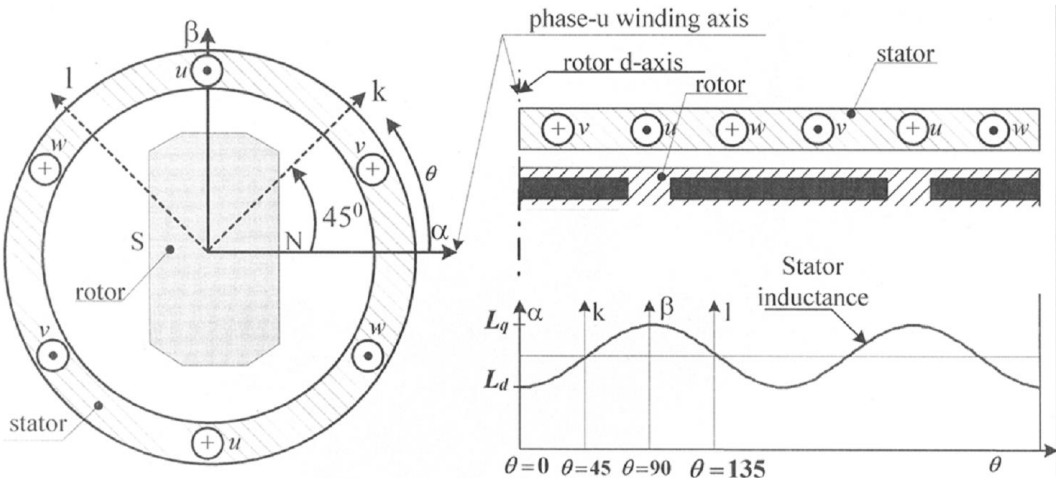

(a) (b)

Figure 4. 1: *IPMSM as a salient-pole synchronous motor (b) Stator winding inductance distribution (phases u-v-w are the same as the phases a-b-c).*

In *figure-4.1*, two stationary reference frames (α - β and k - l) are shown. The use of these two reference frames plays an important role by doubling the rotor-position-dependent part of the stator inductance while by cancelling out the constant part. The real axis of the first reference frame (α-

axis) is aligned with the rotor *d* axis. The other reference frame is 45° in the forward rotation direction from the first reference frame.

Now, assume that the rotor has moved counterclockwise by an angle θ_r (δ as in *figure-4.2*) from the initial position, as shown in *figure-4.2*. The inductance values at the four axes L_α, L_β, L_k and L_l at the α-axis, β-axis, *k*-axis, and *l*-axis, respectively, can be expressed as equations 4.3(a) - 4.3(d) by inspecting *figure 4.2(b)*.

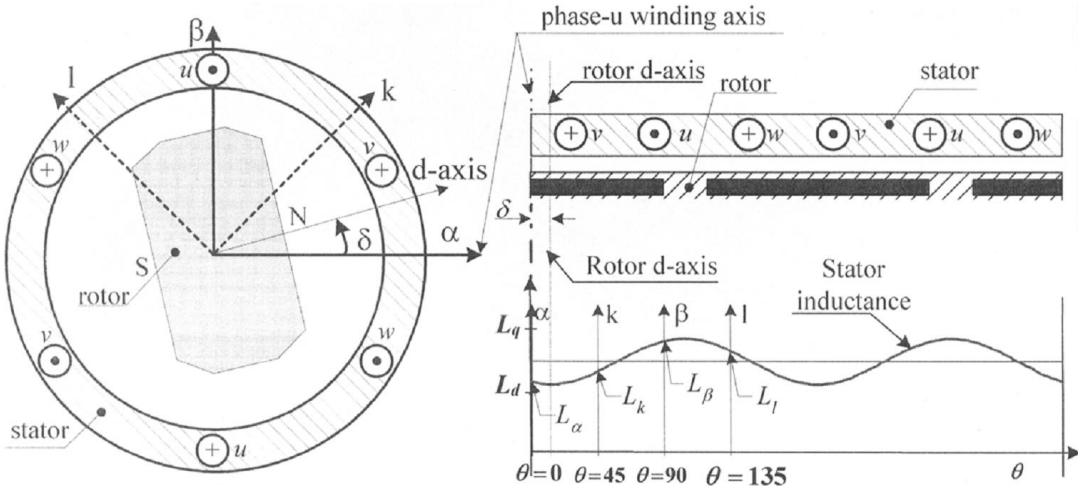

(a) (b)

Figure 4. 2: *Two reference frames α-β and k-l, where α- axis is arbitrarily aligned with phase-u winding axis. (b) Inductance values as the rotor rotates by electrical angle δ (θr) from α- axis. (phases u-v-w are the same as the phases a-b-c).*

$$L_\alpha = L_{sum} - L_{diff}\cos 2(\theta_r) \qquad 4.3(a)$$

$$L_\beta = L_{sum} + L_{diff}\cos 2(\theta_r) \qquad 4.3(b)$$

$$L_k = L_{sum} - L_{diff}\sin 2(\theta_r) \qquad 4.3(c)$$

$$L_l = L_{sum} + L_{diff}\sin 2(\theta_r) \qquad 4.3(d)$$

Where, L_α, L_β, L_k and L_l are the stator inductance at the α-axis, β-axis, *k*-axis, and *l*-axis, respectively.

Subtracting equation *4.3(a)* from *4.3(b)* and *4.3(c)* from *4.3(d)* the constant parts of the inductance values cancel out while the rotor-dependent part doubles are expressed in equations (4.4) and (4.5). From equations (4.4) and (4.5), θ_r can be expressed as in equation (4.6) in terms of the inductance

relative values at the four axes. Note that θ_r is the angle between the rotor *d* axis and α - axis on the stator, and is zero on the axis.

$$L_\beta - L_\alpha = 2L_{diff}\cos 2(\theta_r) \quad 4.4$$

$$L_l - L_k = 2L_{diff}\sin 2(\theta_r) \quad 4.5$$

$$\theta_r = \frac{1}{2}\tan^{-1}\left(\frac{L_l - L_k}{L_\beta - L_\alpha}\right) \quad 4.6$$

4.2.2 Rotor Position Extraction from Carrier-Frequency Signal

In a space vector PWM controlled voltage source inverters (VSI), the required voltage signal's sector and magnitude is identified and the corresponding switching pulses are generated. In this case, the phase shift of the three-phase signal is obtained by the predefined switching sequence. The amplitudes of these voltages are functions of the instantaneous reference voltages and can be expressed as follows [2]:

$$V_{a.cfc} = -\frac{2V_{DC}}{\pi}\cos\left(\frac{\pi v_a}{2V_{DC}}\right)\sin(\omega_c t) \quad 4.7(a)$$

$$V_{b.cfc} = -\frac{2V_{DC}}{\pi}\cos\left(\frac{\pi v_b}{2V_{DC}}\right)\sin\left(\omega_c t - \frac{2\pi}{3}\right) \quad 4.7(b)$$

$$V_{c.cfc} = -\frac{2V_{DC}}{\pi}\cos\left(\frac{\pi v_c}{2V_{DC}}\right)\sin\left(\omega_c t + \frac{2\pi}{3}\right) \quad 4.7(c)$$

Where, V_{DC} is the *DC* link voltage of the inverter, v_a, v_b and v_c are fundamental phase voltages, $V_{a.cfc}$, $V_{b.cfc}$, $V_{b.cfc}$ are carrier frequency component voltages in phases *a*, *b* and *c*, respectively, ω_c is the carrier frequency (which is the frequency of the injected signal) in radians per second.

If the motor speed is low, the back EMF is also low and the terminal voltage (reference voltages v_a, v_b and v_c) can be approximated to be zero. Under such approximation, the carrier-frequency component voltage amplitudes in the previous equations can be approximated to be constant and are given by equations 4.8(a) - (b).

$$V_{a.cfc} \approx -\frac{2V_{DC}}{\pi} sin(\omega_c t) \qquad 4.8(a)$$

$$V_{b.cfc} \approx -\frac{2V_{DC}}{\pi} sin\left(\omega_c t - \frac{2\pi}{3}\right) \qquad 4.8(b)$$

$$V_{c.cfc} \approx -\frac{2V_{DC}}{\pi} sin\left(\omega_c t + \frac{2\pi}{3}\right) \qquad 4.8(c)$$

If the three-phase quantities are transformed to orthogonal two-phase quantities, along the stationary α-β axis, the IPMSM voltage model at the carrier (injected) frequency can be described as equation (4.9) [27], where θ_r is the angle between the α axis and the rotor d axis. In this model, the resistive voltage drop has been neglected since it is very small compared to the inductive reactance at the carrier frequency. Voltage due to rotor speed also has been neglected since the rotor speed is very small compared to the carrier frequency. After mathematical manipulation, equation (4.10), can be written from equation (4.9) assuming θ_r to be constant in one carrier-frequency cycle.

$$\begin{bmatrix} V_{cfc\alpha} \\ V_{cfc\beta} \end{bmatrix} = \begin{bmatrix} L_{sum} + L_{diff} cos(2\theta_r) & L_{diff} sin(2\theta_r) \\ L_{diff} sin(2\theta_r) & L_{sum} - L_{diff} cos(2\theta_r) \end{bmatrix} \frac{d}{dt} \begin{bmatrix} i_{cfc\alpha} \\ i_{cfc\beta} \end{bmatrix} \qquad 4.9$$

$$\begin{bmatrix} i_{cfc\alpha} \\ i_{cfc\beta} \end{bmatrix} = \frac{1}{L_{sum}^2 + L_{diff}^2} \begin{bmatrix} L_{sum} - L_{diff} cos(2\theta_r) & -L_{diff} sin(2\theta_r) \\ -L_{diff} sin(2\theta_r) & L_{sum} + L_{diff} cos(2\theta_r) \end{bmatrix} \begin{bmatrix} \int V_{cfc\alpha} dt \\ \int V_{cfc\beta} dt \end{bmatrix} \qquad 4.10$$

Where, $i_{cfc\alpha}$ and $i_{cfc\beta}$ are α- axis *and* β-axis currents. These are α-β axis transformed currents of the stator currents i_a, i_b and i_c.

If the saliency, $L_q/L_d < 3$, and $\int v_{cfci} dt$ and $\int v_{cfcj} dt$ are sinusoidal and orthogonal (this is an approximation with the reference voltage being very small compared to the *DC*-link voltage), equations 4.11 (a) and (b) can be obtained from equation (4.10) and is given as:

$$\int_0^{T_c} \left| i_{cfc\alpha} \right| dt - \int_0^{T_c} \left| i_{cfc\beta} \right| dt = kL_{diff} \, cos(2\theta_r) \qquad 4.11(a)$$

$$\int_0^{Tc} \left| i_{cfck} \right| dt - \int_0^{Tc} \left| i_{cfcl} \right| dt = kL_{diff} \, cos(2\theta_r) \qquad 4.11(b)$$

Where,

$$k \propto \int_0^{T_{cf}} \left[\int V_{cfcx}\, dt\right] dt \Big/ \left(L_{sum}^2 - L_{diff}^2\right), \qquad x = \alpha, \beta, k, l$$

Equation (4.11) is the same as equations (4.4) and (4.5). Their relations can be described as follows:

$$L_\beta - L_\alpha \propto \left(\int_0^{T_c} \left| i_{cfc\beta} \right| dt - \int_0^{T_c} \left| i_{cfc\alpha} \right| dt \right) \qquad 4.12(a)$$

$$L_l - L_k \propto \left(\int_0^{Tc} \left| i_{cfcl} \right| dt - \int_0^{Tc} \left| i_{cfck} \right| dt \right) \qquad 4.12(b)$$

Using the same approach that is used to reach to equation (4.6), the rotor position can be obtained from the carrier frequency current component as:

$$\theta_r = \frac{1}{2} \arctan \left(\frac{\int_0^{Tc} \left| i_{cfcl} \right| dt - \int_0^{Tc} \left| i_{cfck} \right| dt}{\int_0^{Tc} \left| i_{cfc\beta} \right| dt - \int_0^{Tc} \left| i_{cfc\alpha} \right| dt} \right) \qquad 4.13$$

The above equation shows the extraction of the rotor position from the carrier (injected) frequency component of the stator currents. And also, as it can be seen, no motor parameter is used. Hence, there is no need to know the motor parameters.

The integration of the carrier-frequency component current can be replaced by a moving average of the absolute value of the carrier-frequency component current with a little more than two samples in one carrier-frequency cycle. This eliminates the need for the integration constant. For the purpose of simulation, discrete integral with any arbitrary integration-constant can be used. This constant will cancel out in equation (4.13) and will have no effect on final value.

The following block diagram shows the basic components that are used is determining the rotor's position from the carrier-frequency component current. This is how the rotor position extraction from carrier-frequency component current is carried out.

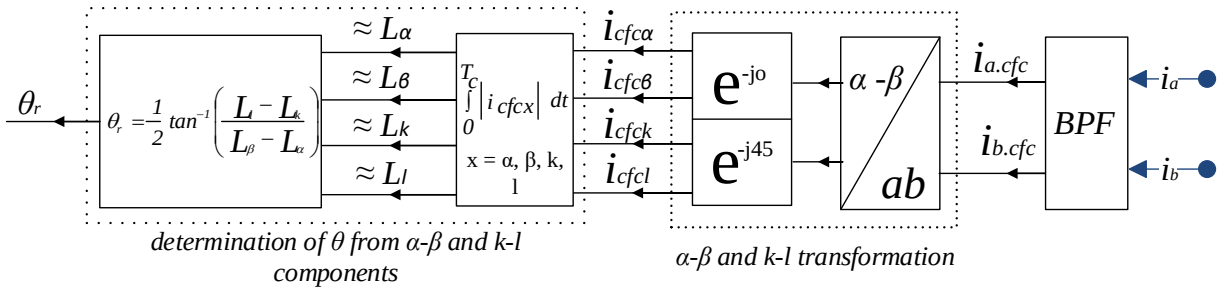

Figure 4. 3: *Rotor Position Extraction from Carrier-Frequency Component of Stator Current.*

Using the above rotor position extraction, and figures 3.1 and 3.4, the overall control system takes the shape shown below. The control of the drive system is thoroughly implemented so that system stability and robust operation is obtained.

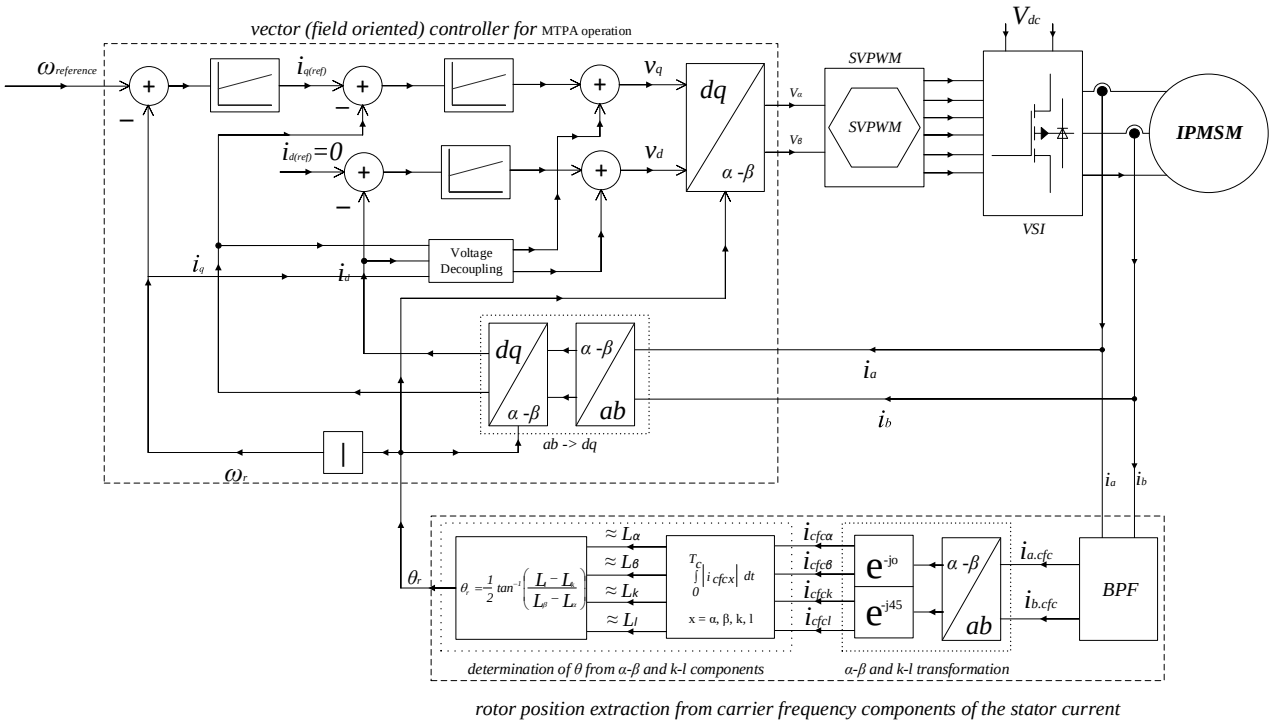

Figure 4. 4: *Vector Control of IPMSM Drive System Using Sensorless Rotor Position Determination from the Carrier Frequency Component of Stator Currents.*

4.3 VECTOR CONTROLLER DESIGN

Proper calculation of PI controller parameters ensures correct operation of vector controller and high precision of the drive. Inputs to the control algorithms for calculation of proportional gain (P component) and integral time constant (I component) are motor parameters together with settling times of current, speed and position control loops, which can be chosen by design. Settling time of each control loop can be changed to achieve the best results of the motion control (speed or position control). Compensation of external load torque acting on the shaft of the motor is included.

As shown in *section-3.3,* PI controllers are used for current compensation and speed control. The independent design approach is used here and is presented as follows.

4.3.1 Current PI Controller Design

For the design of PI-controllers it is necessary to know the closed loop transfer function. To describe appropriate model of IPMSM, *d-q* coordinate system fixed to machine rotor is used. Model is divided into two orthogonal axis enabling independent control of flux and torque component.

To find the closed loop transfer function, block diagrams of permanent magnet synchronous motor (PMSM) in *d* and *q*-axis must be obtained first.

a) Transfer function and block diagram of IPMSM in d axis

Consider equation (2.20) presented in *section 2.2.2,*

$$V_d = R_s i_d - \omega_r L_q i_q + \rho(L_d i_d + \lambda_f) \qquad 4.14$$

Taking the Laplace transform of the above equation gives:

$$V_d(s) = R_s i_d(s) - \omega_r L_q i_q(s) + S L_d i_d(s) \qquad 4.15$$

Since the aim is to control the *d* axis current by varying the *d* axis voltage, the previous equation can be rearranged and represented by the block diagram shown in *figure-4.5*.

If Mason´s formula (*Appendix-I*) is used the transfer function between flux component, i_d and input voltage, V_d, in *d* axis is:

$$\frac{i_d(s)}{V_d(s)} = \frac{\frac{1}{L_d}\frac{1}{S}}{1+\frac{R_s}{L_d}\frac{1}{S}} = \frac{\frac{1}{L_d S}}{\frac{L_d S+R_s}{L_d S}} = \frac{1}{L_d S+R_s} = \frac{\frac{1}{R_s}}{\frac{L_d}{R_s}s+1} = \frac{k_{md}}{\tau_{md}s+1} \qquad 4.16$$

Where, $k_{md}=1/R_s$ is *d* axis motor gain and $\tau_{md}=L_d/R_s$ is *d* axis motor time constant.

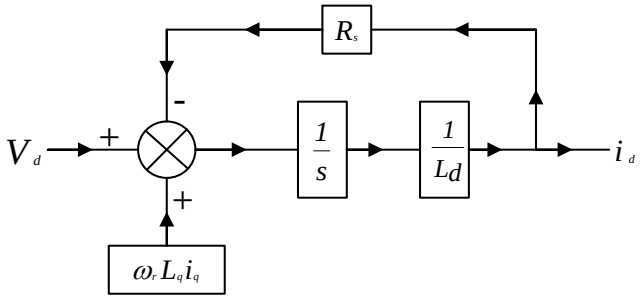

Figure 4. 5: *Block diagram of IPMSM in d axis*

b) Transfer function and block diagram of IPMSM in q axis

Consider equation (2.19)

$$V_q = R_s i_q + \omega_r (L_d i_d + \lambda_f) + \rho L_q i_q \qquad 4.17$$

Taking the Laplace transform of the above equation gives:

$$V_q(s) = R_s i_q(s) + \omega_r (L_d i_d(s) + \lambda_f) + S L_q i_q(s) \qquad 4.18$$

$$V_q(s) = R_s i_q(s) + \omega_r \lambda_d(s) + S L_q i_q(s) \qquad 4.19$$

Where, $\lambda_d(s) = L_d i_d(s) + \lambda_f$

Since the aim is to control the *q* axis current by varying the *q* axis voltage, the equation (4.19) can be further rearranged and represented by the block diagram shown in *figure-4.6*.

If Mason´s formula (*Appendix-I*) is used the transfer function between flux component, i_q and input voltage, V_q, in *q* axis is:

$$\frac{i_q(s)}{V_q(s)} = \frac{\frac{1}{L_q}\frac{1}{S}}{1+\frac{R_s}{L_q}\frac{1}{S}} = \frac{\frac{1}{L_q S}}{\frac{L_q S+R_s}{L_q S}} = \frac{1}{L_q S+R_s} = \frac{\frac{1}{R_s}}{\frac{L_q}{R_s}s+1} = \frac{k_{mq}}{\tau_{mq}s+1} \qquad 4.20$$

Where, $k_{mq}=1/R_s$ is q axis motor gain and $\tau_{mq}=L_q/R_s$ is q axis motor time constant.

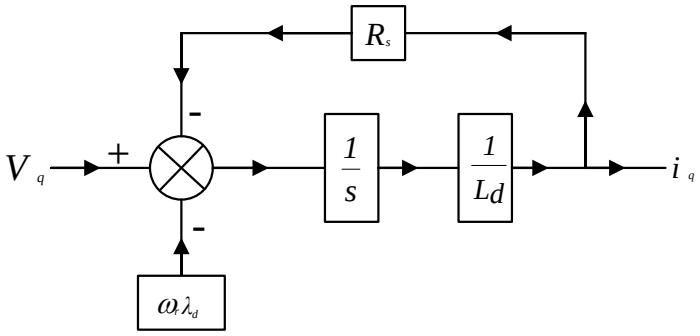

Figure 4. 6: *Block diagram of IPMSM in q axis.*

For the q axis transfer function, since the speed of the motor depends on the q axis current i_q, it is necessary to refer the torque equation of the motor. Therefore, equating equations (2.26) and (2.27), we obtain:

$$T_L + B\omega_m + J\frac{d\omega_m}{dt} = \frac{3}{2}\left(\frac{P}{2}\right)\left(\lambda_d i_q - \lambda_q i_d\right) \qquad 4.21$$

substituting, $\lambda_d(s) = L_d i_d(s) + \lambda_f$ *and* $\lambda_q = i_q L_q$

$$T_L + B\omega_m + J\frac{d\omega_m}{dt} = \frac{3}{2}\left(\frac{P}{2}\right)\left(\left(L_d i_d + \lambda_f\right)i_q - L_q i_q i_d\right) \qquad 4.22$$

Taking the Laplace transform of the above equation we obtain:

$$T_L + B\omega_m(S) + SJ\omega_m(S) = \frac{3}{2}\left(\frac{P}{2}\right)\left(\left(L_d i_d(S) + \lambda_f\right)i_q(s) - L_q i_q(s) i_d(s)\right) \qquad 4.23$$

After further simplification and rearranging, we obtain the equation:

$$\omega_m = \left[\frac{1}{B+Js}\right]\left\{\frac{3p}{4}\left[\left(L_d - L_q\right)i_d i_q + \lambda_f i_q\right] - T_L\right\} \qquad 4.24$$

The block diagram of equation (4.24) is shown below.

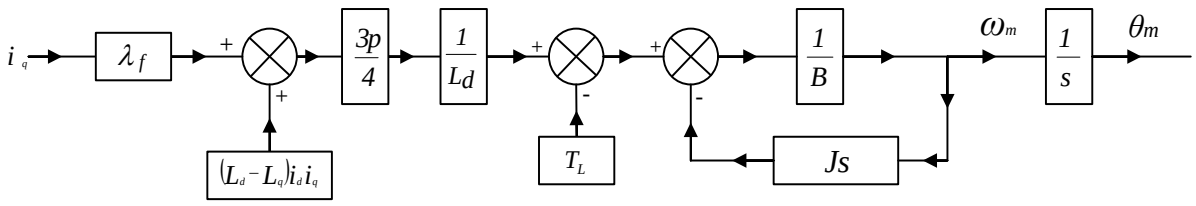

Figure 4. 7: *Block diagram of the relationship between i_q and ω_m.*

The complete q axis model of IPMSM is obtained from *figures 4.6* and *4.7*. And the resulting block diagram is:

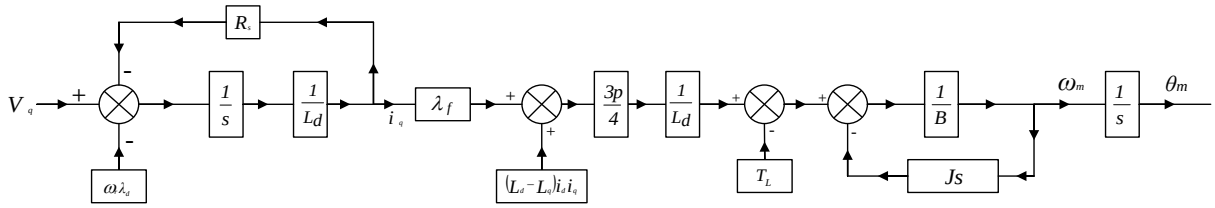

Figure 4. 8: *The complete q axis block diagram of IPMSM.*

Both transfer functions in *d-q* coordinate system have been replaced by the first order transfer functions with gain $K_{mm} = k_{mq} = k_{md}$ and with electrical time constants τ_{md} and τ_{mq}.

For the design of PI controller of magnetic flux control in *d* axis, the following block diagram is used:

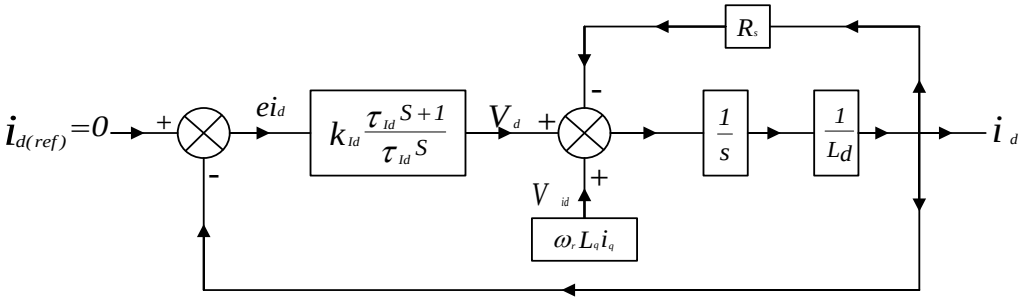

Figure 4. 9: *Current loop of IPMSM in d axis.*

Where, $k_{Id}\frac{\tau_{Id}S+1}{\tau_{Id}S}$ is a *d* axis PI controller with proportional gain of k_{Id}, and an integral time constant of τ_{Id}.

To achieve best results of the motion control and full flux of the machine condition $i_{d(ref)} = 0$ must be secured (*Section 3.3*). If current PI controller in *d* axis secures such condition, then the only magnetic flux created will be flux of permanent magnets. Closed loop transfer function with PI controller can be written in following way (first order transfer function obtained in equation 4.16 is used):

$$\frac{i_d(s)}{i_{d(ref)}(s)} = \frac{k_{Id}\frac{\tau_{Id}S+1}{\tau_{Id}S}\frac{k_{md}}{\tau_{md}s+1}}{1+k_{Id}\frac{\tau_{Id}S+1}{\tau_{Id}S}\frac{k_{md}}{\tau_{md}s+1}} = \frac{1}{\frac{\tau_{Id}}{k_{Id}k_{mm}}s+1} \qquad 4.25$$

For the design of PI controller by *pole placement method*, the demanded transfer function given by equation (4.25) of corresponding order is compared with denominator of closed loop transfer function:

$$(s+\omega_0)^n \qquad 4.26$$

Where *n* is order of the system and ω_0 is minimal natural frequency obtained from Dodd´s formula equation (4.27) [28], which respects prescribed settling time T_s of corresponding loop. Equation (4.27) shows Dodd's formula for 5% settling time criterion.

$$T_S = {}^{3}\!/_{2}(1+n)\frac{1}{\omega_0} \qquad 4.27$$

The comparison of the ideal first order transfer function with denominator of the closed-loop transfer function of current control loop results in values of proportional gain K_{Id} and time integral constant τ_{Id} of PI controller in *d* axis while respecting prescribed settling time:

$$\frac{T_{Sd}}{3}S+1 \;\leftrightarrow\; \frac{\tau_{Id}}{k_{Id}k_{mm}}S+1 \qquad 4.28$$

Where, T_{sd} is settling time of current loop in q axis. Setting $\tau_{Id} = \tau_{md} = L_d/R_s$, the solution for equation (4.28) will be:

$$k_{Id} = \frac{3L_d}{T_{Sd}}, \qquad \tau_{Id} = \tau_{md} = \frac{L_d}{R_S} \qquad 4.29(a,b)$$

In similar way, constants of current PI controller in q axis can be calculated. For the design of PI controller of current loop in q-axis for control of electromagnetic PMSM torque the block diagram shown in figure-4.10 is used. This block diagram is a result of the implementation of PI controller for the block shown in figure-4.6. In the block diagram of figure-4.10, $k_{Iq}\frac{\tau_{Iq}S+1}{\tau_{Iq}S}$ is a q axis PI controller with proportional gain of k_{Iq}, and an integral time constant of τ_{Iq}.

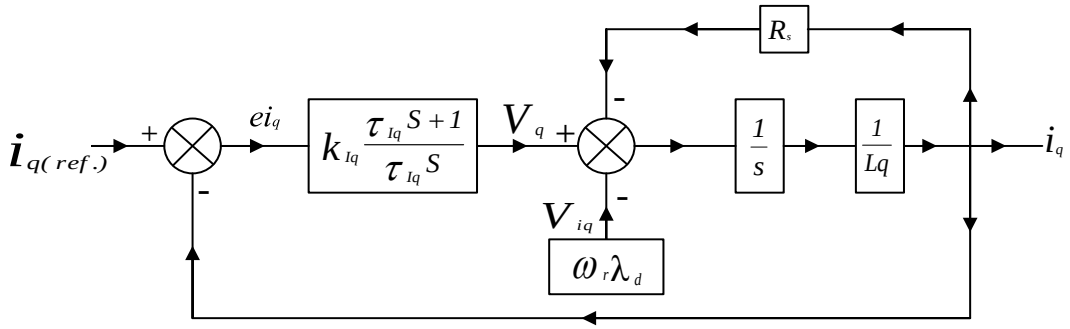

Figure 4. 10: *Current loop of IPMSM in q axis.*

Values of current PI controller parameters in q axis are calculated in a similar way as it was calculated for d axis and the results are:

$$k_{Iq} = \frac{3L_q}{T_{Sq}}, \qquad \tau_{Iq} = \tau_{mq} = \frac{L_q}{R_S} \qquad 4.30(a,b)$$

Where, T_{sq} is settling time of current loop in q axis, K_{iq} is proportional gain and τ_{Id} is time integral constant of PI controller in q axis.

4.3.2 Speed PI Controller Design

For the design of speed PI controller, block diagram shown on figure-4.11 is used. Inner current control loop is replaced by its first order transfer function satisfying settling time of current control loop T_{sq}, where τ_{qi} is time constant of current loop. Following relation between these two time constants given in equation (4.28), which similarly can be used for *q* axis current loop. The *q* axis current loop is expressed by first order transfer function:

$$\frac{i_q}{i_{q(ref.)}} = \frac{1}{\frac{\tau_{Id}}{k_{Id}k_{mm}}s+1} = \frac{1}{\tau_{qi}s+1} \qquad 4.31$$

The relationship between T_{sq} and τ_{qi} is obtained from equation (4.28) as:

$$\tau_{qi} = \frac{T_{Sq}}{3} \qquad 4.32$$

The torque block shown in figure-4.8 can be divided in to two parts; motor constant and mechanical part. The motor constant, K_M, is sometimes referred as torque constant or motor size constant and is obtained from the provided motor parameters. The mechanical part comprises the motor viscous friction constant *B*, and the inertia of the motor, *J*. Taking the above discussions in to consideration, the speed control loop of IPMSM is shown in figure-4.11.

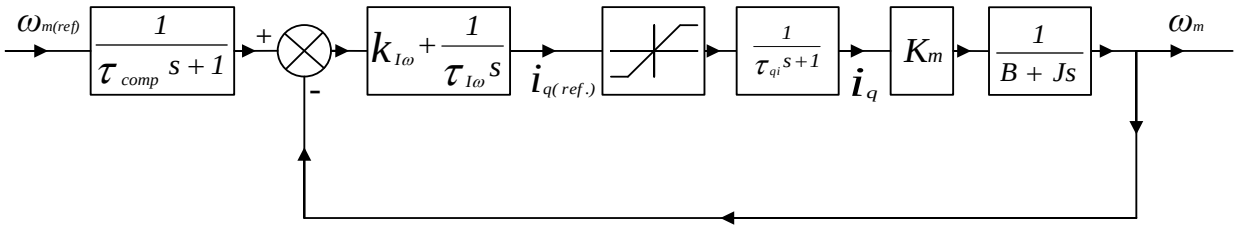

Figure 4. 11: *Speed loop of IPMSM in q axis.*

The closed loop diagram for speed control of IPMSM includes filtering block on the input of demanded speed (*the first order transfer function*), which compensates overshooting of speed. Time constant of compensator τ_{comp} is then given by:

$$\tau_{comp} = K_{I\omega}\tau_{I\omega} \qquad 4.33$$

Closed loop transfer function of speed control loop with PI-controller is as follows:

$$\frac{\omega_m}{\omega_{m(ref)}} = \frac{\left(k_{I\omega}+\frac{1}{\tau_{I\omega}s}\right)\left(\frac{1}{\tau_{qi}s+1}\right)\left(\frac{k_m}{Js+B}\right)}{1+\left(k_{I\omega}+\frac{1}{\tau_{I\omega}s}\right)\left(\frac{1}{\tau_{qi}s+1}\right)\left(\frac{k_m}{Js+B}\right)}\frac{1}{(\tau_{comp}s+1)}$$

$$= \frac{\frac{k_m(k_{I\omega}\tau_{I\omega}s+1)}{\tau_{I\omega}s(\tau_{qi}s+1)(Js+B)}}{1+\frac{k_m(k_{I\omega}\tau_{I\omega}s+1)}{\tau_{I\omega}s(\tau_{qi}s+1)(Js+B)}}\frac{1}{(\tau_{comp}s+1)}$$

$$= \frac{k_m(k_{I\omega}\tau_{I\omega}s+1)}{\tau_{I\omega}s(\tau_{qi}s+1)(Js+B)+k_m(k_{I\omega}\tau_{I\omega}s+1)}\frac{1}{(\tau_{comp}s+1)}$$

from equation (4.33)

$$= \frac{k_m}{\tau_{qi}\tau_{I\omega}Js^3+\tau_{I\omega}(J+B\tau_{qi})s^2+(k_m k_{I\omega}\tau_{I\omega}+B\tau_{I\omega})s+k_m}$$

$$= \frac{\frac{k_m}{J\tau_{qi}\tau_{I\omega}}}{s^3+\frac{J+B\tau_{qi}}{J\tau_{qi}}s^2+\frac{k_{I\omega}k_m+B}{J\tau_{qi}}s+\frac{k_m}{\tau_{qi}\tau_{I\omega}J}} \qquad 4.34$$

For designing speed PI controller by pole placement method, denominator of closed-loop speed transfer function is compared with ideal transfer function of the same order, which for order n = 3 is as follows:

$$S^3+3\omega_0 S^2+3\omega_0^2 S+\omega_0^3 \qquad 4.35$$

For calculation of proportional gain $K_{I\omega}$ and integral time constant $\tau_{I\omega}$ of speed PI controller, ideal transfer function given by equation (4.35) is designed exploiting Dodd´s formula, equation (4.27), which satisfies the settling time of speed control loop. Then, the ideal transfer function satisfying settling time of speed control loop is:

$$S^3 + \frac{18}{T_{s\omega}} S^2 + \frac{108}{T_{s\omega}^2} S + \frac{216}{T_{s\omega}^3} \qquad 4.36$$

Comparing equations (4.36) with (4.34), the speed controller (PI controller) parameters are obtained as:

$$s^3 + \frac{J + B\tau_{qi}}{J\tau_{qi}} s^2 + \frac{k_{I\omega} k_m + B}{J\tau_{qi}} s + \frac{k_m}{\tau_{qi}\tau_{I\omega} J} \quad \leftrightarrow \quad S^3 + \frac{18}{T_{s\omega}} S^2 + \frac{108}{T_{s\omega}^2} S + \frac{216}{T_{s\omega}^3} \qquad 4.37$$

$$k_{I\omega} = \frac{108J\tau_{qi}}{k_m T_{s\omega}^2} - \frac{B}{k_m}, \qquad \tau_{I\omega} = \frac{k_m T_{s\omega}^3}{216J\tau_{qi}} \qquad 4.38(a,b)$$

For the proper function of speed control loop with chosen settling time $T_{s\omega}$, settling time of current loop in *q* axis should be adjusted to satisfy following condition:

$$\frac{1}{\tau_{qi}} = \frac{18}{T_{S\omega}} - \frac{B}{J} \rightarrow \frac{1}{T_{Sq}} = \frac{6}{T_{S\omega}} - \frac{B}{3J} \qquad 4.39$$

If the condition set in equation (4.39) is respected, speed loop for chosen settling time will work with high precision. On the other hand, if settling time of current control loop in q axis does not satisfy the condition, the dynamics of speed control loop will differ from the demanded.

For the safety operation of the IPM drive, the control systems is equipped with current range limiter, saturation block on figure-4.11.

Following the above analysis, the controllers' responses, *d* and *q* axis currents and speed drive, can be checked using motor parameters. The following table shows the parameters of a 1500rpm, 1.5KW IPMSM.

NO.	Description	Parameter	Unit	Value
1	Rated Voltage	V_{rated}	Volt (V)	200
2	Rated Current	I_{rated}	Ampere (A)	6.5
3	Stator Phase Resistance	R_s	Ohm (Ω)	0.18
4	Armature Inductance	L_d, L_q	Henry (H)	$8.5x10^{-3}$, $8.5x10^{-3}$
5	PM Flux Linkage	λ_f	Volt Second (V.s)	0.07145
6	Torque Constant	K_m	Newton-meter per Ampere (Nm/A)	0.4287
7	Inertia	J	Kilogram meter-squared ($Kg.m^2$)	$6.2x10^{-4}$
8	Viscous Friction Dumping Constant	B	Newton meter second (N.m.s)	$3.035x10^{-4}$
9	Number of Poles	P	-	8

Table 4. 1: *IPMSM parameters.*

According to the parameters that are given in the above table and using the 5% settling time PI controller calculation shown in equations (4.25) through (4.38), the following values are obtained.

For the *d* axis current controller, the PI parameters are:

$$K_{ID} = 0.1275, \qquad \tau_{Id} = 0.0472, \qquad K_{mm} = 5.56, \qquad \tau_{md} = 0.0472$$

This *d* axis current controller is implemented in SIMULINK® as shown in figure-4.12. And the corresponding step, impulse and frequency response graphs are shown in figure 4.13.

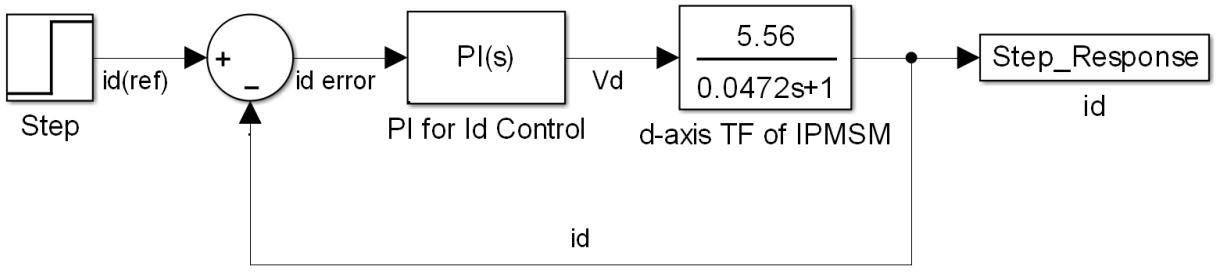

Figure 4. 12: *SIMULINK® Implementation of d-axis Current Control Loop.*

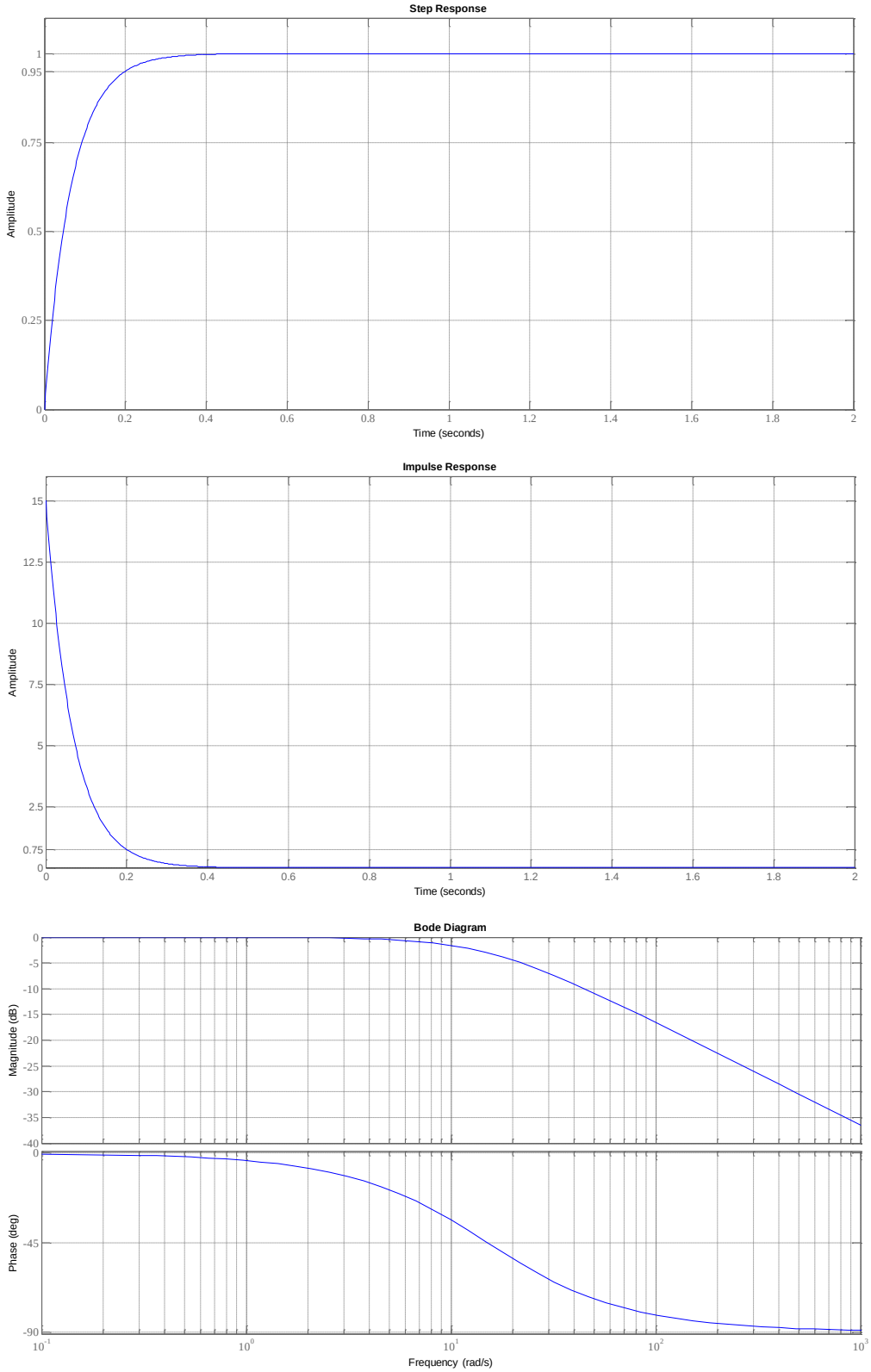

Figure 4. 13: *Step and Impulse Responses and bode plot of d axis Current Control Loop*

From the step and impulse responses of the above figure, the settling time observed is the same as that of the designed value. From the bode diagram, it can be observed that the current loop is always stable.

Similarly, for the *q* axis current controller, the PI parameters are:

$$K_{Iq} = 0.1275, \qquad \tau_{Iq} = 0.0472, \qquad K_{mm} = 5.56, \qquad \tau_{mq} = 0.0472$$

The *q* axis current controller is implemented in SIMULINK® as shown in figure-4.14, and it is the same as the *d* axis current control loop shown in figure-4.12. Hence, the same step, impulse and frequency response, as shown in figure-4.13.

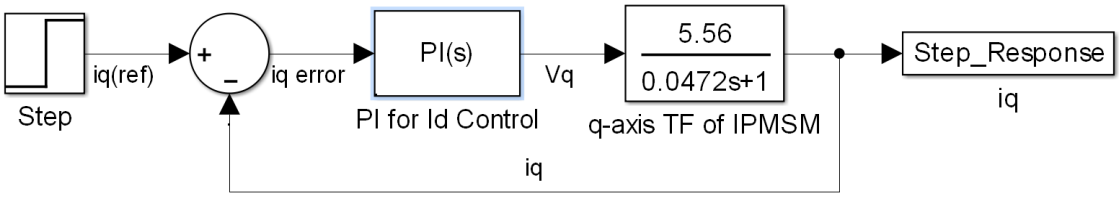

Figure 4. 14: *SIMULINK® Implementation of q axis Current Control Loop.*

The speed control loop is implemented using on SIMULINK® as shown in figure-4.15. For the chosen settling time to work with high precision, it has to satisfy equation (4.39). Then, according to equation (4.39), the speed controller settling time is, $T_{s\omega}$ = 1.162 s. Using the value of this settling time the PI controller parameters are found to be:

$$K_{I\omega} = 0.007, \qquad \tau_{I\omega} = 74.960, \qquad \tau_{qi} = 0.067 \qquad \tau_{Comp} = 0.5247$$

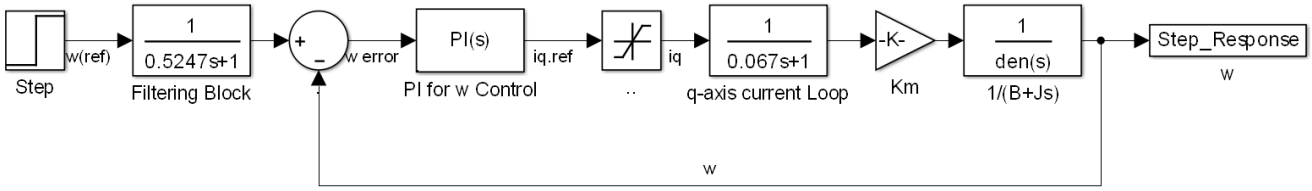

Figure 4. 15: *SIMULINK® Implementation of the Speed Control Loop with Filter.*

From the figure below the settling time observed is the same as that of the designed value. From the bode diagram; it can be observed that the speed loop is indefinitely stable.

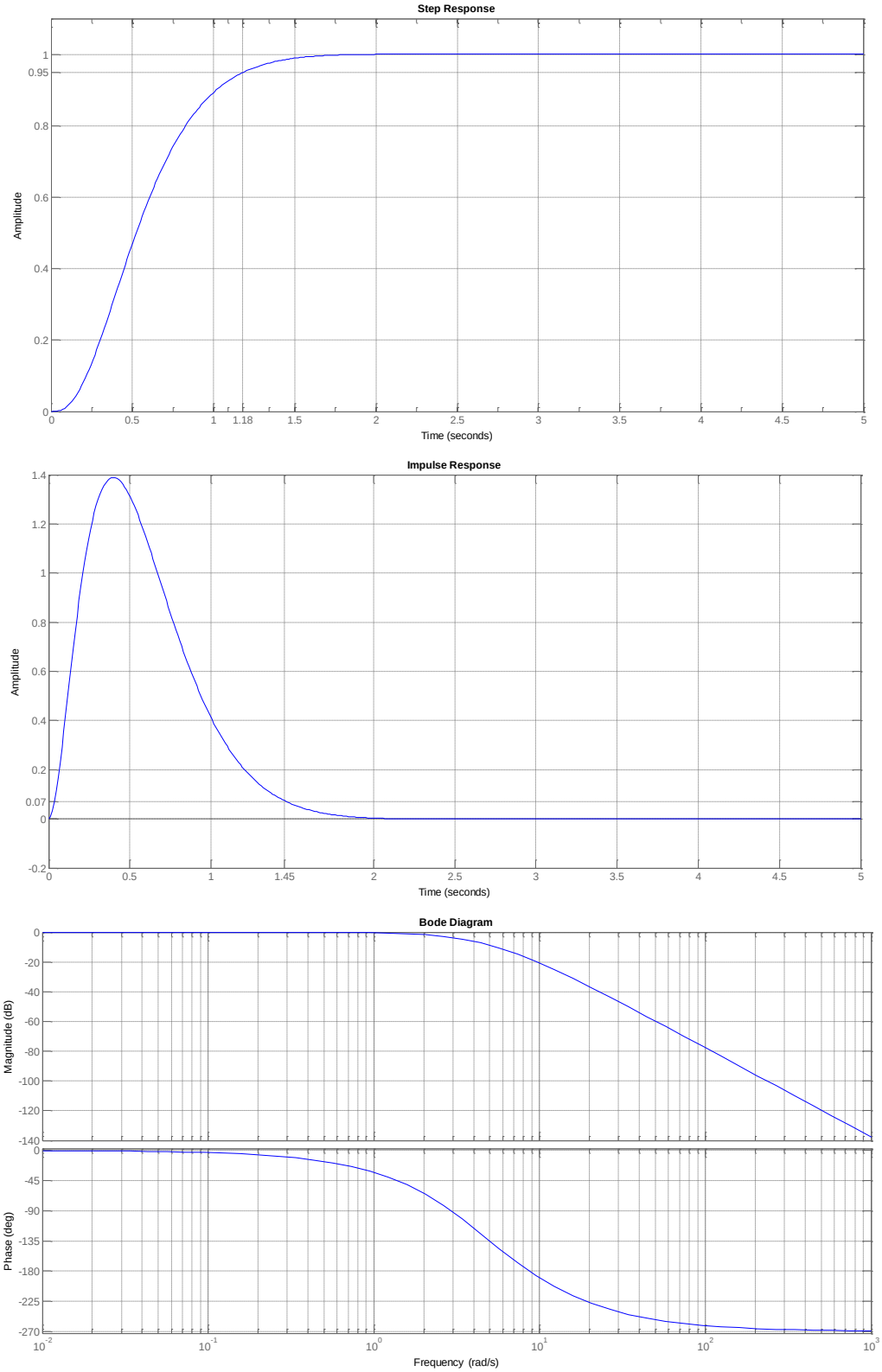

Figure 4. 16: *Step and Impulse Responses and bode plot of Speed Control Loop.*

CHAPTER 5
SIMULATION RESULTS AND DISCUSION

5.1 INTRODUCTION

The *d-q* model of IPMSM is realized and a complete drive system is designed and implemented in SIMULINK® as shown in figure-5.1.

The motor, IPMSM, is directly driven by the voltages V_a, V_b, and V_c, which are outputs of the three phase VSI. The three phase VSI's switching pattern is controlled by the SVM generator, which obtains the required reference voltage signals from the PI controller of the vector control block. The resulting motor stator currents are taken using high frequency and efficient current transformers. For this drive system, only two of the three phase currents are obtained. This is because, high frequency currents transformers are very expensive and it is possible to obtain the *α-β* transformation of these currents as long as the three phase applied voltages to the motor are balanced, which is right for closed loop VFD drives.

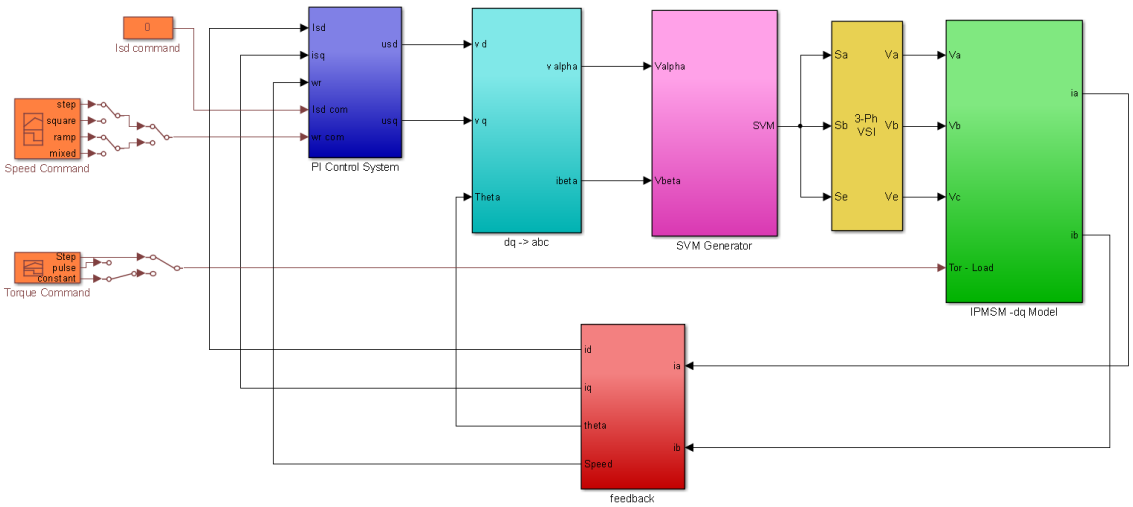

Figure 5. 1: *SIMULINK® Realization of the Complete Sensorless Drive System.*

The *α-β* transforms are further used to determine the *d-q* and *k-l* axis rotary and stationary reference frame transforms, respectively. The *α-β* and *k-l* transforms are used to determine the rotor's position and speed. These closed loop continues indefinitely satisfying the torque and speed command through the vector controller.

5.2 PERFORMANCE OF THE SVM SIGNAL GENERATOR

The SVM is realized as shown in appendix-II. The MATLAB function shown in appendix-III performs the required six sector operation. For the reference signal in the first sector, i.e. its space vector $V_a+V_b+V_c$ has an angle between 0 and $\pi/3$, the switching sequence shown in figure-5.2 is obtained.

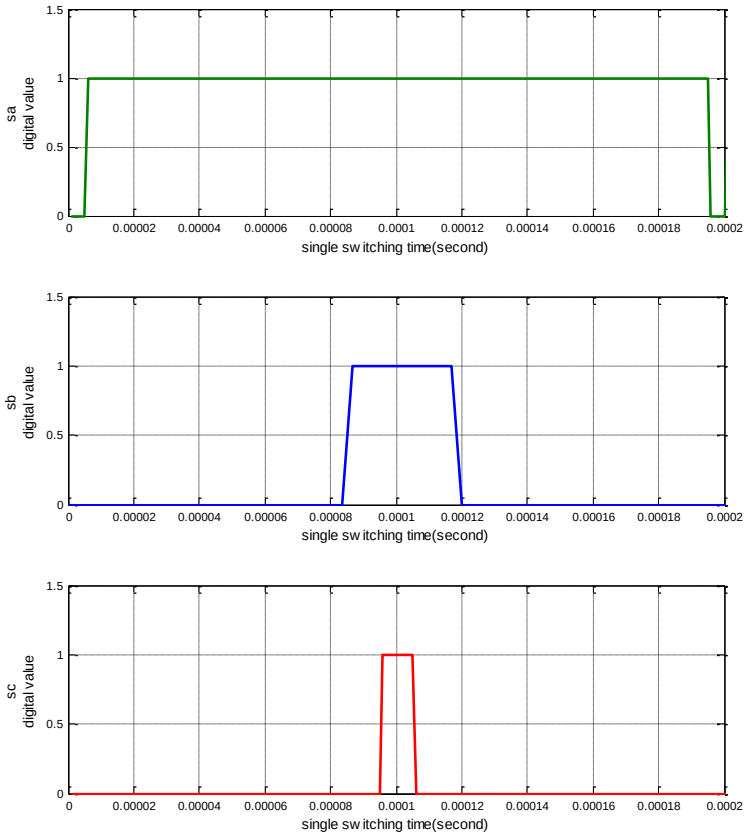

Figure 5. 2: *Switching Sequence Output of the SVM Generator in the First Sector. .*

All switchings' sequences are generated from the SVM generator for the six sectors and this repeats all over again. This process continues indefinitely and ensures the availability of the required voltages to the motor. The required voltages that are acquired from PI controllers are represented by these switchings. A VSI, then, converts this series of digital signals to a three phase signal shown in figure-5.3(b). Since the stator of the motor acts as a low pass filter, the filtered signal will take the form shown in figure-5.3(c). Figure-5.3 summarizes the VSI and stator voltage waveforms. As discussed in *section-3.4.1*, VSI plays an important role in voltage inversion.

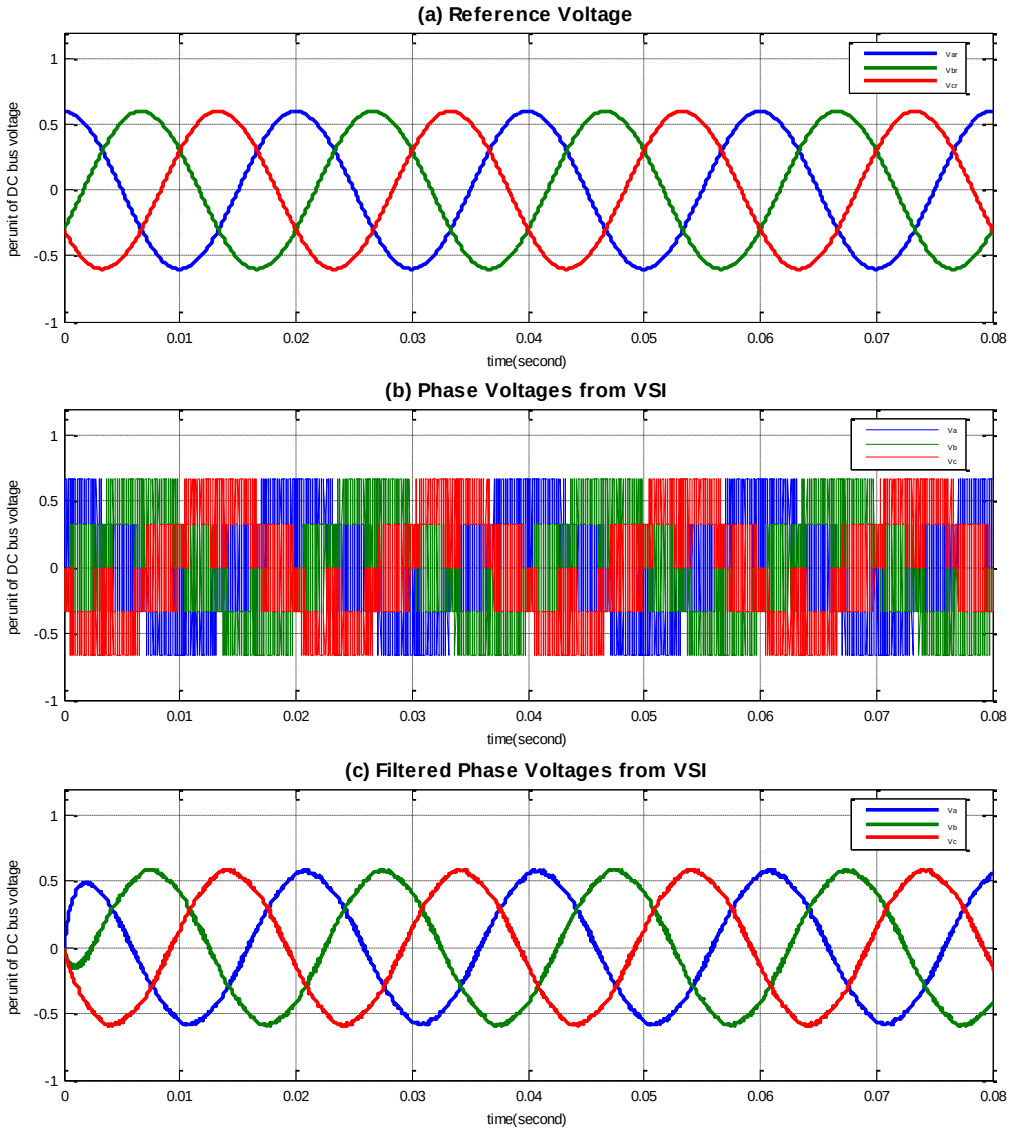

Figure 5. 3: *Reference, VSI and Filtered Phase Voltages.*

The α-β transforms of the signals shown in figure-5.3(b) and (c) are shown in figure-5.4(a), (b) and (c). The 90 degree phase shift between the α and β components is clearly seen on the figure. The complex plane (α-β) plot, in figure-5.4(d), shows the hexagon incorporating the six sectors.

The inscribed circle is the α-β plot of the filtered signal. The radius of this circle represents the amplitude of the reference three phase voltage. As long as the reference voltage's amplitude is less than or equal to this value the SVM generator works in the linear modulation region. In the other modulation regions the concept of SVM degrades slowly as the amplitude value is increased.

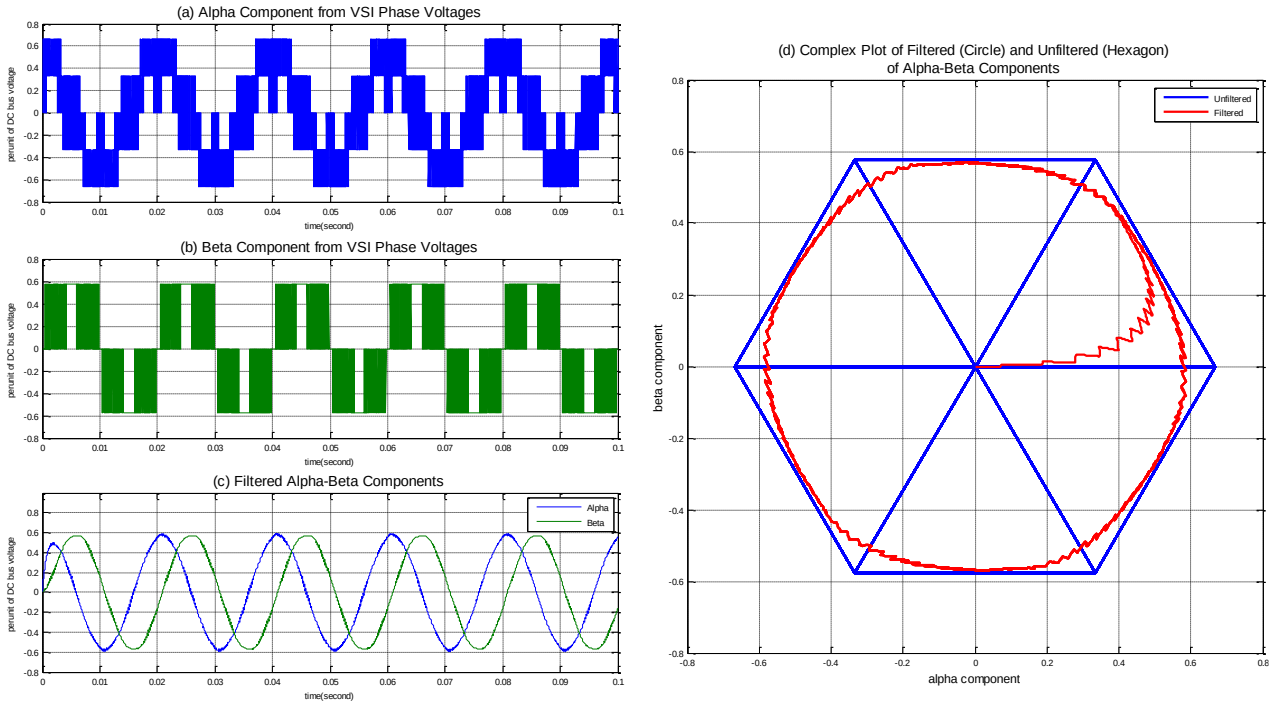

Figure 5. 4: *α-β transforms of VSI and Stator Phase Voltages and Their Complex Plane Plot.*

In order to study the harmonics and the spectrum of SVPWM technique, a three-phase SPWM is implemented as shown on *Appendix-IV*. The resulting voltage wave forms are shown in figure-5.5 and figure-5.6. The figures show, the waveform for one of the phases, V_{an}, and the corresponding FFT spectrum and THD value.

The result shown in figure-5.5, comprises the signal V_{an} and the frequency spectrum. From the frequency spectrum, it can be clearly seen that, only the spectrum of the fundamental and switching components has contribution on the signal. But in figure-5.6, the harmonic values take part in the composition of the modulated phase voltage $V_{an.}$ As a result, the THD of the former is less than that of the later. There is about *22%* of THD difference. Even the peak value of the waveform in figure-5.5 is *0.57* and in figure-5.6 is *0.47*, which implies that, the conversion ratio from DC to AC is larger in SVPWM than SPWM.

Having lower THD in SVPWM implies lower switching loses than SPWM. This lower THD value ensures the reliability and flexibility of SVPWM. Apart from motor drives, this PWM technique can be used in different modern non-linear systems, where the presence of harmonics is inevitable and the THD should be in the limit standard expressed by [29].

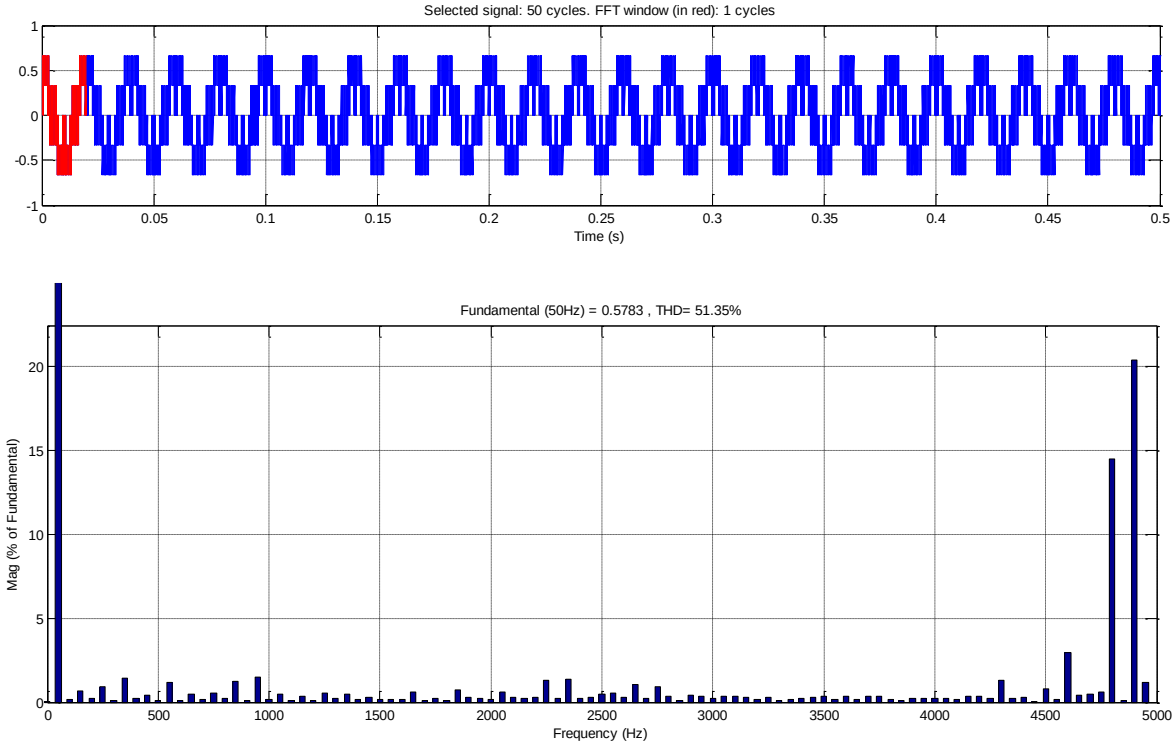

Figure 5. 5: *Waveform and Frequency Spectrum Plot of Phase Voltage V_{an} of SVPWM.*

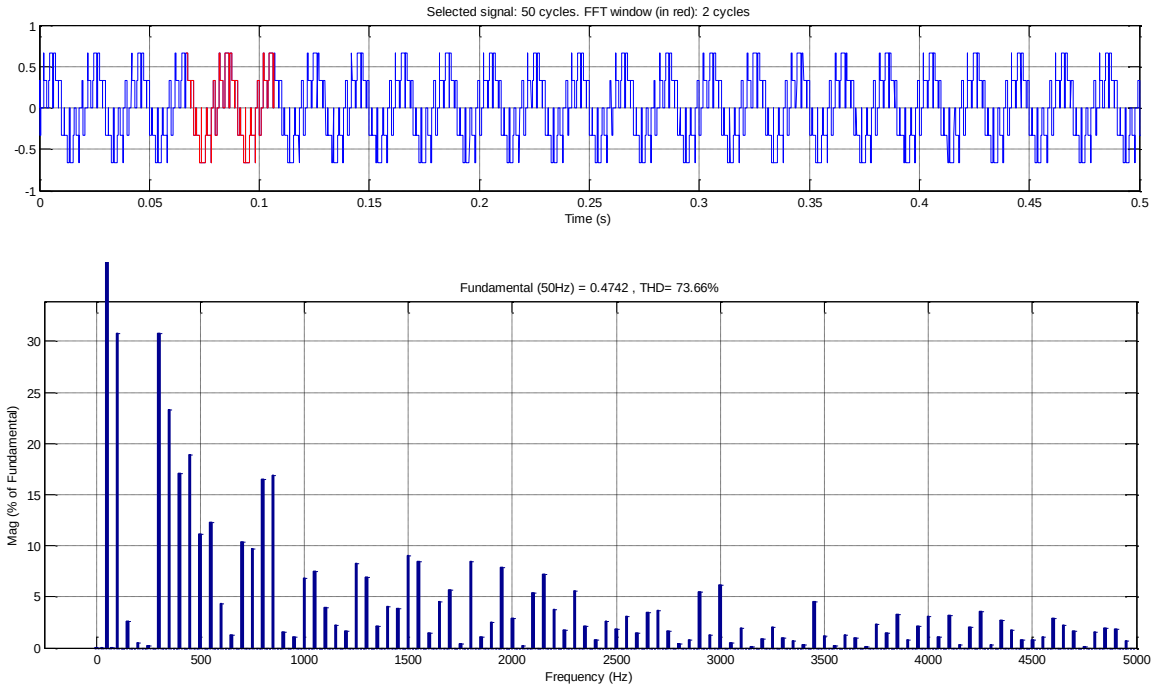

Figure 5. 6: *Waveform and Frequency Spectrum Plot of Phase Voltage V_{an} of SPWM.*

If a signal of high frequency is injected, as this paper uses (implemented as in *Appendix-II*, figure-II.4), the increase in THD and a different type of spectrum is expected.

A three phase signal of frequency *2-KHz* having very small amplitude, i.e. 5% of the reference voltage, is injected as shown in Appendix-II (*the smaller value of peak voltage is to keep the total signal inside the linear modulation range*). The resulting phase voltage and frequency spectrum is shown in figure-5.7. As in the figure, the THD value is 53.65% and an additional of a 2-KHz signal's spectrum is obtained. From figure-5.5, this plot has an additional of 2.3% of THD. This is due to the high frequency injection signal.

Even with the injection this SVPWM signal has smaller THD than SPWM.

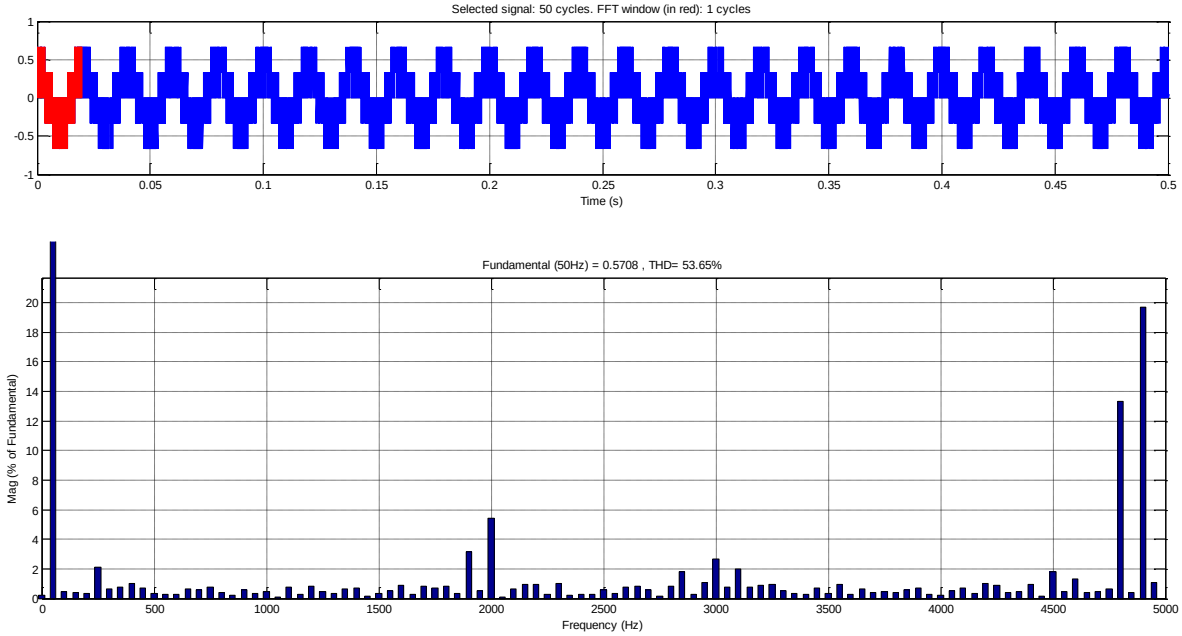

Figure 5. 7: *Waveform and Frequency Spectrum Plot of Phase Voltage V_{an} of SVPWM with a 2KHz Injection Signal having 5% of Fundamental Signal's Amplitude.*

Higher frequency for switching and injection can be used. And, the resulting waveform and frequency domain plot is shown in figure-5.8. As shown in the figure, increasing the switching and injection frequencies results an increase in THD and decline in fundamental signal quality. Therefore, using an optimal frequency value, as shown in figure-5.8, results in better fundamental signal quality and smaller THD while providing wider bandwidth for extracting the injection signal.

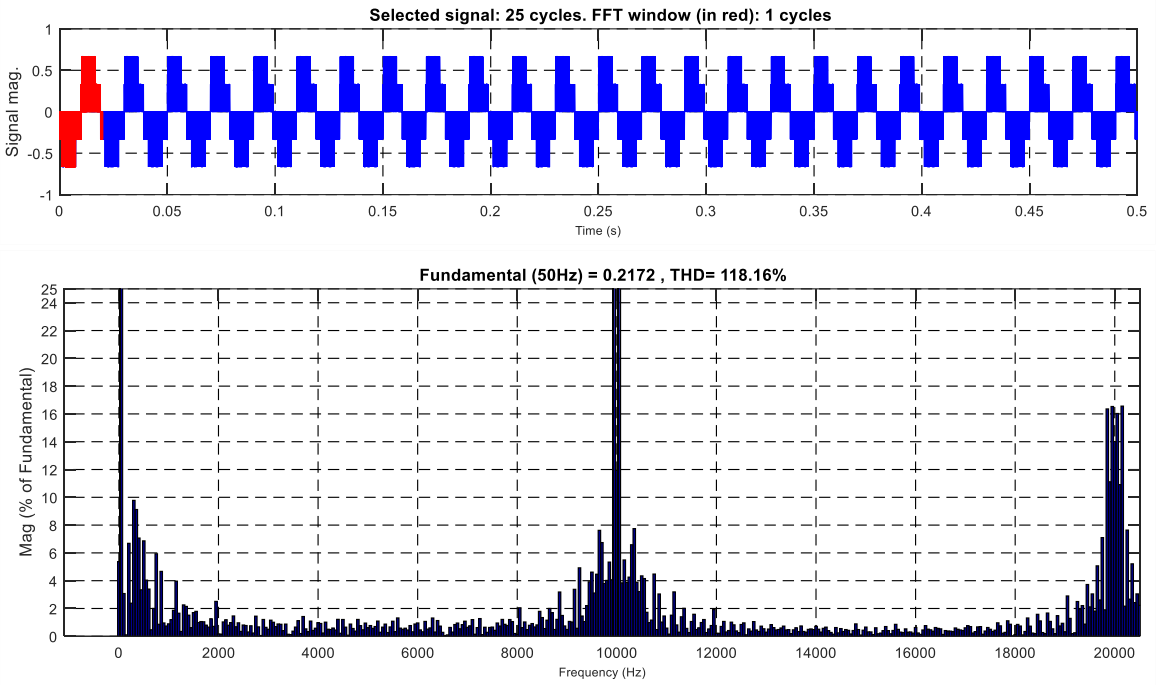

Figure 5. 8: *Waveform and Frequency Spectrum Plot of Phase Voltage Van of SVPWM with a 10KHz Injection Signal having 5% of Fundamental Signal's Amplitude with 20KHz of Switching Frequency.*

5.3 PERFORMANCE OF SPEED CONTROL

The performance of the speed control of the drive system under no-load condition is inspected under different conditions. Figure-5.9 shows the performance of the drive for constant speed command. Until the steady-state speed is attained, the motor is pushed to increase torque, hence, speed. This is made possible by increasing the *q*-axis current. For MTPA operation, the d-axis current is controlled to be zero. Therefore, the current i_q is a starting current where maximum torque is required to start the motor under no-load condition. As the motor approaches steady state operation, and since the load torque is zero, a very small amount of *q*-axis current is required to keep the motor running. Figure-5.9 also shows the rotors instantaneous position in radians. The speed of the motor is obtained by taking the time derivative of the position vector. The instantaneous slop of the position corresponds to the instantaneous speed.

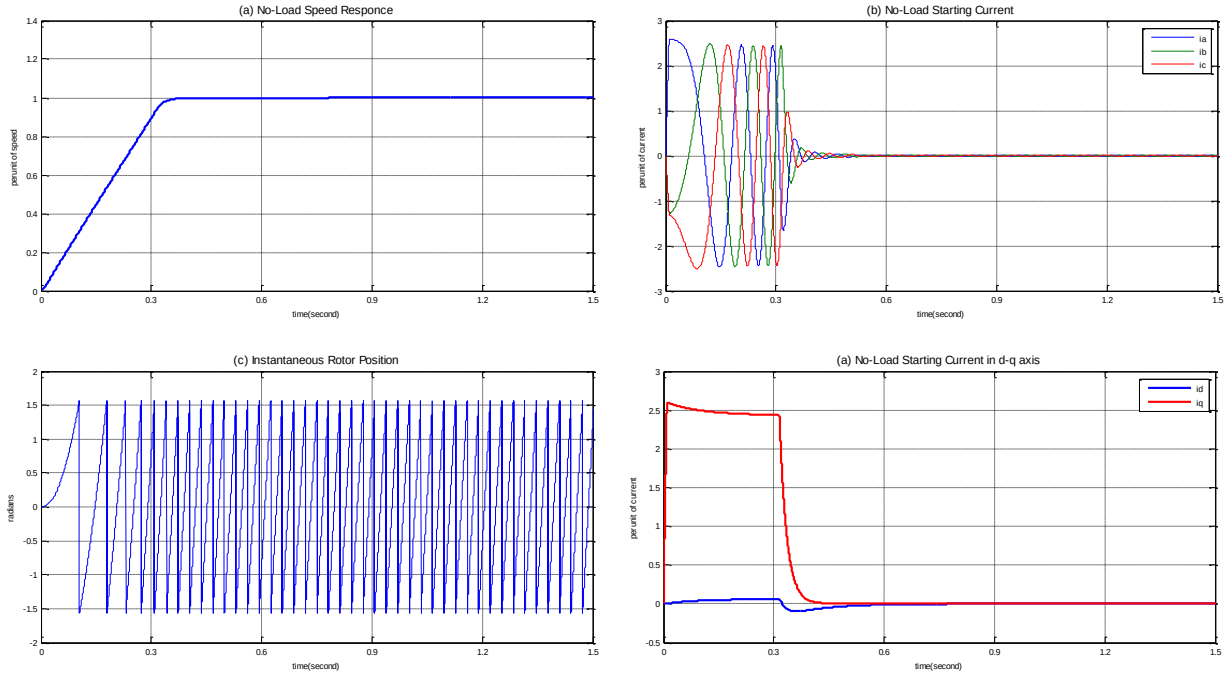

Figure 5. 9: *No-Load Speed and Position Transients, and Steady State Operations.*

Figure-5.10 shows the operation of the drive system for direction reversal speed command. As the motor drive obtains speed decreasing command, it tries to slow down the motor by creating a negative *q*-axis current which in turn creates torque in opposite direction. From figure-5.10, the negative i_q can be seen and it is the result of the reversed current sequence shown in figure-5.10(b). The position of the motor is shown in figure-5.10(c), where at zero speed the slop of the position plot is zero. After this zero slop value, the negative slop inverse-tangent plot follows and continues this way as long as the required speed is in the negative/reverse direction.

Figure-5.11 shows the increasing staircase operation of the drive system. After the motor reaches steady state of the current reference, the operating *q*-axis current is very small. When step speed increase command is obtained, the motor increases torque by increasing *q*-axis current. Which in

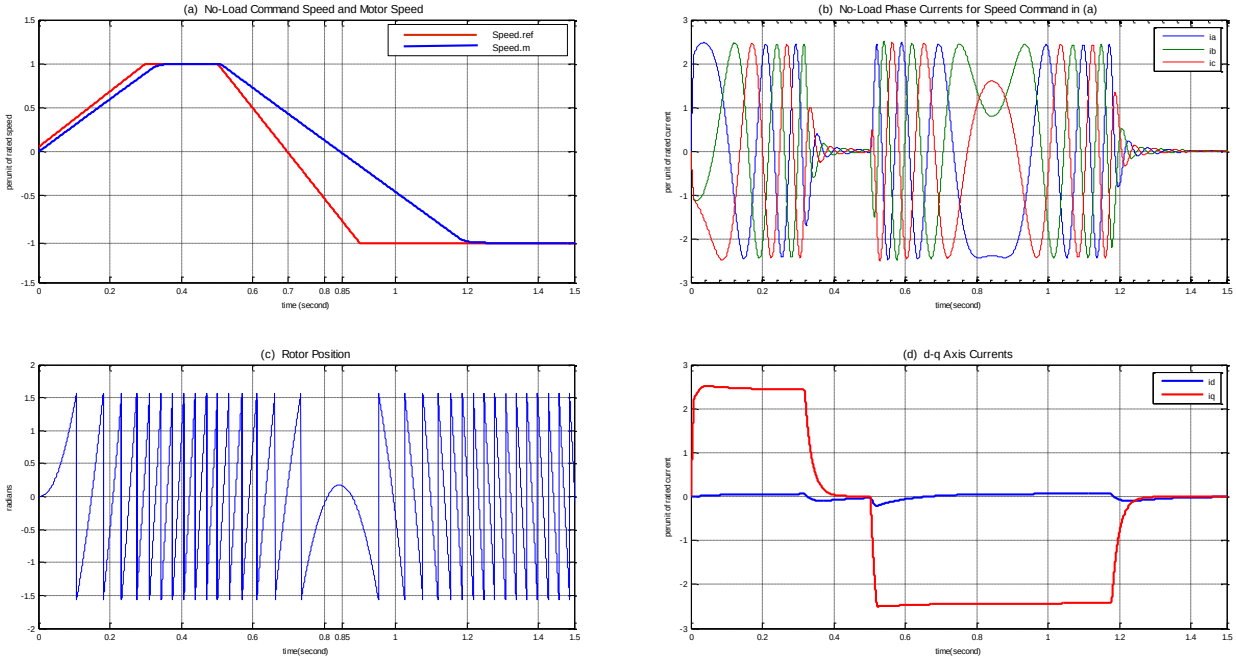

Figure 5. 10: *Speed Reversal Operation Under No-Load.*

-decreases and maintains small value at this secondary speed reference. This operation continues and maintains very small *q*-axis current value for no-load operation. Figure-5.11(d) shows the conditions of the d-q axis currents.

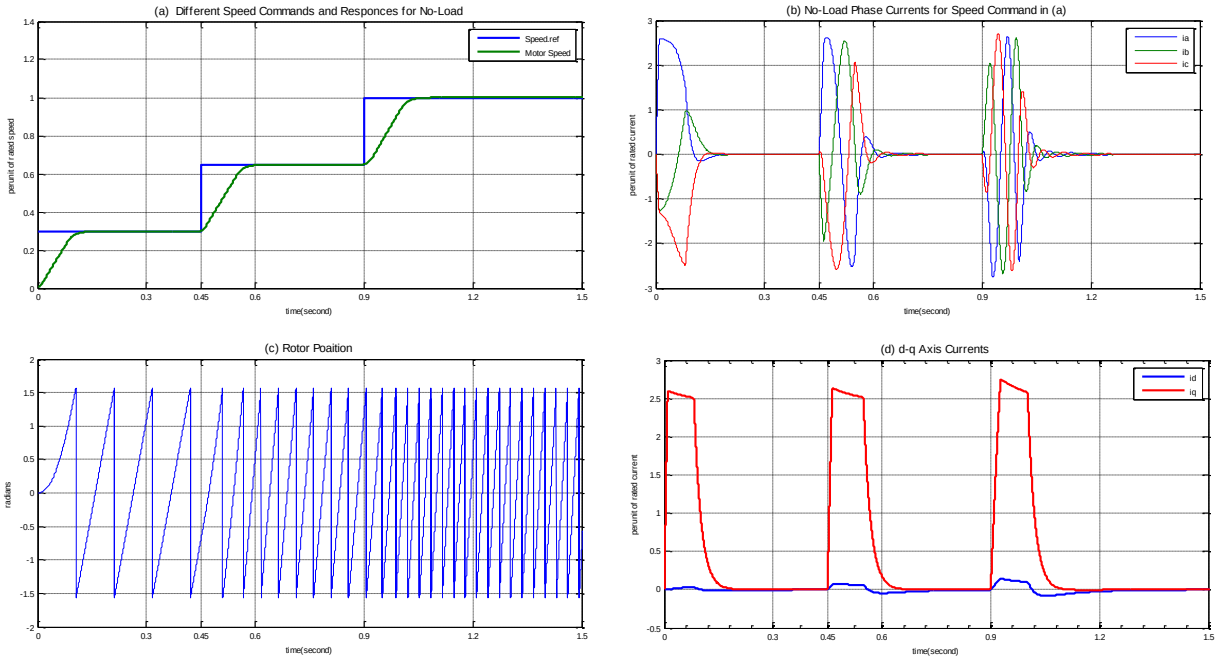

Figure 5. 11: *Increasing Staircase Speed Command Operation Under No-Load.*

For case of the decreasing staircase operation, the motor operates in a similar way as in the case of the increasing staircase operation except that negative torque is used to decrease the speed of the motor. Figure -5.12 shows this operation. In this case, the negative torque (*q*-axis current) is obtained by decreasing the driving electrical speed, which is frequency. So, figures-5.12(b) and (d) show, decreasing frequency of stator phase currents and negative value of *q*-axis current, respectively.

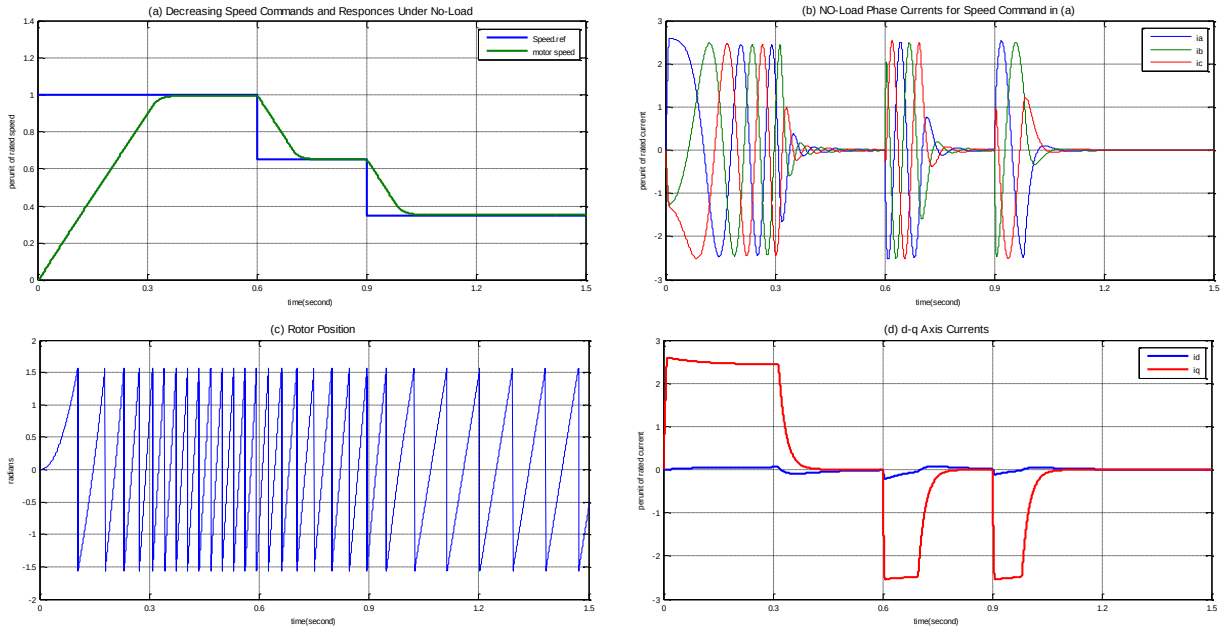

Figure 5. 12: *Decreasing Staircase Speed Command Operation Under No-Load.*

5.4 TORQUE CHARACTERISTICS AND PERFORMANCE

Before starting discussion about starting the motor under-load, it is better to see the effect of applying load to a motor which has started with no-load. Consider Figure-5.13. The motor operates as the same way as shown in Figure-5.9 until a load is applied at $t = 0.5s$. At this time, the motor's *q*-axis current increases from the very small value it has been to some higher value and is maintained at this value in order to keep the motor running at the required speed by driving the load specified. In Figure-5.13(b) and (d), the increase in these currents' values is illustrated.

If the load is introduced to the motor beginning from the starting time, the q-axis current will not decrease to a very small value. Instead it maintains a value that allows the motor to produce enough torque in order to drive the load torque at the required peed. Figure-5.14 shows this operation. The

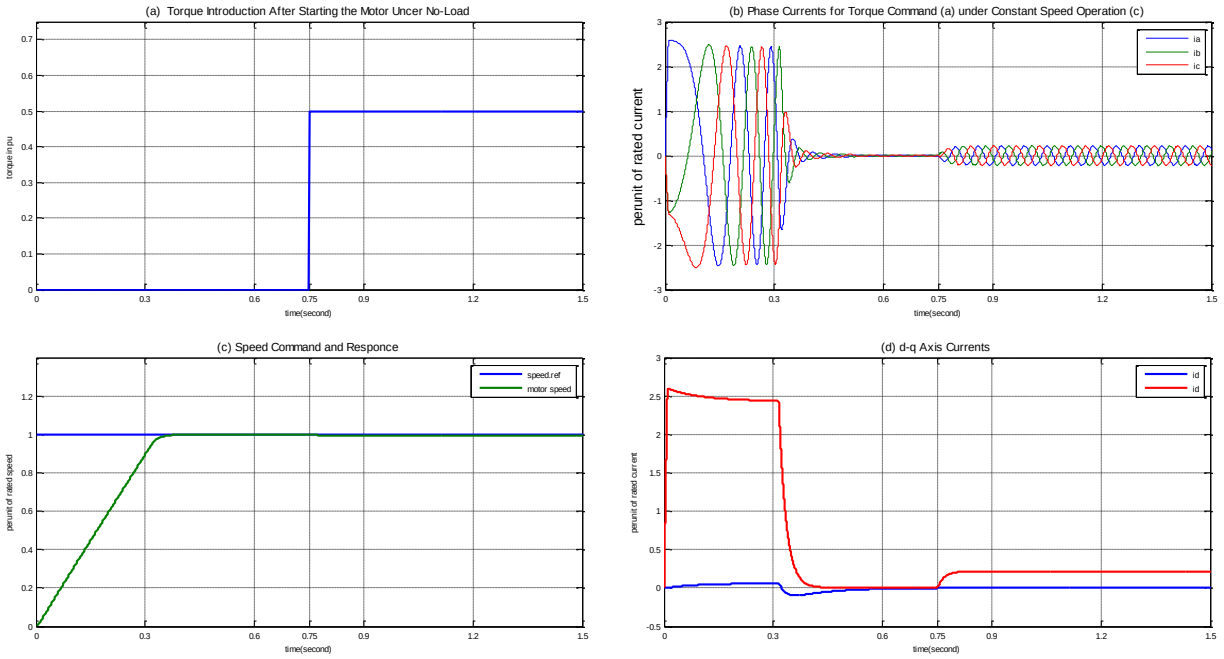

Figure 5. 13: *Load Introduction to the Motor after Starting Under No-Load.*

-starting current of the motor is very large and it, most of the time, reaches at a value of 2.6pu. From the figure, it can be seen that, the motor's operation satisfies MTPA condition, i.e. $i_d = 0$. This criteria increases the conversion of the power supplied to motor torque.

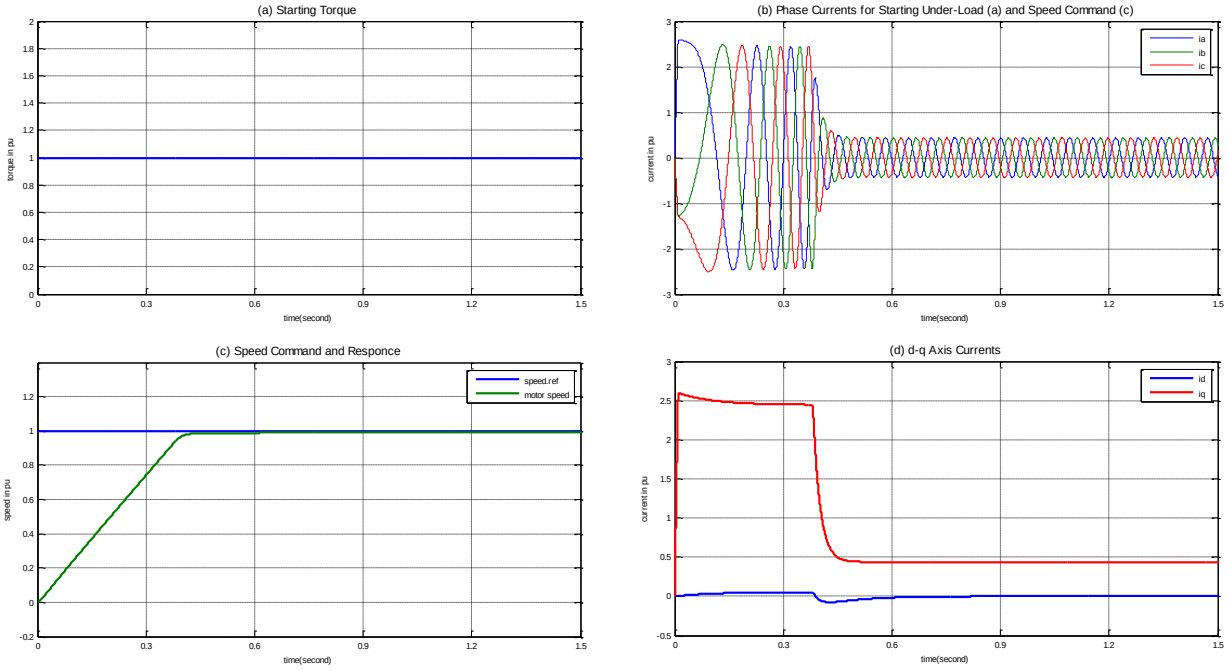

Figure 5. 14: *Speed and Position Transients, and Steady State Operations Under-Load.*

The increasing and decreasing operation of the motor under load condition given in Figures-5.15 and 5.16 are the same as that of no load operations except that the q-axis currents have higher value to support the load.

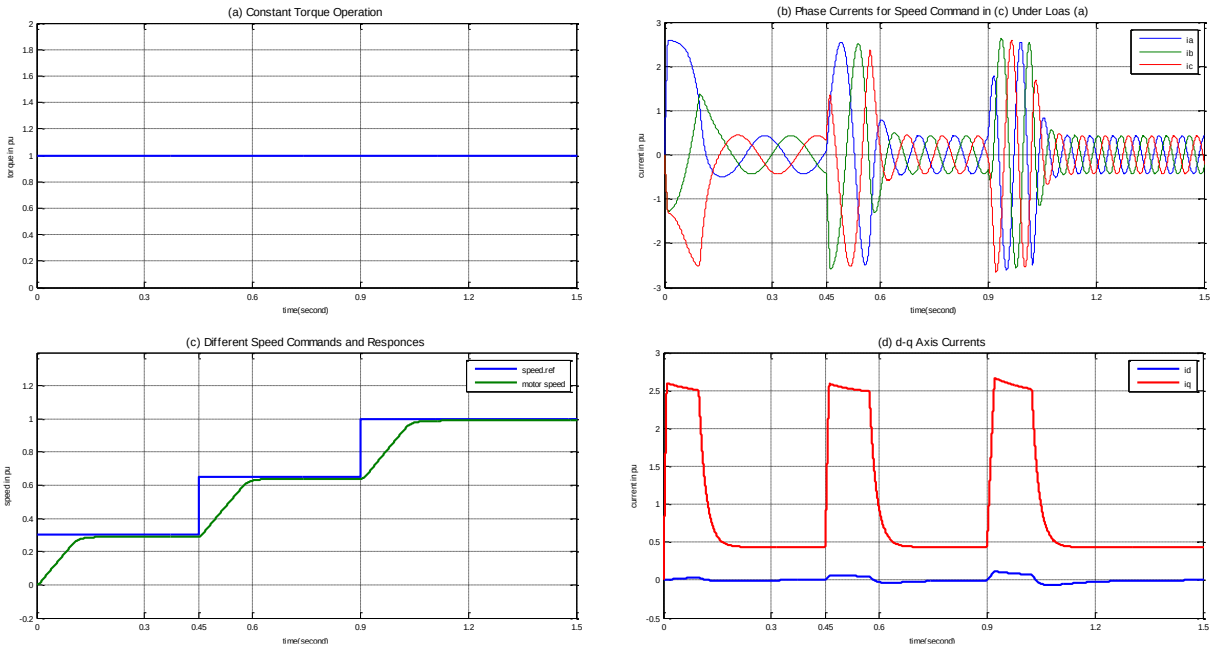

Figure 5. 15: *Increasing Staircase Speed Command Operation under Load.*

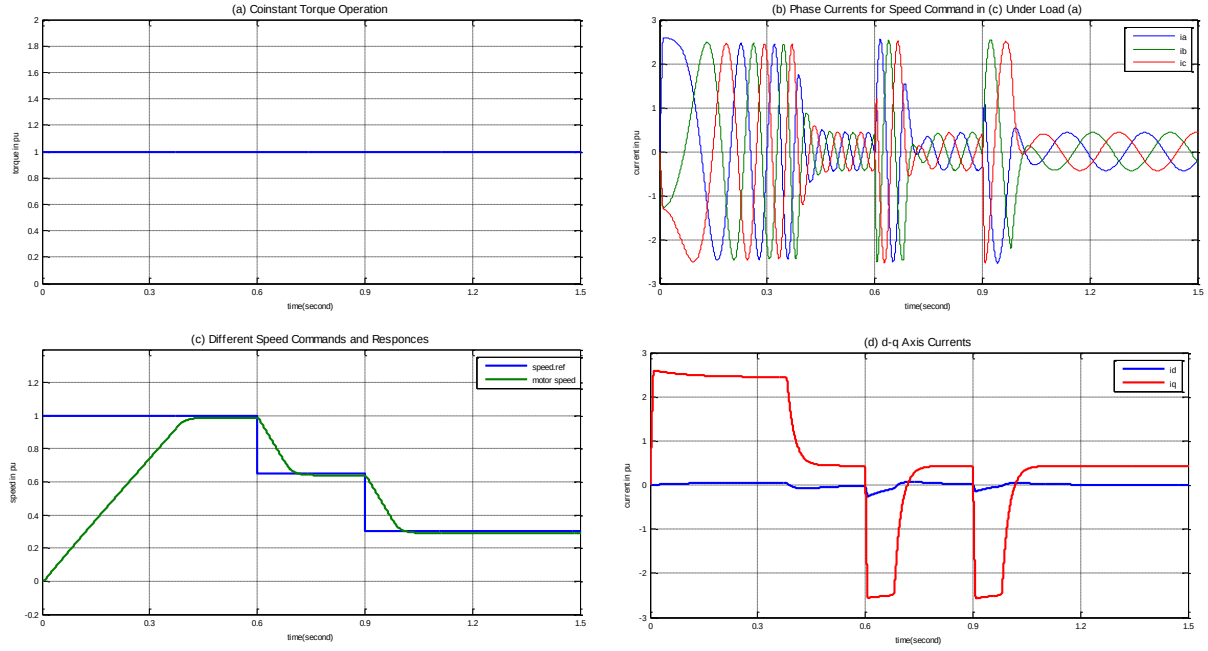

Figure 5. 16: *Decreasing Staircase Speed Command Operation under Load.*

The speed reversal operation under-load is can be seen from two different load types. The first one is conveyer operation and the other is fan operation.

For conveyer operation, the load-torque reverses direction with the motor. The torque and speed command and their effect on operation of the motor is shown in Figure-5.17. Similarly, decreasing speed is performed by decreasing the frequency of the phase voltages, hence phase currents. Once the direction of the motor is changed, the direction will be handled by changing the sequence of the phase currents and the speed will be increased by increasing the frequency of this sequence changed signal. Due to the presence of load, the *q*-axis current will have a non-small negative value, which maintain to drive the conveyer load in the other direction.

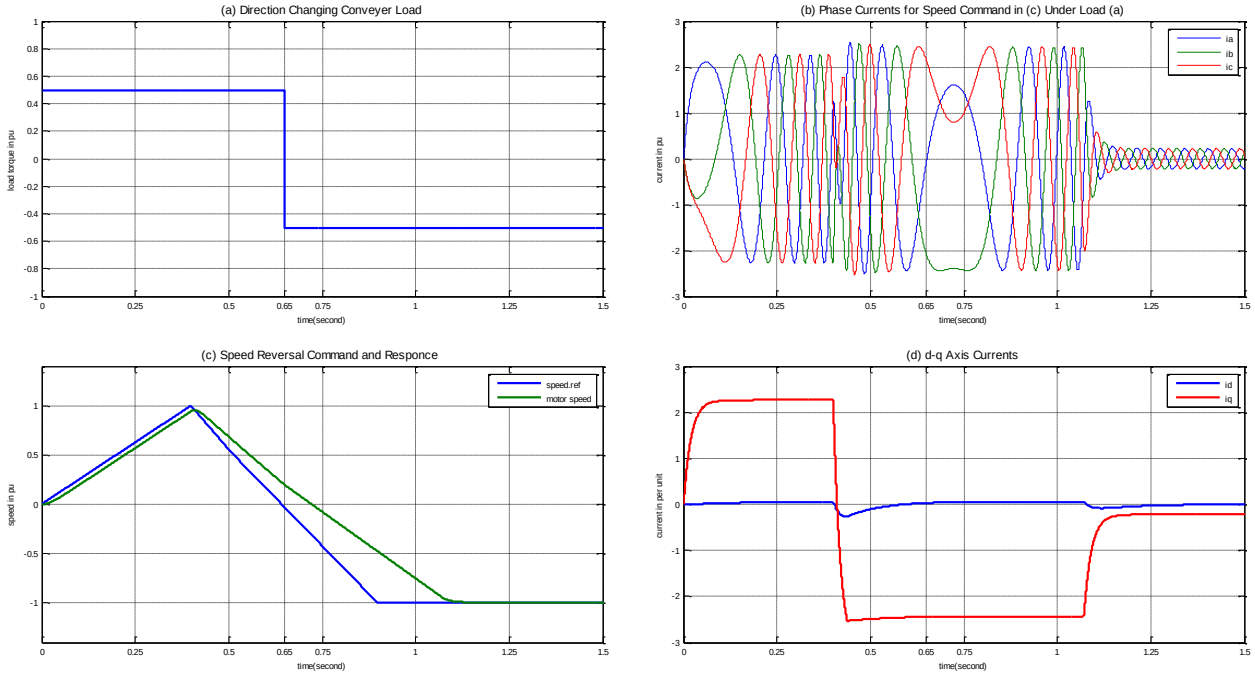

Figure 5. 17: *Speed Reversal Operation under Conveyer Type Load Operations.*

For fan operation, the load torque has a zero value in reverse direction. The operation is shown in Figure-5.18. The same speed control procedure is used here. The only difference from the conveyer type load is that the *q*-axis current will have a very small negative value in the reverse direction due to the absence of load.

From the previous discussions, the torque is found to be directly proportional to the *q*-axis current. IPMSM, like induction motors, has a torque-speed characteristics curve. But, unlike ACIMs, this

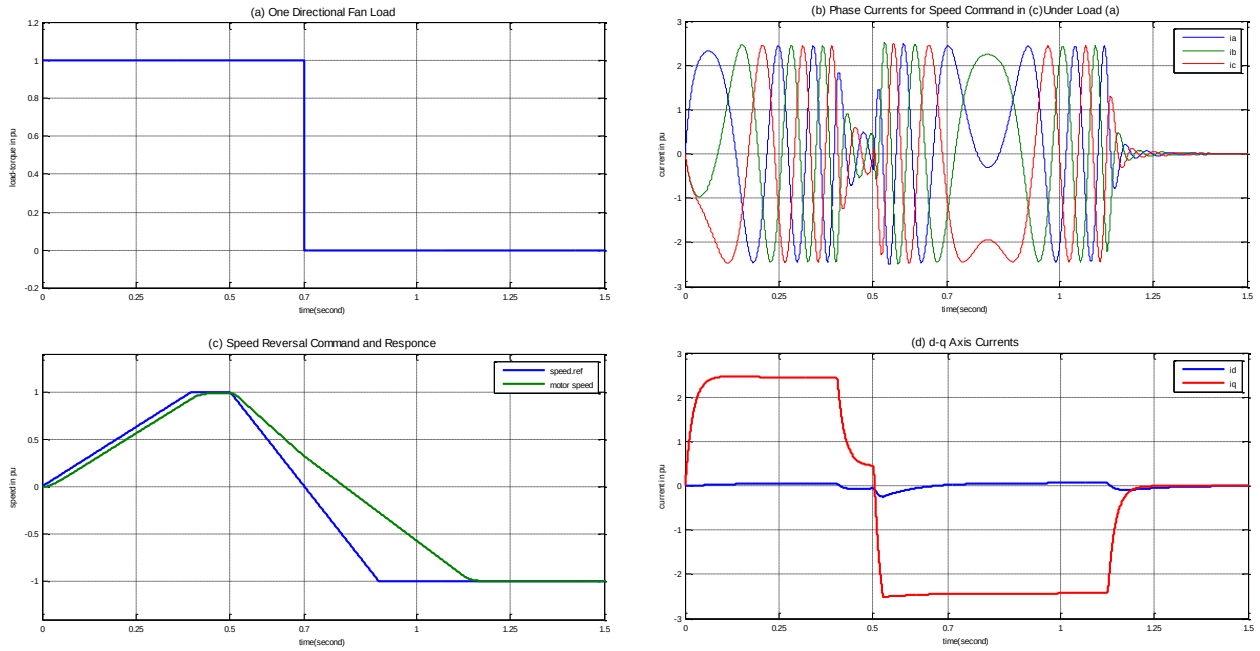

Figure 5. 18: *Speed Reversal Operation under Fan Type Load Operations.*

-motor can operate at the synchronous speed. Consider the figure shown below (Figure-5.19). The torque speed characterizes is given by (c) is for the conveyer type load which is specified by the commands (a) and (b). At speed -1pu, the motor has a non-zero torque. The torque decrease from

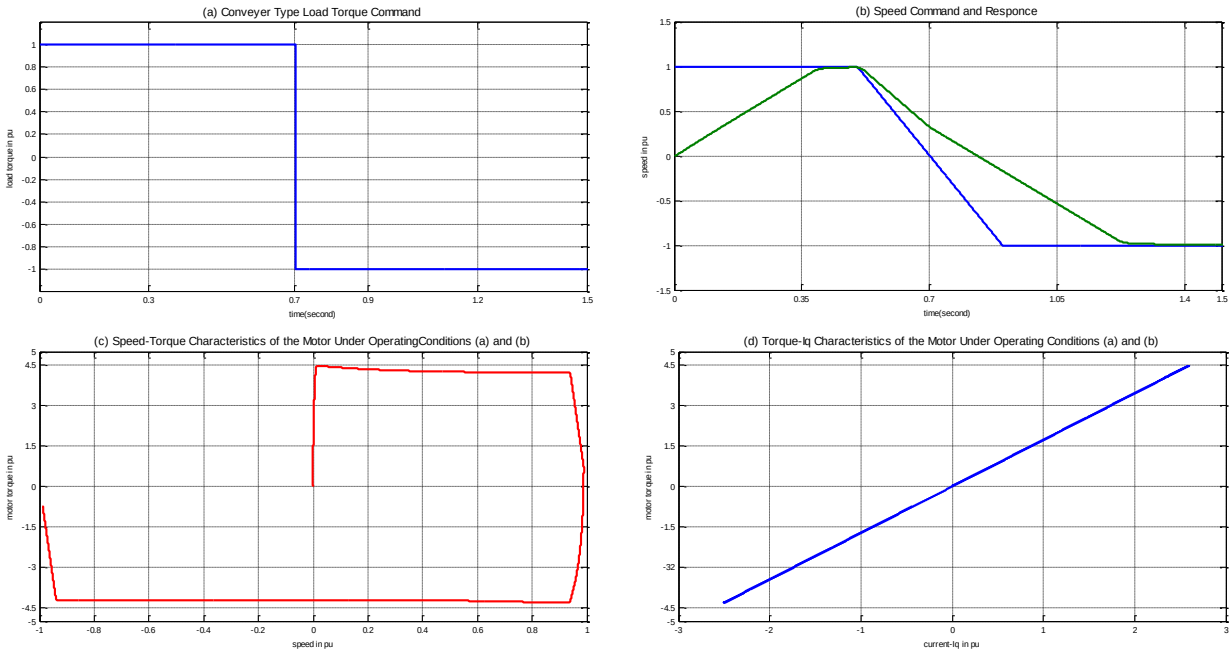

Figure 5. 19: *Torque-Speed and Torque-i_q Characteristics.*

-from peak value and maintains a constant value. The peak is due to the high starting current. For different types of load-speed commands, different torque speed characteristic curves are obtained.

According to [3], the performance of IPMSM can be implicitly described using the *torque*, i_d and i_q 3D curve. For MTPA operation, $i_d = 0$. Therefore, the 3D curve can be replaced by a 2D curve containing *torque* and i_q. This curve is the intersection of the 3D curve and the plane $i_d = 0$. Figure-5.19(d) shows this 2D curve. This curve (*linear plot of Torque Vs* I_q) can be used for any direction operation of IPMSM. This plot shows that, the relationship between the motor torque and *q*-axis current is linear.

CHAPTER 6
CONCLUSSIONS, RECOMMENDATIONS AND FUTURE WORK

6.1 CONCLUSIONS

For low power applications, switching losses are acceptable for specific range but for high power applications, switching losses become more significant. Because of switching losses, high frequencies (greater than 20 kHz) are less efficient than lower frequencies (as low as 100 Hz). Due to this, efficiency of a system reduces as switching losses increase. But in order to reduce filtering requirements, we have to increase switching frequency, which results in greater switching losses. Although switching losses can be reduced by modifying carrier signal in SPWM.

SVPWM has greater flexibility to reduce switching losses. In SVPWM reduced switching losses are because of the changing of any one switching state, which results in one single phase voltage change every time. If system needs further reduction in switching losses, then another technique could be used for switching loss reduction based on stopping the control pulses of SVPWM for some duration and this duration depends upon angle of the load power factor. For different modulation indexes, extra switching can be eliminated in SVPWM.

During the investigations, we realized harmonics and switching losses in both techniques. For this purpose extensive simulations of these techniques are performed using MATLAB tools. It has been observed that SVPWM has showed superior performances due to less THD and less switching losses; this is because, SVPWM utilizes advance computational switching technique to reduce THD. It also reduces switching losses because of the changing of any one switching state which results in one single phase voltage change every time. Furthermore, at high switching frequencies SVPWM gives better results as compared to SPWM.

IPMSM's saliency, unlike other motor types, provides an information about the exact position of the rotor. The saliency is due to the non-uniform air gap between the stator and rotor of the motor. When the motor is modeled using the rotating *d-q* axis, the variation of inductance in this to axis's become observable. By injecting high frequency signals the inductance value can be made measurable by increasing the bandwidth for filter design. In order to obtain the exact rotor position,

the rotating reference frame's representation should be transformed to two stationary reference frames which are 45-degrees out of phase.

Using the saliency and high frequency signal injected SVPWM, a vector controlled sensorless drive system of IPMSM using carrier frequency component of the rotor current is designed and extensive simulations of this drive system is performed using MATLAB tools.

Thus, based on all obtained results, we concluded that SVPWM technique provides greater overall performance and efficiency as compared to SPWM technique. The rotor position of the motor is obtained using carrier frequency component method. And all the necessary motor performance measures are taken and their values are discussed.

All the objectives stated in Chapter-1 are met and this makes the thesis successful.

6.2 RECOMMENDATION

In this paper, many important motor parameters are assumed. Some of this parameters are magnetic core saturation, ohmic and core losses, and field current dynamics. In the investigation of the performance of the drive system, frictional viscous coefficient is ignored. As a result, a good performing drive systems is investigated. By considering the above key motor parameters, the non-linearity is introduced. This leads to the investigation of non-linear system models and controllers, which are robust.

6.3 FUTURE WORK

For the future work, it opens a way to investigate the application of SVPWM using multilevel inverters. This might decrease the THD value. The other future work recommended point is a sensorless drive of multiphase IPMSMs using CFCM.

REFERENCES

[1]. T. Jahns, J. B. Kliman and T. W. Neumann, *Interior Permanent-Magnet Synchronous Motors for Adjustable-Speed Drives*, IEEE Transactions on Industry Applications, Vol.IA-22, No.4, July/August 1986.

[2]. Mengesha Mamo, K. Izle, M. Sawamura and J. Oyama, *Novel Rotor Position Extraction Based on Carrier Frequency Component Method (CFCM) Using Two Reference Frames for IPM Drives*, IEEE Transactions on Industrial Electronics, Vol. 52, No. 2, April 2005.

[3]. Jung-Ik Ha, Kozo Idle, Toshihiro Sawa, Seung-Ki Sul, *Sensorless Rotor Position Estimation of an Interior Permanent-Magnet Motor from Initial States,* IEEE Transactions of Industrial Electronics, Vol. 39, No. 3, May/June 2003.

[4]. S. Sayeef, G. Foo and M. F. Rahman, *Rotor Position and Speed Estimation of a Variable Structure Direct-Torque-Controlled IPM Synchronous Motor Drive a Very Low Speeds Including Standstill*, IEEE Transactions of Industrial Electronics, Vol. 57, No. 11, November 2010.

[5]. S. Albatran, Y. Fu, A. Albanna, R.Schrader and M. Mazzola, *Hybrid 2D-3D Space Vector Modulation Control Algorithm for Three Phase Inverters*, IEEE Transactions on Sustainable Energy, Vol. 4, No. 3, July 2013.

[6]. V. T. Ranganathan, *Space Vector Pulse Width Modulation – A Status Review*, Sādhanā, Vol. 22, Part 6, December 1997, (pp. 675-688).

[7]. Dorin O. Neacsu, *Space Vector Modulation – An Introduction*, IECON'01: The 27th Annual Conference of the IEEE Industrial Electronics Society.

[8]. Fouad Giri, *AC Electric Motors Control: Advanced Design Techniques and Applications*, Wiley, United Kingdom, 2013. *(pp. 398 – 428)*

[9]. R. Krishnan *Permanent Magnet Synchronous and Brushless DC Motor Drives*, CRC Press, Virginia, USA, 2010.

[10]. R. Krishnan *Electric Motor Drives: Modelling, Analysis and Control*, Prentice Hall, New Jersey, USA, 2001.

[11]. Seung-Ki Sul *Control of Electric Machine Drive Systems*, Wiley, IEEE PRESS, New Jersey, 2011.

[12]. Chee-Mun Ong *Dynamic Simulation of Electrical Machinery: Using Matlab/Simulink*, Prentice Hall, New Jersey, 1998.

[13]. Paul Krause, Oleg Wasynczuk, Scott Sudhoff, Steven Pekarek, *Analysis of Electric Machinery and Drive Systems*, Wiley, IEEE PRESS, Third Edition, New Jersey, 2013.

[14]. S. S. Kulkarni, A. G. Thosar, *Mathematical Modeling and Simulation of Permanent Magnet Synchronous Machine*, International Journal of Electronics and Electrical Engineering Vol. 1, NO. 2, June 2013.

[15]. Rasmus Andersson, Andreas Gillström *Sensorless Control of a Permanent Magnet Synchronous Machine using Signal Injection*, Chalmers University of Technology, Goteborg, Sweden, 2008.

[16]. Persson J, Markovic M, Perriard Y., *A New Standstill Position Detection Technique for Non-salient Permanent-Magnet Synchronous Motors Using the Magnetic Anisotropy Method*, IEEE Transactions On Magnetics, Vol. 43, No. 2, February 2007.

[17]. Vas, P. *Sensorless Vector and Direct Torque Control*, Oxford University Press Oxford, 1998.

[18]. Bose, B. K. "*Power Electronics and Motor Drives: Advances and Trends*," Academic Press, Elsevier, 2006.

[19]. Kazmierkowaski, M. P., Krishnan, R., Blaabjerg, F. *Control in Power Electronics*, Selected Problems. Academic Press, USA, 2002.

[20]. Holmes, D. G. and Lipo, T. A. *Pulse Width Modulation for Power Converters: Principles and Practice*, IEEE Power Engineering Series, Wiley Inter-science, USA, 2003.

[21]. Holtz, J., Khamabdkone, A. M., and Lotzkat, W. *On continuous control of PWM inverters in the over modulation range including the six-step mode*, IEEE Trans. Power Elect., 8(4), 546–553, 1993.

[22]. Lee, D. C. and Lee, G. M. *A novel over-modulation technique for space vector PWM inverter*, IEEE Trans. Power Elect., 13(6), 1144–1151, 1998.

[23]. Mathworks, Inc. *SimpowerSystems™: For use with Simulink®*, Version 3, 1998-2003.

[24]. Michael Meyer, Joachim Böcker, *Optimum Control for Interior Permanent Magnet Synchronous Motors (IPMSM) in Constant Torque and Flux Weakening Range*, EPE-PEMC, Portorož, Slovenia, 2006.

[25]. P. Brandstetter, T. Krecek *Estimation of PMSM Magnetic Saliency Using Injection Technique*, Elektronika IR Elektrotechnika, ISSN 1392-1215, VOL. 20, NO. 2, 2014.

[26]. Antti Piippo, Marko Hinkkanen, Jorma Luomi, *Analysis of an Adaptive Observer for Sensorless Control of Interior Permanent Magnet Synchronous Motors*, IEEE Transactions on Industrial Electronics, VOL. 55, NO. 2, February 2008.

[27]. M. Mamo, J. Oyama, T. Abe, T. Higuchi, and E. Yamada, *Carrier frequency component method for position sensorless control of IPM motor in lower speed range*, Inst. Elect. Eng. Jpn. Trans. Ind. Appl., vol. 120-D, no. 2, Feb. 2000.

[28]. Stephen J. Dodds, *Settling Time Formulae for The Design of Control Systems With Linear Closed Loop Dynamics*, Advances in Computing and Technology, The School of Computing and Technology 3rd Annual Conference, University of East London, pp.31-39, 2008.

[29]. IEEE Std, 519-1992, *IEEE Recommended Practices and Requirements for Harmonic Control in Electrical Power Systems*, New York, NY: IEEE.

APPENDICES

APPENDIX I: Mason's Gain Formula

Mason's formula allows one to compute the transfer function $G(p)$ of any system composed of interconnected subsystems. Under the non-limiting assumption that signals are only summed (and not subtracted) the formula is:

$$G(p) = \frac{\sum_k C_k(p)\Delta_k(p)}{\Delta(p)} \qquad I.1$$

Where, $C_k(p)$, $\Delta(\rho)$, and $\Delta_k(\rho)$ are called, respectively, *transfer function of the direct input—output path, determinant* of the system, and *reduced determinant* with respect to the k^{th} direct path. The transfer function $C_k(p)$ is simply the product of the transfer functions of all the systems composing the k^{th} direct {*i.e.*, not containing cycles) path from input to output. The determinant $\Delta(\rho)$ is given by:

$$\Delta(p) = 1 - \sum_i L_i(p) + \sum_i \sum_j L_i(p)L_j(p) - \sum_i \sum_j \sum_k L_i(p)L_j(p)L_k(p) + \ldots \qquad I.2$$

Where, $L_i(p)$ is the transfer function of the i^{th} closed path (loop), that is, the product of the transfer functions of all the subsystems composing the i^{th} closed path exiting in the system. The first sum in the formula concerns all the loops, the second all the disjoint pairs of loops *(i.e.*, loops that do not touch each other) and so on. Finally, the reduced determinant Δ_k is the determinant Δ without all the terms corresponding to loops that are touched by the k^{th} direct path. On occasions, it may not be easy to find all the direct paths and all the loops by inspection of the graph representing the inter-connected system. However, in many cases of practical interest, Mason's formula is straightforward to apply, particularly when there are no disjoint loops.

APPENDIX II: SIMULINK® Blocks

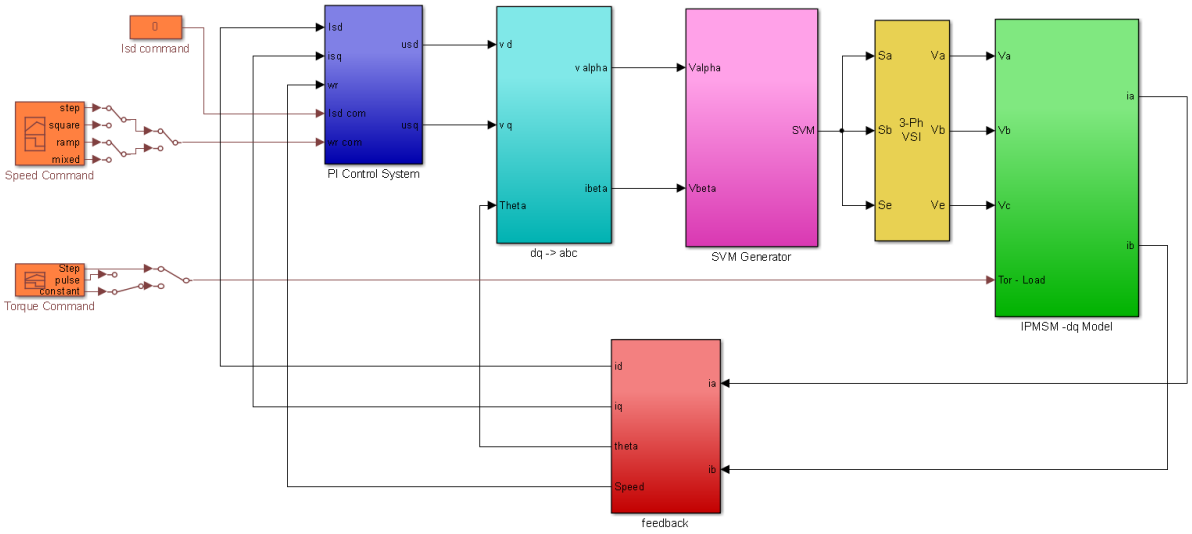

***Figure-II.1**: SIMULINK® Realization of the Sensorless Drive System.*

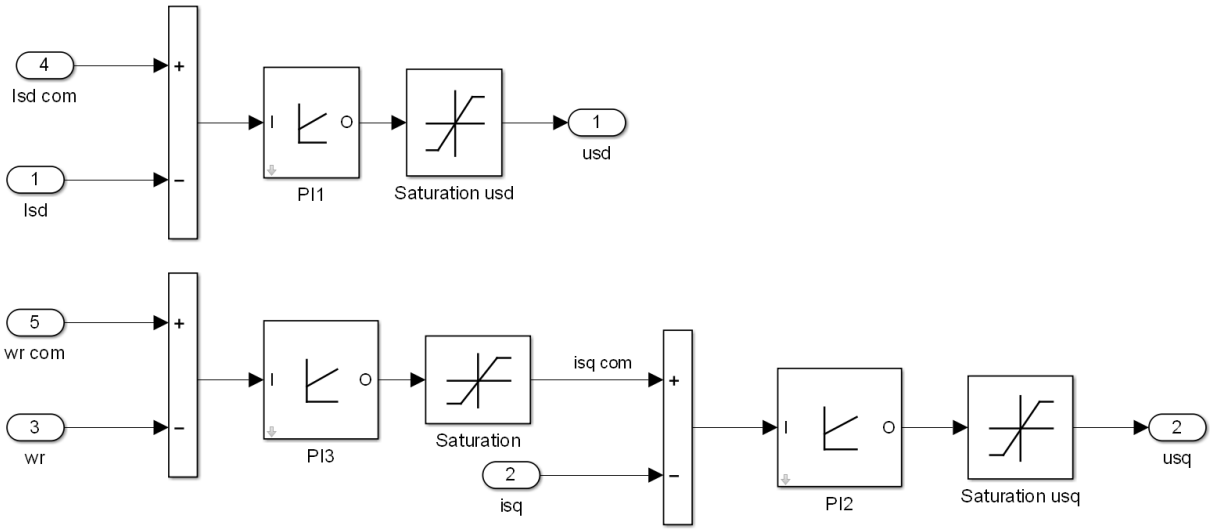

***Figure-II.2**: Realization of the PI Control System.*

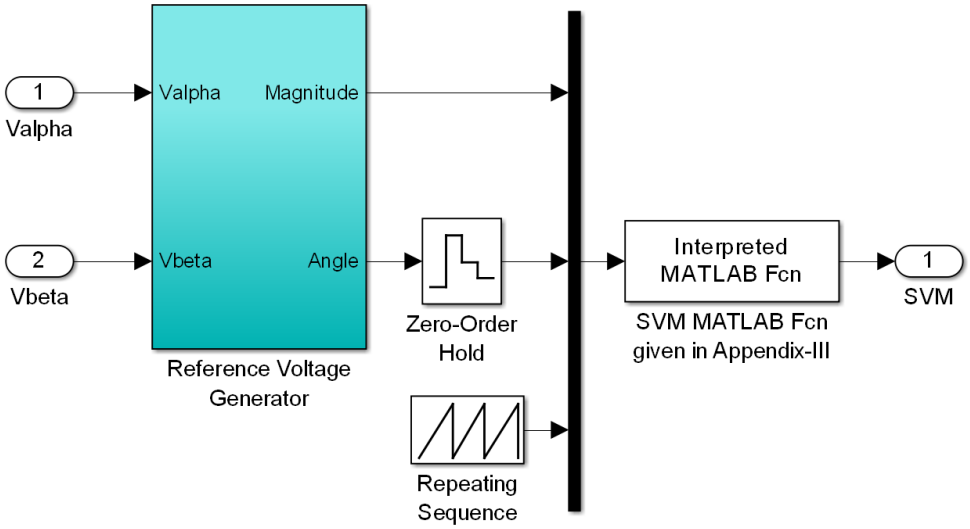

***Figure-II.3**: Realization of the SVM Generator*.

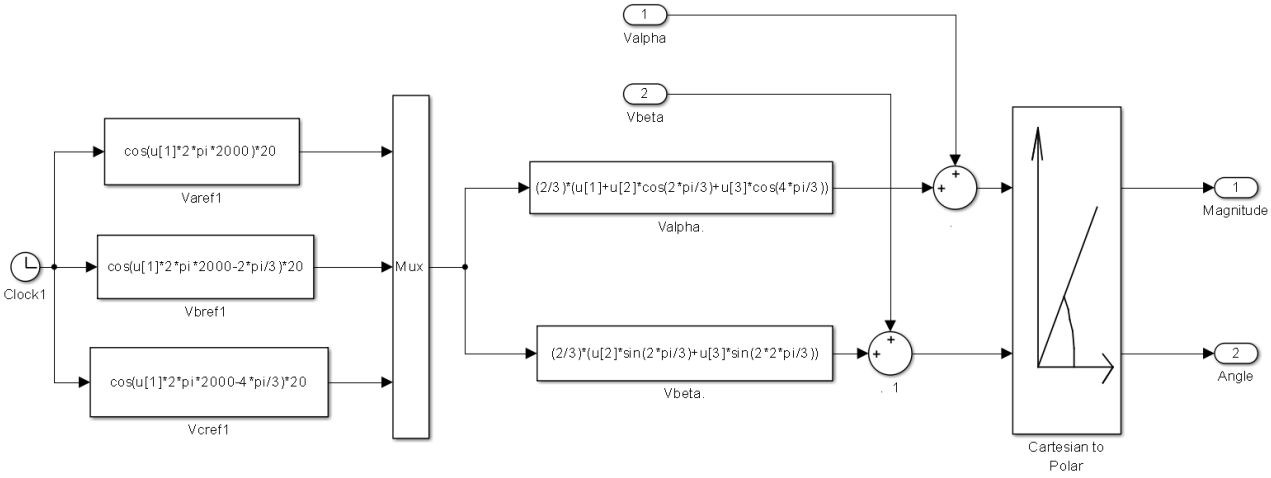

***Figure-II.4**: Realization of the Reference Voltage Generator, from PI Controller Output and Injection Signal inside SVM Generator Block.*

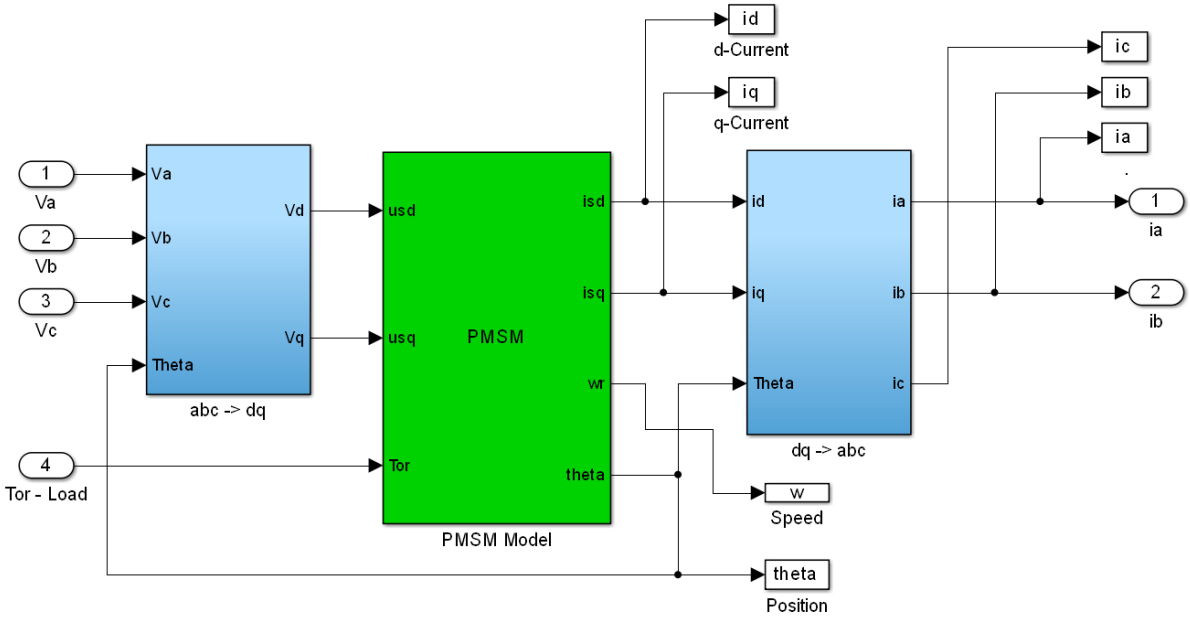

***Figure-II.5**: Realization of the IPMSM Block.*

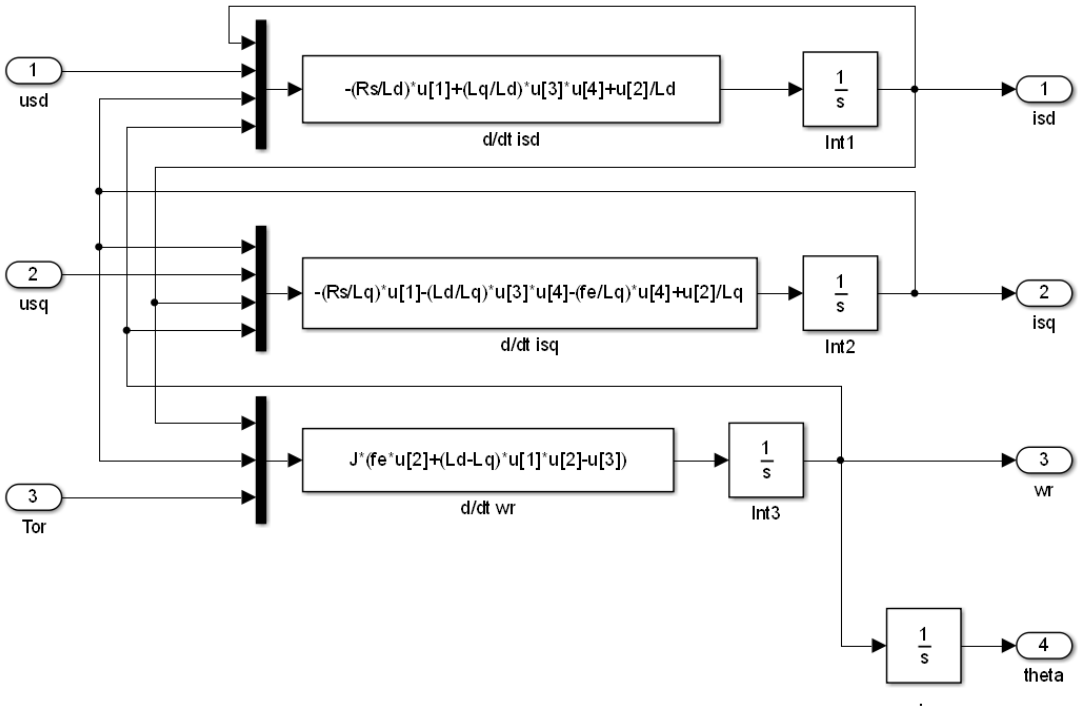

***Figure-II.6**: Realization of the IPMSM in d-q Reference Frame.*

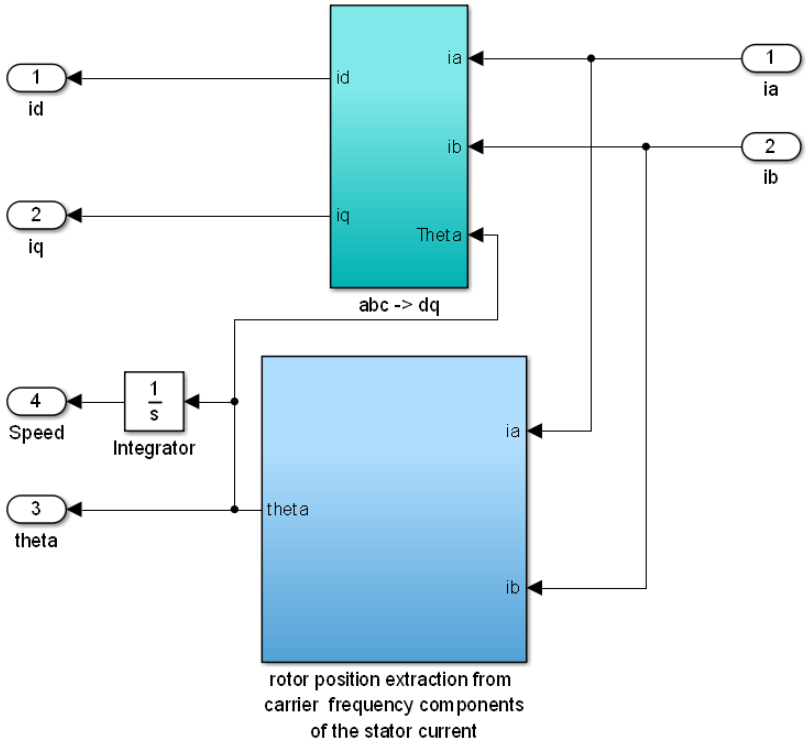

***Figure-II.7**: Realization of the Feedback Block.*

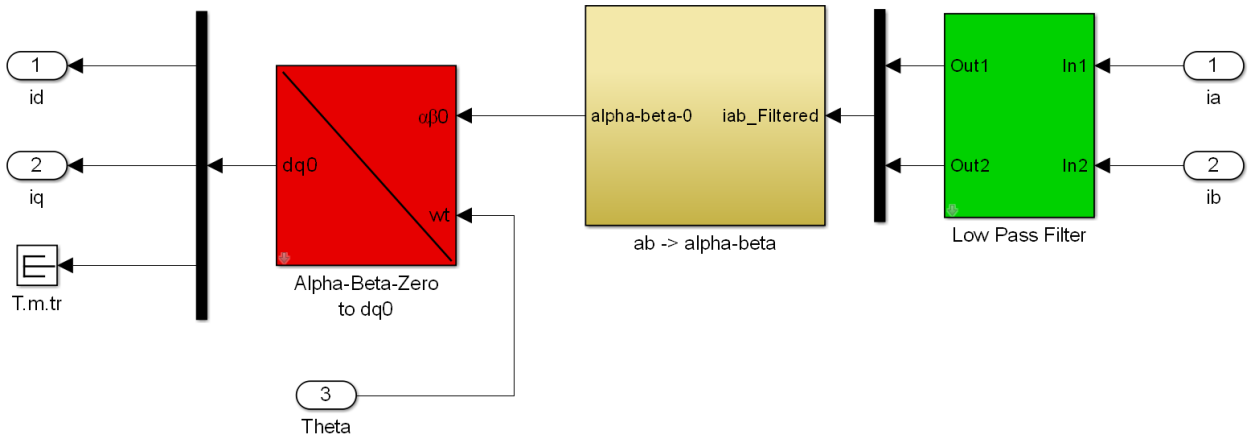

***Figure-II.8**: Realization of abc → dq0 Converter.*

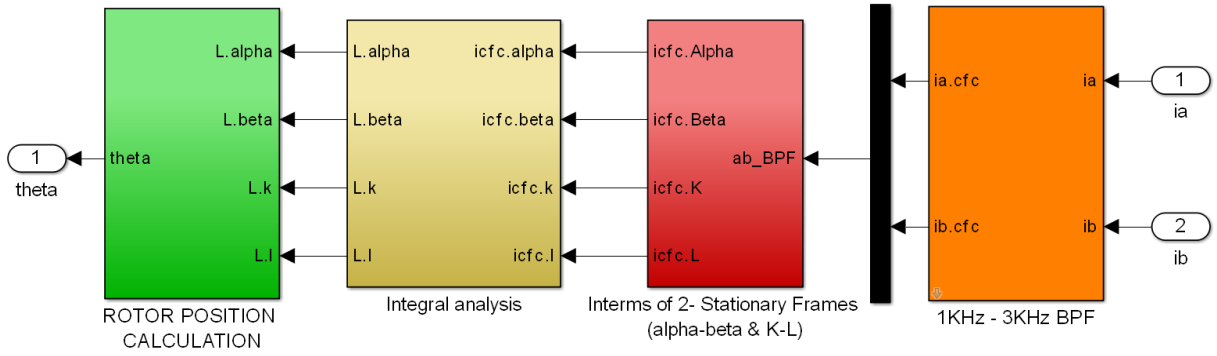

***Figure-II.9**: Realization of the Position Extraction Block.*

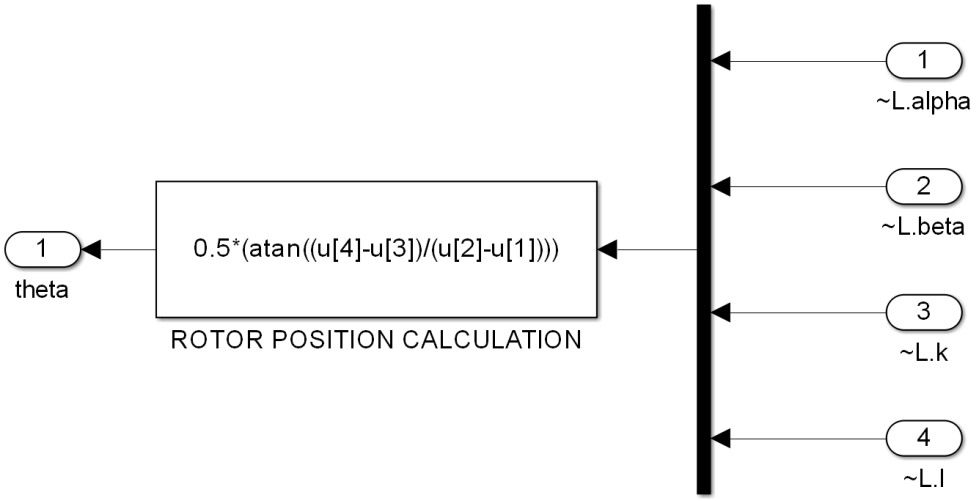

***Figure-II.10**: Realization of Rotor Position Computation.*

APPENDIX III: SVM Implementation Code for per Unit DC Bus Voltage

```
% inputs are
        % magnitude u1(:)
        % angle u2(:);

function [sf]=3phaseSVPWM(u)  %Function Declaration.

f=50;       %Fundamental Frequency in Hz
ts=0.0002;  % %Switching time. Switching Frequency of 5KHz.
vdc=1;      %Per unit DC bus Voltage
peak_phase_max = vdc/sqrt(3);   %Maximum Possible Pick Value of SVPWM output

x=u(2);

y=u(3);
mag=(u(1)/peak_phase_max) * ts;

%SECTOR-1 IDENTIFICATION AND SWITCHING SYMMETRIC SEQUENCE GENERATION
%_____________________________________________________________________
if (x>=0) & (x<pi/3)

    ta = mag * sin(pi/3-x);
    tb = mag * sin(x);
    t0 =(ts-ta-tb);

    t1=[t0/4 ta/2 tb/2 t0/2 tb/2 ta/2 t0/4];
    t1=cumsum(t1);

    v1=[0 1 1 1 1 1 0];
    v2=[0 0 1 1 1 0 0];
    v3=[0 0 0 1 0 0 0];

    for j=1:7
        if(y<t1(j))
            break
        end
    end

    sa=v1(j);
    sb=v2(j);
    sc=v3(j);

end

%_____________________________________________________________________
%SECTOR-2 IDENTIFICATION AND SWITCHING SYMMETRIC SEQUENCE GENERATION
%_____________________________________________________________________

if (x>=pi/3) & (x<2*pi/3)

    adv= x-pi/3;

    tb = mag * sin(pi/3-adv);
    ta = mag * sin(adv);
    t0 =(ts-ta-tb);
```

```
        t1=[t0/4 ta/2 tb/2 t0/2 tb/2 ta/2 t0/4];
        t1=cumsum(t1);

        v1=[0 0 1 1 1 0 0];
        v2=[0 1 1 1 1 1 0];
        v3=[0 0 0 1 0 0 0];

    for j=1:7
        if(y<t1(j))
            break
        end
    end

    sa=v1(j);
    sb=v2(j);
    sc=v3(j);

    end

    %_____________________________________________________________________
    %SECTOR-3 IDENTIFICATION AND SWITCHING SYMMETRIC SEQUENCE GENERATION
    %_____________________________________________________________________

    if (x>=2*pi/3) & (x<pi)

        adv=x-2*pi/3;
        ta = mag * sin(pi/3-adv);
        tb = mag * sin(adv);
        t0 =(ts-ta-tb);

        t1=[t0/4 ta/2 tb/2 t0/2 tb/2 ta/2 t0/4];
        t1=cumsum(t1);
        v1=[0 0 0 1 0 0 0];
        v2=[0 1 1 1 1 1 0];
        v3=[0 0 1 1 1 0 0];

    for j=1:7
        if(y<t1(j))
            break
        end
    end

    sa=v1(j);
    sb=v2(j);
    sc=v3(j);

end

    %_____________________________________________________________________
    %SECTOR-4 IDENTIFICATION AND SWITCHING SYMMETRIC SEQUENCE GENERATION
    %_____________________________________________________________________

    if (x>=-pi) & (x<-2*pi/3)

                adv = x  + pi;

        tb= mag * sin(pi/3 - adv);
        ta = mag * sin(adv);
        t0 =(ts-ta-tb);
```

```
        t1=[t0/4 ta/2 tb/2 t0/2 tb/2 ta/2 t0/4];
        t1=cumsum(t1);
    v1=[0 0 0 1 0 0 0];
    v2=[0 0 1 1 1 0 0];
    v3=[0 1 1 1 1 1 0];

    for j=1:7
        if(y<t1(j))
            break
        end
    end

    sa=v1(j);
    sb=v2(j);
    sc=v3(j);

end

    %_____________________________________________________________________
    %SECTOR-5 IDENTIFICATION AND SWITCHING SYMMETRIC SEQUENCE GENERATION
    %_____________________________________________________________________

    if (x>=-2*pi/3) & (x<-pi/3)

        adv = x+2*pi/3;

        ta = mag * sin(pi/3-adv);
        tb = mag * sin(adv);
        t0 =(ts-ta-tb);

        t1=[t0/4 ta/2 tb/2 t0/2 tb/2 ta/2 t0/4];
        t1=cumsum(t1);
        v1=[0 0 1 1 1 0 0];
        v2=[0 0 0 1 0 0 0];
        v3=[0 1 1 1 1 1 0];

    for j=1:7
        if(y<t1(j))
            break
        end
    end

    sa=v1(j);
    sb=v2(j);
    sc=v3(j);

end

    %_____________________________________________________________________

    %SECTOR-6 IDENTIFICATION AND SWITCHING SYMMETRIC SEQUENCE GENERATION
    %_____________________________________________________________________

    if (x>=-pi/3) & (x<0)

        adv = x+pi/3;
```

```
        tb = mag * sin(pi/3-adv);
        ta = mag * sin(adv);
        t0 =(ts-ta-tb);

        t1=[t0/4 ta/2 tb/2 t0/2 tb/2 ta/2 t0/4];
        t1=cumsum(t1);
        v1=[0 1 1 1 1 1 0];
        v2=[0 0  0 1 0 0 0];
        v3=[0 0 1 1 1 0 0];

    for j=1:7
        if(y<t1(j))
            break
        end
    end
    sa=v1(j);
    sb=v2(j);
    sc=v3(j);
end



    sf=[sa, sb, sc];
```

APPENDIX IV: Sinusoidal PWM Implementation

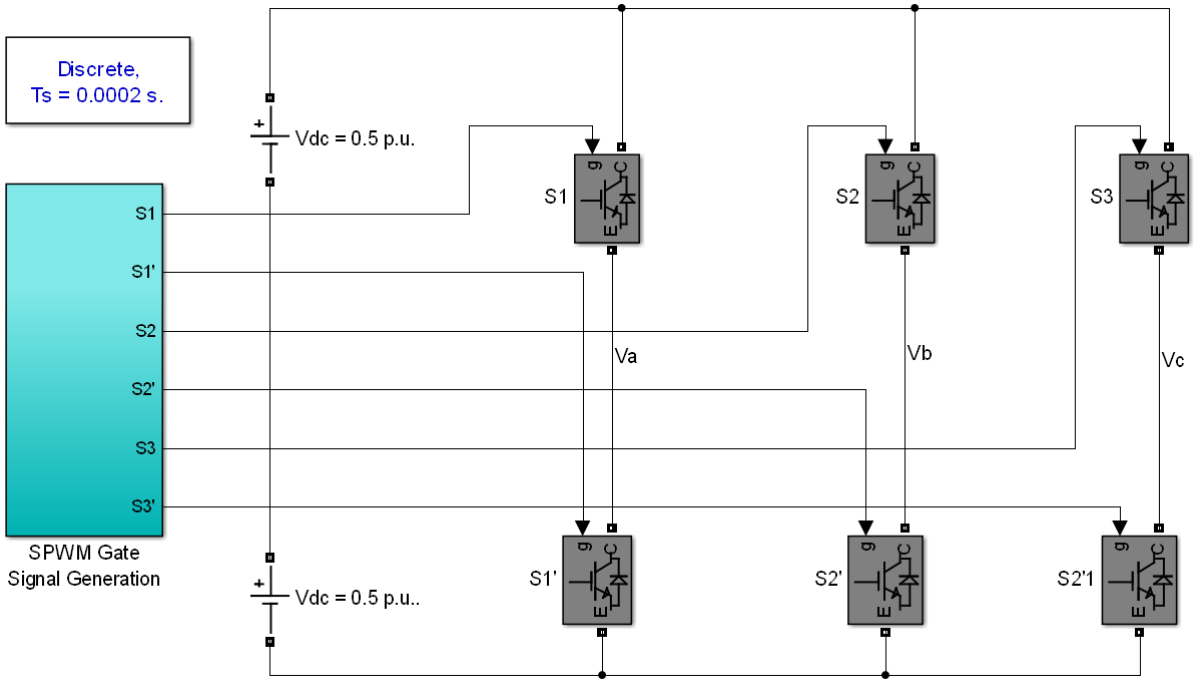

***Figure-IV.1**: Implementation of Sinusoidal PWM Technique.*

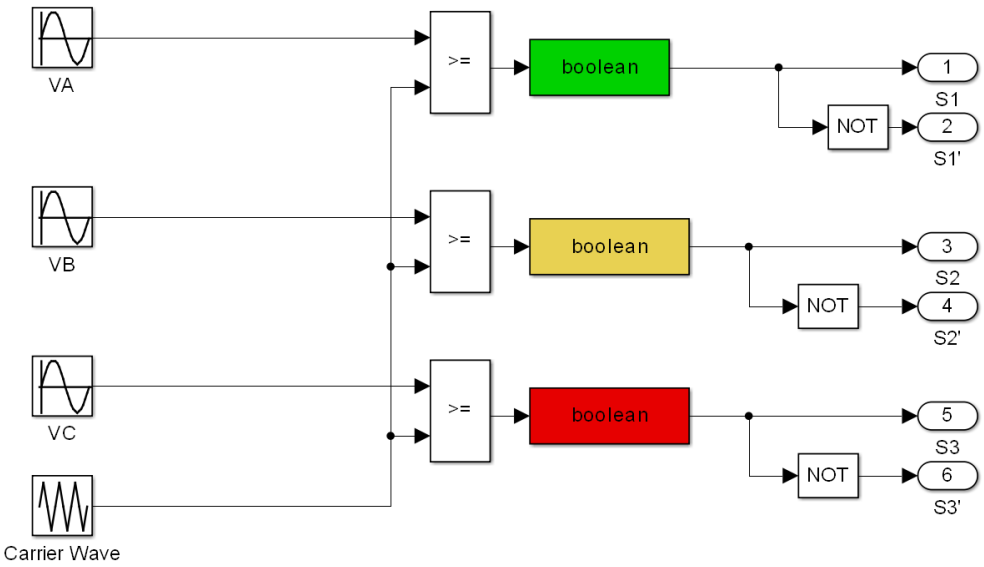

***Figure-IV.2**: Realization of Sinusoidal PWM Gate Signal Generation.*

DECLARATION

I, the undersigned, declare that this thesis work is my original work, has not been presented for a degree in this or any other universities, and all sources of materials used for the thesis work have been fully acknowledged.

Nebiyu Tenaye Woldegebriel _____
Name Signature

Place: Addis Ababa Institute of Technology, AAiT
Addis Ababa University, AAU
Addis Ababa,
Ethiopia.

Submitted in: September 2015.

This thesis has been submitted for examination with my approval as a university advisor.

Dr. Mengesha Mamo _____
Name Signature